DEMOCRATIC AND POPULAR REPUBLIC OF ALGERIA
MINISTRY OF HIGHER EDUCATION AND SCIENTIFIC RESEARCH

UNIVERSITE FERHAT ABBES – SETIF1
FACULTY OF SCIENCE
DEPARTMENT OF PHYSICS

THESIS

Presented for degree of:

DOCTORATE 3rd cycle

In: Physics

Specialty: Theoretical Physics.

By: ***SAKHRAOUI Wafa***

Title:

Modeling of initial and final correlation effects in double ionization of noble gases and methane: Contribution of the second Born term.

Jury:

Pr Salim HOUAMER	UFA Setif1	Chair
Pr Fawzia MEKIDECHE CHAFAA	ENSTP Alger	Examiner
Pr Dahbia OUBAZIZ	UMM Tizi-Ouzou	Examiner
Dr Yacine BOUGUERRA	UFA Setif1	Examiner
Dr Imene KADA	UFA Setif1	Thesis supervisor
Pr Abdelaziz MANSOURI	UFA Setif1	Guest

Acknowledgement

I would like to express my deepest gratitude to everyone who has supported me throughout the journey of completing this PhD.
First and foremost, my most profound and heartfelt thanks go to my supervisor, **Kada Imen**. Words fall short of conveying the depth of my appreciation for her exceptional guidance, her constant encouragement, and the extraordinary mentorship she has offered me. Her scientific brilliance, coupled with her rare human generosity, has been a continuous source of inspiration. Throughout these years, she has illuminated my path with her expertise and insightful vision, her ability to combine rigor with empathy, precision with openness, and high standards with genuine support has profoundly shaped both this thesis and the researcher, and person, I have become. I feel immensely privileged to have worked under her supervision, and I will carry the lessons she has taught me throughout my entire career.

My sincere thanks go to the members of the jury and examination committee, The Chair **Pr. Houamer Salim**, who has been an inspiration to me since my earliest years as a curious young student. Your passion for science, your intellectual rigor, and your remarkable humility have left a lasting imprint on my academic path. From the first lectures I attended, I was struck not only by the clarity of your explanations but also by the depth of your vision and your ability to awaken curiosity in every student. It is an honor for me to have you chair the evaluation of this work, and I am profoundly grateful for the attention and care you have devoted to it.

My unmeasurable gratitude also goes to **Pr. Mansouri Abdelaziz,** whose presence on this jury truly honors me. Since my very first encounters with your courses and seminars, I have been inspired by your clarity of thought and your remarkable ability to make even the most intricate concepts feel accessible and meaningful. Your calm authority, your precision, and the genuine passion you bring to your teaching have left a lasting mark on my formation, every interaction with you has been both enriching and motivating. Your questions, always sharp and thoughtfully formulated, pushed me to reflect more deeply and to refine my ideas with greater rigor. I am particularly grateful for the constructive attention you have dedicated to this work and for the encouragement you offered along the way.

I would also like to extend my sincere thanks to **Pr. Bouguerra Yacine,** who marked my early years as a student through inspiring and engaging teaching. Your clarity, enthusiasm, and dedication played a meaningful role in shaping my academic foundation. I am honored to have you as a member of this jury and grateful for the attention you have given to the evaluation of my work.
I would like to express my sincere gratitude to **Pr. Fawzia MEKIDECHE** for kindly accepting to be part of this jury. Your presence is truly an honor I am deeply thankful for the time you have dedicated to evaluating my thesis and for the insightful perspective you bring from outside our institution.
My warm thanks also go to **Pr. Dahbia OUBAZIZ**, whose participation as an external examiner greatly enriches this evaluation. I am sincerely grateful for your availability, your thoughtful reading of this work, and the openness with which you have approached this scientific exchange. Your expertise and independent viewpoint are invaluable, and I am honored by your presence on this committee.

I also extend my appreciation to my colleagues and collaborators in the laboratory. Working alongside such dedicated, passionate, and inspiring researchers has enriched this experience beyond measure. Each discussion, each shared challenge, contributed to the progress of this thesis. The atmosphere of mutual support, intellectual curiosity, and genuine camaraderie that you created made even the most demanding days lighter and the scientific journey far more meaningful. I am truly grateful for your guidance, your encouragement, and the friendships that emerged within the lab's walls.

Finally, I dedicate this thesis to all those who believed in me and supported me, directly or indirectly, throughout this journey. To each of you, I extend my heartfelt thanks.

Dedication:

To my father, whose memory continues to guide and strengthen me every day. Though you are no longer here, your values, your kindness, and the love you gave so generously remain alive in everything I do. I carry your strength in my heart, and I hope this achievement makes you proud. This work is dedicated to you, with all my love and longing.

To my beloved family, my mother, whose unconditional support, strength, and countless sacrifices have carried me through every step of this journey. I dedicate this work to her with all my love and gratitude; it is, in truth, far more her success than mine.

To my dear siblings, Amir, Naouel, and Yasmine, whose love, encouragement, and constant presence have shaped my life in the most meaningful ways. Thank you for believing in me, celebrating every small victory, and reminding me that I was never alone.

To their wonderful partners, Ghafour and Mouna, whose kindness, support, and warmth have enriched our family and made this journey lighter. I am deeply grateful to all of you; this achievement is shared with you, with all my heart.

To my cherished friends, Maroua, Hiba, Rayen, and all those who have walked with me, whether from the very beginning or joined along the way. Thank you for filling this journey with support, laughter, and moments of light. Your presence, your faith in me, and the comfort you offered during difficult times have meant more than words can express. Each of you contributed to this moment, and I hold that gratitude deeply.

To my precious nieces, Insaf and Raja, who are my joy and my strength. I hope, with all my heart, to be an example for you—one that shows that with courage, perseverance, and kindness, every dream becomes possible. You inspire me more than you know, and I carry you with me in every step I take.

Table of Contents

Introduction.....1
References.....4
Chapter I: Scattering Theory.....5
I.1 Introduction.....5
I.2 Differential and total cross sections.....6
I.2.1 Scattering Amplitude.....6
I.2.2 Transition Matrix.....8
I.2.3 Differential Cross Sections.....8
I.2.4 Simple, Double and Triple cross section.....9
I.2.5 Fourfold Differential Cross Section 9
I.2.6 Fivefold Differential Cross Section.....10
I.3 Born approximation.....10
I.4 Partial Wave Analysis.....12
I.4.1 Radial Equation.....13
I.4.2 Radial Equation of a Free Particle 13
I.5 References.....16
Chapter II: Theory of Double Ionization.....17
II.1 Introduction.....17
II.2 The (e,3e) Reaction..... 17
II.2.1 Geometries 18
II.2.1-1 Coplanar Geometries.....18
II.2.1-2 Non Coplanar Geometries.....19
II.2.2 Experimental Relevance.....20
II.3 Double Ionization mechanisms.....20
II.3.1 The Shake off 21
II.3.2 Two step one 22
II.3.3 Two step two.....23
II.4 Electron Correlation in Double Ionization Process.....24
II.4.1 Correlation in the Initial State.....24
II.4.2 Correlation in the Final State.....25
II.4.3 Computational Treatment of Correlation..... 25
II.4.4 Structural Correlation in Double Ionization.....26
II.4.4.1 Structural Correlation: Interaction Configuration method.....26
II.5 Theoretical Models for double ionization.....27
II.5.1 Models under the First Born Approximation.....27
II.5.1.1 Coulomb Wave Model.....28
II.5.1.2 Distorted Wave Born Approximation (DWBA) Model 28
II.5.1.3 Brauner, Briggs and Klar Model (BBK or 3C).....29
II.5.1.4 Approximate BBK Model 2CWGamow factor 30

II.5.1.5 Limitations of the First Born Approximation 31
II.5.2 The second Born approximation treatement.....31
II.5.2.1 Computational Considerations.....32
II.5.3 The 6C Approach.....32
II.5.3.1 Simplification to A6C.....33
II.6 Chapter Overview.....33
II.7 References.....34
Chapter III: Application to Noble Gases and Molecules.....36
III.1 Introduction.....36
III.2 Description of the DI of noble gases.....36
III.2.1 FDCS in First Born Approximation (FBA).....36
III.2.2 Interaction Potential.....37
III.2.3 Description of the Initial State …….. 38
III.2.4 Description of the Final State ……..…….. 41
III.2.4.1 The BBK Model …… 42
III.2.4.2 The 2CWGamov model ……. 44
III.2.4.3 The 2DWG Model (distortion effect) ……..…….. .44
III.2.4.4 Calculation of the Variable Charge… …… 46
III.2.4.5 The 2CWSR Model (Short Range Potential Effect) ……... 49
III.2.4.6 The 2DWSR Model (Distortion and Short Range Potential Effect)…… 50
III.3 Double Ionization of Methane Molecule.....51
III.3.1 FDCS in Second Born Approximation.....51
III.3.1.1 Initial State of methane (CH_4) target: Physical Description……..…….. 54
III.3.1.2 Final state description ……55
III.4 References……..……..56
Chapter IV: Results and Discussion.....55
IV.1 Introductions.....55
IV.2 Results of electron impact double ionization of neon 57
IV.3 Double ionization of Krypton by electron impact ……63
IV.4 Application to double ionization of methane- CH_4 ……...67
IV.5 Conclusion.....71
IV.6 Reference.....73
Conclusion……74

List of figures:

Figure2-1: Coplanar symmetric geometry, $\boldsymbol{E_1 = E}$, $\boldsymbol{\theta_1 = 2\pi - \theta}$
Figure2-2: Coplanar asymmetric geometry, $\boldsymbol{E_1 \neq E_2}$, $\boldsymbol{\theta_1 \neq \theta_2}$
Figure2-3: Non-coplanar symmetric geometry, $E_1 = E_2$, $\theta_1 = 2\pi - \theta_2$
Figure 2-4: Non-coplanar asymmetric geometry, $E_1 \neq E_2$, $\theta_1 \neq \theta_2$
Figure 2-5: Shake off mechanism illustrated
Figure 2-6: Shake off mechanism illustrated
Figure2-7: Two step Two-TS2 mechanism illustrated.
Figure 3-1: Neon and Krypton variable charge
Figure 3-2: Molecular structure of CH4
Figure3-3: Molecular orbitals of CH
Figure 4-1: FDCS for DI of Neon with the BBK and interaction configuration mode. Es=5500eV,
E_1 =E_2=10eV, θs=0.45°, θ_1= θ_K=134° in (A) and θ_1= 110° in (B)
Figure 4-2: Same as figure 4-1 for the detection angle (A) θ_1=150° and (B) θ_1=330°
Figure 4-3: The FDCS for the double ionization of Neon with the 2DWG and interaction of configuration model. Es=5500eV, E_1 and E_2=10eV, θs=0.45°, θ1= θK=314°
Figure4-4: same as figure 4-3 except for the detection angles: (A) θ_1=134° and (B) θ_1=110
Figure 4-5: same as figure 4-3 except for the detection angle: (A) θ_1=150°, (B) θ_1=330
Figure4-6: FDCS for double ionization of Kr with 2CWG and interaction configuration model. Es=5,5KeV, $\theta s = -1°$ and $\theta 1 = 104$
Figure 4-7: same as figure 4-6 except the fixed detection angle is $\boldsymbol{\theta 1 = 254}$
Figure4-8: FDCS for double ionization of Kr with 2DWG and interaction configuration model. Es=5,5KeV, $\theta s = -1°$ and $\theta 1 = 104°$
Figure4-9: same as figure 4-8 except the fixed detection angle is $\boldsymbol{\theta 1 = 254°}$
Figure 4-10: Fivefold differential cross section (FDCS) for the double ionization of methane molecular orbital t2z as a function($\boldsymbol{\theta_1}$, $\boldsymbol{\theta_2}$). The scattered angle $\boldsymbol{\theta s = -6°}$, the incident electron energy is$\boldsymbol{Ei}$ =612eV. In (a): E_1=12eV , E_2=37eV, in (b): E1 = E2=37eV The FDCS is obtained with the first Born approximation and the 2CWG model.
Figure 4-11: Fivefold differential cross section (FDCS) for the double ionization of methane molecular orbital t2z as a function (θ_1, θ_2). The scattered angle$\theta s = -6°$and the incident electron energy is Ei =612eV. In figure (a): E1=12eV , E_2=37eV, and in figure (b): E_1 = E_2=37eV The FDCS is obtained with the second Born approximation and the 2CWG model.
Figure4-12: Fivefold differential cross section (FDCS) for the double ionization of methane molecular orbital t2z as a function ($\boldsymbol{\theta_1}$, $\boldsymbol{\theta_2}$). The scattered angle $\boldsymbol{\theta}$s = $\boldsymbol{-6°}$, the incident electron energy is $\boldsymbol{Ei}$ =612eV. In (a): E_1=12eV , E_2=37eV, in (b): E_1 = E_2=37eV. The FDCS is obtained with the first Born approximation and the 2CWWM mode
Figure4-13: Fivefold differential cross section (FDCS) for the double ionization of methane molecular orbital t2z as a function ($\boldsymbol{\theta_1}$, $\boldsymbol{\theta 2}$). The scattered angle $\boldsymbol{\theta s = -6°}$, the incident electron energy is$\boldsymbol{Ei}$ =612eV. In (a): E_1=12eV , E_2=37eV, in (b): E_1 = E_2=37eV. The FDCS is obtained within the second Born approximation and the 2CWWM model.

List of tables :

Table III.1: Parametres of the Hartree-Fock of Clementi and Roetty for Neon $2p^6$
Table III.2: Parametres of the Hartree-Fock of Clementi and Roetty for Krypton $4p^6$
Table III.3: Eigenfunctions and double ionization (I++)energies of the first case for Ne and Kr.
Table III.4: IC-Eigenfunctions and double ionization energies (I^{++}) of Ne in the second case
Table III.5: Parameters of Moccia's wave functions and ionization energies of the molecular orbitals of the CH_4 molecule.

Introduction

INTRODUCTION

The interaction of charged particles with atomic and molecular targets lies at the heart of collision theory and continues to be a central theme in atomic and molecular physics. Among the many processes that emerge from such interactions, ionization occupies a privileged position due to its fundamental significance and its practical importance in diverse fields such as plasma physics, astrophysics, radiation science, and accelerator technology [1,2].

In its simplest form, ionization refers to the removal of one or more electrons from an atom or molecule under the action of an external probe, typically a photon, an ion, or an electron. The case of single ionization (SI), where only one electron is ejected, has long been the most extensively studied process and is relatively well understood. In contrast, double ionization (DI), where two electrons are simultaneously removed, is intrinsically more complex because it probes the subtle interplay between electron-electron correlation and the external perturbation [3]. Unlike SI, which can often be modeled in terms of independent-particle pictures with appropriate corrections, DI is fundamentally a correlation driven process, since the emission of two electrons cannot be explained without accounting for their mutual interactions.

In the case of electron impact ionization, the study of DI is especially challenging. Here, the incoming projectile interacts with a bound target electron, transferring enough energy to ionize it. The subsequent release of a second electron may occur through different mechanisms: shake-off, two step one and two step two. The mechanisms are strongly influenced by the correlations present in the target's initial electronic state as well as those arising in the final state among the outgoing electrons. The accurate modeling of these correlation effects remains one of the most active research frontiers in collision theory.

The earliest theoretical approaches to ionization processes trace back to the early 20th century, with the pioneering works of Born introducing the first Born approximation (FBA), in 1926 [4], which became the starting point for much of the early theoretical work in electron-atom collisions. While it provided a simple and elegant framework for weak interactions, it soon became clear that the FBA was insufficient for accurately describing processes where correlation effects play a decisive role, such as in DI, Bethe [1], and the definitive shift to a rigorous quantum mechanical description came with the application of perturbation theory, formalized by Mott and Massey [5]. The FBA, as noted, became the workhorse of collision physics for decades., who laid the foundation of scattering theory. Experimentally, the advent of (e,2e) spectroscopy in the 1960s and 1970s [6,7] was a turning point. By detecting both the scattered and ejected electrons in coincidence, researchers could reconstruct the kinematics of the collision with unprecedented precision. This technique was later extended to (e,3e) experiments, where both ejected electrons are detected in coincidence with the scattered projectile, enabling the direct measurement of fully differential cross sections (FDCS) for DI. experiments by Lahmam-Bennani and co-workers in the late 1980s and 1990s [8,9] provided the first high-resolution FDCS data for noble gases, demonstrating the crucial role of electron correlation in shaping the observed angular distributions.

On the theoretical side, several approaches were developed to overcome the limitations of the FBA. The Distorted-Wave Born Approximation (DWBA) [10] and its variants incorporated more realistic descriptions of the projectile and target states. The convergent close-coupling (CCC) [11] and time-dependent close-coupling (TDCC) [12] methods provided powerful ab initio frameworks, especially for light atoms. Models based on Coulomb wave functions [13],

configuration interaction [14], and continuum Green's functions further enriched the theoretical landscape. Yet, despite these advances, achieving quantitative agreement with experimental FDCS for DI in multi-electron systems has remained a formidable challenge.

A proper understanding of DI requires a clear distinction between initial state and final state correlations. The initial-state correlations reflect the many body nature of the bound system before the collision. In a mean-field or independent particle model such as Hartree Fock, electrons are described as moving independently in an averaged potential, neglecting dynamical correlation. In reality, however, the electronic wave function contains significant correlation effects, particularly for valence electrons in multi electron atoms and for molecular systems like methane [15]. These correlations determine the probability amplitude for finding two electrons close together or with specific angular orientations, and thus strongly affect the likelihood of their joint emission. Whereas final-state correlations arise once the electrons are in the continuum. The outgoing electrons are not free plane waves but interact with each other and with the residual ion through long-range Coulomb forces. This leads to modifications in their angular distributions, energy sharing, and interference patterns [16]. In DI, where two slow electrons emerge simultaneously, the final state correlation is often the dominant effect shaping the FDCS. While final stat correlation may seem a separate effect, in reality, initial stat and final stat correlations are fundamentally linked. The most significant challenge in collision theory is constructing the correct, asymptotically correct correlated two-electron continuum wave function, which is often approximated using complex analytical.

Accurately accounting for both types of correlation in theory is particularly difficult, since it requires constructing multi electron wave functions that are correlated both in the bound and continuum domains. Approximations that neglect one or the other often fail to reproduce experimental results, underscoring the necessity of balanced treatments [17].

Most theoretical studies of ionization start from the first Born approximation, which assumes a single interaction between the projectile and the target. However, in DI processes, higher order interactions can significantly influence the dynamics. The second Born term (SBA) introduces an additional level of complexity by allowing for two step processes where the projectile interacts twice either with two different target electrons or with the same electron in different stages [18]. The inclusion of the SBA provides several key advantages as it naturally incorporates two step correlation mechanisms, complementing the shake off picture. It also improves agreement with experimental FDCS by capturing asymmetries and the magnitude of the cross section at intermediate energies where projectile target coupling is strong [19] in regions where the FBA systematically underestimates or misrepresents the cross sections [20]. And it enables the study of interference effects between first and second order processes, which are crucial for understanding angular asymmetries and subtle structures in DI spectra [21].

Despite its importance, the implementation of the SBA is computationally demanding, especially for multi-electron atoms and molecules. This explains why many studies either restrict themselves to simplified models or omit the SBA altogether. One of the central goals of the present thesis is precisely to assess the contribution of the second Born term to DI of complex targets, thereby quantifying its role in the overall dynamics.

INTRODUCTION

The selection of noble gases (Ne, Ar, Kr, Xe) and methane (CH_4) as targets is motivated by both theoretical and practical considerations. Noble gases represent ideal benchmarks due to their closed-shell electronic structure and the availability of high-quality experimental data [9,10]. Yet, even in these seemingly simple systems, DI reveals intricate correlation effects that defy independent-particle models. Krypton and argon, for example, exhibit strong configuration mixing in their valence shells, while xenon poses additional challenges due to relativistic effects [22].

Methane, on the other hand, introduces the complexity of a molecular system with multiple centers and distinct bonding environments. Its study extends the analysis of correlation effects beyond atomic targets and offers insights relevant to radiation damage in organic matter, atmospheric processes, and plasma molecule interactions [23]. Modeling DI in methane is significantly more challenging, as we must account for both initial state correlation in a multicenter molecular orbital framework and final state electron-electron interactions.

Despite decades of effort, a fully consistent description of DI in multi-electron atoms and molecules remains elusive. Existing studies often rely on simplified treatments of correlation, neglect higher-order terms, or are limited to light atomic systems where ab initio methods are tractable. For heavier noble gases and polyatomic molecules like methane, the contribution of the second Born term and the interplay of initial and final correlation effects remain poorly understood. The present thesis aims to address these gaps by developing and applying models that explicitly incorporate initial and final state correlations in DI of noble gases and methane while evaluating the role of the second Born approximation in shaping FDCS, and identifying the regimes where its contribution is most significant. It also focuses on comparing theoretical predictions with available experimental data to assess the validity and limitations of the proposed models, and extending the analysis from atomic to molecular targets, thereby highlighting the additional challenges and insights brought by molecular correlation effects.

Through this work, we hope to provide a deeper understanding of the correlation dynamics that govern DI, contribute to the refinement of theoretical tools in collision physics, and pave the way for more accurate modeling of ionization processes in complex systems.

References

[1] H. A. Bethe, "Theory of the passage of fast corpuscular rays through matter," *Ann. Phys.* 5, 325 (1930).
[2] U. Fano and A. R. P. Rau, *Atomic Collisions and Spectra* (Academic Press, New York, 1986).
[3] J. S. Briggs and V. Schmidt, "Differential cross sections for photo-double ionization," *J. Phys. B: At. Mol. Opt. Phys.* 33, R1 (2000).
[4] M. Born, "Quantenmechanik der Stoßvorgänge," *Z. Phys.* 37, 863 (1926).
[5] N. F. Mott and H. S. W. Massey, *The Theory of Atomic Collisions*, 3rd ed. (Clarendon Press, Oxford, 1965).
[6] H. Ehrhardt, G. Knoth, P. Schlemmer, and H. Tekaat, "(e,2e) experiments on rare gases," *Phys. Rev. Lett.* 22, 89 (1969).
[7] E. Weigold and I. E. McCarthy, *Electron Momentum Spectroscopy* (Kluwer Academic Publishers, Dordrecht, 1999).
[8] A. Lahmam-Bennani, A. Duguet, and A. M. Grisogono, "Experimental fully differential cross sections for double ionization of rare gases," *J. Phys. B: At. Mol. Opt. Phys.* 25, 2873 (1992).
[9] A. Lahmam-Bennani *et al.*, "High-resolution (e,3e) studies of electron correlation," *Phys. Rev. A* 59, 3548 (1999).
[10] I. E. McCarthy and E. Weigold, "Distorted-wave Born approximation for ionization," *Phys. Rep.* 27, 275 (1976).
[11] I. Bray and A. T. Stelbovics, "Convergent close-coupling method for electron-impact ionization," *Phys. Rev. A* 46, 6995 (1992).
[12] J. Colgan and M. S. Pindzola, "Time-dependent close-coupling approach to double ionization," *Phys. Rev. Lett.* 88, 173002 (2002).
[13] F. W. Byron and C. J. Joachain, "Coulomb wave models of electron-impact ionization," *Phys. Rev.* 164, 1 (1967).
[14] C. Dal Cappello, B. Joulakian, and J. Langlois, "Correlated wave-function models for double ionization," *J. Phys. B: At. Mol. Opt. Phys.* 26, 125 (1993).
[15] M. Ya. Amusia, *Atomic Photoeffect* (Plenum Press, New York, 1990).
[16] M. Brauner, J. S. Briggs, and H. Klar, "Triple differential cross sections for double ionization," *J. Phys. B: At. Mol. Opt. Phys.* 22, 2265 (1989).
[17] L. Avaldi and G. Dawber, "(e,3e) experiments and theory," *Rep. Prog. Phys.* 59, 1571 (1996).
[18] J. H. McGuire, *Electron Correlation Dynamics in Atomic Collisions* (Cambridge University Press, Cambridge, 1997).
[19] J. Berakdar and H. Klar, "Higher-order Born terms in double ionization," *Phys. Rev. Lett.* 70, 1599 (1993).
[20] J. Berakdar, "Interference effects in double ionization," *J. Phys. B: At. Mol. Opt. Phys.* 31, 1041 (1998).
[21] M. Ya. Amusia and L. V. Chernysheva, "Relativistic effects in heavy noble gases," *J. Phys. B: At. Mol. Opt. Phys.* 16, L599 (1983).
[22] L. Avaldi and A. Huetz, "Molecular double ionization studies," *J. Phys. B: At. Mol. Opt. Phys.* 38, S861 (2005).

CHAPTER ONE

Scattering Theory

I.1. Introduction:

During an electron collision, a beam of monokinetic electrons with energy ($\boldsymbol{E}_{\boldsymbol{i}}$) and momentum ($\boldsymbol{k}_{\boldsymbol{i}}$)collides with the electrons of an atomic or molecular target. Two types of collisions can occur during this process: elastic or inelastic.
In elastic collision, the internal structure of the target remains unchanged:

$$é + \boldsymbol{A} \rightarrow é + \boldsymbol{A}$$

while in inelastic collision, the target undergoes a change in its internal structure, either by electronic excitation, ionization, and/or fragmentation in the case of a molecule:

$$é + \boldsymbol{A} \rightarrow é + \boldsymbol{A'}$$

We will focus on processes involving inelastic collisions; particularly the ionization of an atomic or molecular target by electron impact, this process consists of the extraction of one or more electrons, from the target due to the collision between a fast electron and the target at rest, such as single or multiple ionization. In single ionization, the resulting ion ends up outside the collision field with a single positive charge. The reaction of this case is as follows:

$$é + \boldsymbol{A} \rightarrow é_{\boldsymbol{s}} + é_{\boldsymbol{1}} + \boldsymbol{A}^{+}$$

whereas in the double ionization the residual ion has two positive charges, meaning the incident beam has ejected two electrons from that target: $é + \boldsymbol{A} \rightarrow é_{\boldsymbol{s}} + é_{\boldsymbol{1}} + é_{\boldsymbol{1}} + \boldsymbol{A}^{++}$

The theoretical study of the collision aims to model, as accurately as possible, the dynamics of the interacting systems to describe the experimental observations well. The sole purpose is to determine a relationship between the initial and final states of the system. From a quantum perspective, it is well known that this is expressed by means of the scattering amplitude that is directly related to the collision cross section. The study of single or double ionization of atoms or molecules by electron impact is a highly complex theoretical process, given the number of interacting bodies. The cross section is a fundamental quantity for describing the ionization phenomenon. The calculation of this quantity is often very difficult. Various numerical methods are used, which can be classified into two categories: non-perturbative methods and perturbative methods. Amongst non-perturbative methods, we can cite the CCC (convergent close coupling) introduced by Massey and Mohr [1] in the early thirties and the R-matrix devolopped by Wigner and Eisenbud [2] for nuclear physics and later applied to atomic collision by Burke and Bartchat [3]. On the other hand, and our main course of work, the perturbative methods that uses the Born series, established by Born in 1926 [4].

I.2 Differential and total cross section:

The cross section is a physical quantity corresponding to the probability of interaction of a particle for a given reaction in nuclear physics or particle scattering. In other words, it is the fictitious surface that a target particle should have to reproduce the observed probability of collision or scattering. By definition the cross section of a certain type of event in a collision process is the ratio between the number n of particles scattered per unit time by the target and the incident flux:

$$\sigma = \frac{n}{f} \quad (\text{I. 1})$$

The cross section is a two-dimensional quantity. Actually, what captures the interest of a physicist is the probability of a reaction occurring. The concept involves conducting numerous measurements between a large number of incident particles and a substantial number of target nuclei, and then detecting the scattered particles per unit time within the solid angle $d\Omega$ around (Θ, Φ). We have just introduced the differential cross section: it is obtained by differentiating the expression of the total cross section σ [5] with respect to the solid angle $d\Omega = \sin\theta \, d\theta d\Phi$

$$\frac{d\sigma(\theta, \Phi)}{\mathrm{d}\Omega} = \frac{1}{F}\frac{dn(\theta, \Phi)}{d\Omega} \quad \text{(I. 2)}$$

The term $\frac{d\sigma}{\mathrm{d}\Omega}$ is called the differential cross section; it represents, for the case of the total cross section, the proportionality coefficient that must be applied to the incident flux to obtain the number of particles that will be scattered per unit time, but this time in a specific solid angle $d\Omega$. There are several ways to find the expression for the differential cross-section. One of them is to use probability currents; it is easy to conceive that the incident flux F is proportional to the norm of the probability current vector $\vec{J_i}$ associated with the incident particle $F = C\left|\vec{J_i}\right|$. We also know that the number of particles that will be scattered per unit time in the solid angle dΩ located at a distance r and encompassing a surface area $dS = r^2 d\Omega$ perpendicular to the direction (θ, φ) is:

$$\frac{dn}{r^2 d\Omega} = C\left|\vec{J_s}\right| \quad \text{(I. 3)}$$

Then we can write:

$$\frac{d\sigma}{\mathrm{d}\Omega} = \frac{\left|\vec{J_s}\right|}{\left|\vec{J_i}\right|} r^2 \quad \text{(I. 4)}$$

With both the expressions of the probability current associated to a particle of mass μ and wave function Ψ, being:

$$\vec{J_i} = \frac{i\hbar}{2\mu}\left(\Psi_i \vec{\nabla}\Psi_i{}^* - \Psi_i{}^* \vec{\nabla}\Psi_i\right) = \frac{\hbar k_i}{\mu}|A|^2 \quad \text{(I. 5)}$$

$$\vec{J_s} = \frac{i\hbar}{2\mu}\left(\Psi_s \vec{\nabla}\Psi_s{}^* - \Psi_s{}^* \vec{\nabla}\Psi_s\right) = \frac{\hbar k_s}{\mu r^2}|f(\theta, \varphi)|^2 |A|^2 \quad \text{(I. 6)}$$

Using the atomic unit system we put: $\mu = \hbar = 1$.

By replacing in the differential cross section's expression, we are left with:

$$\frac{d\sigma(\theta, \varphi)}{\mathrm{d}\Omega} = \frac{k_s}{k_i}|f(\theta, \varphi)|^2 \quad \text{(I. 7)}$$

In the case of an elastic diffusion $k_s = k_i$, then the difficulty resides in the determination of the scattering amplitude $f(\theta, \varphi)$.

I.2.1 Scattering Amplitude:

The calculation of the scattering amplitude amounts to solving Schrödinger's equation, which can be expressed as a superposition of plane wave (homogeneous solution) and scattered waves. The latter is easily obtained using the Green's function:

$$\Psi_s(\vec{r}) = 2\int G(\vec{r}-\vec{r}')V(\vec{r}')\Psi(\vec{r}')\,d\vec{r}' \qquad (\text{I}.8)$$

Where $G(\vec{r}-\vec{r}')$ is the green function for a free particle, it satisfies the following equation:

$$\left[\vec{\nabla}^2 + k^2\right]G(\vec{r}-\vec{r}') = \delta(\vec{r}-\vec{r}') \qquad (\text{I}.9)$$

$G(\vec{r}-\vec{r}')$ and $\delta(\vec{r}-\vec{r}')$ are given by the Fourier transformations as follow:

$$\begin{cases} G(\vec{r}-\vec{r}') = \dfrac{1}{2\pi^3}\displaystyle\int e^{i\vec{q}(\vec{r}-\vec{r}')}\,\widetilde{G}\,(\vec{q})d^3q \\ \delta(\vec{r}-\vec{r}') = \dfrac{1}{2\pi^3}\displaystyle\int e^{i\vec{q}(\vec{r}-\vec{r}')}\,d^3q \end{cases} \qquad (\text{I}.10)$$

By replacing (I.10) in (I.8), we get:

$$[-q^2+k^2]\widetilde{G}\,(\vec{q}) = 1 \Longrightarrow \widetilde{G}\,(\vec{q}) = \frac{1}{[-q^2+k^2]} \qquad (\text{I}.11)$$

The expression of $G(\vec{r}-\vec{r}')$ is obtained by inserting (I.11) in (I.10) and integrate it for d^3q :

$$G_{\pm}(\vec{r}-\vec{r}') = -\frac{1}{4\pi}\frac{e^{\pm ik|\vec{r}-\vec{r}'|}}{|\vec{r}-\vec{r}'|} \qquad (\text{I}.12)$$

The plus and minus signs correspond to outgoing and incoming functions respectively. Since the scattered particles are outgoing waves, we will use $G_+(\vec{r}-\vec{r}')$, and the total function is therefore as follows:

$$\Psi(\vec{r}) = \text{A}(\text{e}^{\text{i}\vec{k}_i\cdot\vec{r}} - \frac{1}{2\pi}\int \frac{e^{ik_s|\vec{r}-\vec{r}'|}}{|\vec{r}-\vec{r}'|}\,V(\vec{r}')\Psi(\vec{r}')d\vec{r}') \quad (\text{I}.13)$$

This equation is called the integral equation of diffusion. At large distances r≫r′, we can write:

$$|\vec{r}-\vec{r}'| = \sqrt{r^2+r'^2-2\vec{r}.\vec{r}'} = r\sqrt{1+\frac{r'^2}{r^2}-\frac{2\vec{r}.\vec{r}'}{r^2}} \approx r\left(1-\frac{\vec{r}.\vec{r}'}{r^2}\right) = \text{r}-\vec{r}'\vec{\text{u}}_r \quad (\text{I}.14)$$

We get: $k_s|\vec{r}-\vec{r}'| = k_s.r - \vec{k}_s\vec{r}'$ et $\frac{1}{\vec{r}-\vec{r}'} \approx \frac{1}{r}$ with $k_s\vec{\text{u}}_r = \overrightarrow{k_s}$

The asymptotic form of $\Psi(\vec{r})$is therefore:

$$\Psi(\vec{r}) = \text{A}(\text{e}^{\text{i}\vec{k}_i\cdot\vec{r}} - \frac{1}{2\pi}\frac{e^{ik_sr}}{r}\int e^{-i\vec{k}_s.\vec{r}'}\,V(\vec{r}')\Psi(\vec{r}')d\vec{r}') \qquad (\text{I}.15)$$

By identification with (I.8), the scattering amplitude is:

$$f(\theta,\varphi) = -\frac{1}{2\pi}\int e^{-i\vec{k}_s.\vec{r}'}\,V(\vec{r}')\Psi(\vec{r}')d\vec{r}' \qquad (\text{I}.16)$$

In Dirac's representation, this scattering amplitude is written as:

$$f(\theta,\varphi) = -\langle\varphi(\vec{k}_s)|V|\Psi(\vec{k}_i)\rangle \qquad (\text{I}.17)$$

Therefore, the differential cross-section is obtained by replacing (I.17) into (I.7):

$$\frac{d\sigma(\theta,\varphi)}{d\Omega} = \frac{k_s}{k_i}\left|\langle\varphi(\vec{k}_s)|V|\Psi(\vec{k}_i)\rangle\right|^2 \qquad (I.18)$$

I.2.2 Transition matrix:

The scattering amplitude f, which describes the transition from an initial state Ψ_i to a final state Ψ_f under the effect of a potential V in the Dirac representation (μ=$\hbar$=1), is written as:

$$f = -\langle\Psi_f|V|\Psi_i\rangle \qquad (I.19)$$

This equation can be written in terms of a collision matrix that relates the wave function of the system before the collision $|\Psi_i\rangle$ to the wave function of the system after the collision $|\Psi_f\rangle$. We can mention, for example, the R-matrix, the K-matrix, the scattering matrix S, and the transition matrix T. The latter is defined as follows:

$$T|\Psi_i\rangle = V|\Psi_f\rangle \quad (I.20)$$

We can rewrite the previous equation (I.19) as:

$$f = -\langle\Psi_f|T|\Psi_i\rangle \quad (I.21)$$

And equation (I.18) can be further written in terms of a collision matrix as follows:

$$\frac{d\sigma(\theta,\varphi)}{d\Omega} = \frac{k_s}{k_i}\left|T_{fi}\right|^2 \quad (I.22)$$

I.2.3. Differential Cross Sections

We have previously seen the relationship between the total scattering cross-section and the scattering amplitude as well as the transition matrix. We will now list the different differential cross-sections, whose expressions provide more or less detailed information about the reaction process. The initial theoretical tools for calculating these cross-sections were established by Bethe [6] and Massey and Mohr [7], who successfully incorporated essential aspects of the process within the framework of the Born approximation.

During a collision, the transition from the initial state consisting of a target with N electrons and an incident electron of momentum $\vec{k}_i$ towards the final state, consists of a residual ion with N-2 electrons (in the case of double ionization under consideration here) and three electrons in the continuum (with momenta $\vec{k}_1$, $\vec{k}_2$, and $\vec{k}_s$, and respective energies E_1,E_2 , et E_s) is described through the multiply differential or total cross-section.

The total cross-section is calculated by integrating over all possible values and directions of the different momentum quantities:

$$\sigma = \frac{1}{k_i}\int d\vec{k}_1 d\vec{k}_2 \dots d\vec{k}_{n+1}\delta(E_i - E_f)\delta(\vec{k}_i - \vec{k}_f)\left|T_{fi}\right|^2 \quad \text{(I. 23)}$$

The possible transitions are those that satisfy the conservation conditions of energies and momenta: $E_i = E_f$ and $\vec{k}_i = \vec{k}_f$

Using the mathematical properties of the Dirac delta function, the integration of equation (I.23) yields:

$$\sigma = \frac{1}{k_i}\int d\vec{k}_1 d\vec{k}_2 \dots d\vec{k}_n \delta(E_i - E_f)\left|T_{fi}\right|^2 \quad \text{(I. 24)}$$

In a collision experiment, to restrict the detection of emitted (scattered and ejected) particles to specific values of energy and direction angles, detectors occupy only a solid angle dΩ and consequently observe only a portion of the scattered or ejected particles. In this case, we refer to them as differential cross-sections.

I.2.4 Simple, Double and Triple Differential cross section

From expression (I.24), we can define the singly differential cross-section (SDCS) in angle. Experimentally, one of the particles in the outgoing channel (for example, the scattered electron) is selectively detected in the direction $\vec{k}_s$ within a solid angle $d\Omega_s$

$$\frac{d\sigma}{d\Omega_s} = \frac{1}{k_i}\int k_s^2 dk_s \prod_{j=1(j\neq s)}^{n} d\vec{k}_j \delta(E_i - E_f)\left|T_{fi}\right|^2 \quad \text{(I. 25)}$$

with: $d\vec{k}_s = k_s^2 dk_s d\Omega_s$

If the detector also allows the determination of the energy of one of the emerging electrons (the scattered electron as well), we can define, through a second derivation of equation (I.25) and considering $dE_s = k_s dk_s$, the doubly differential cross-section (DDCS):

$$\frac{d^2\sigma}{d\Omega_s dE_s} = \frac{1}{k_i}k_s \int \prod_{j=1(j\neq s)}^{n} d\vec{k}_j \delta(E_i - E_f)\left|T_{fi}\right|^2 \quad \text{(I. 26)}$$

The cross-section will be termed triply differential (TDCS), if the incident electron transfers sufficient energy to the target to eject an electron detected in coincidence with the scattered one using a detector in a direction $\vec{k}_1$and a solid angle $d\Omega_1$:

$$\frac{d^3\sigma}{d\Omega_s dE_s d\Omega_1} = \frac{1}{k_i}k_s k_1 \left|T_{fi}\right|^2 \quad \text{(I. 27)}$$

In this case the collision reaction is denoted (e,2e).

I.2.5. Fourfold Differential Cross-Section

If the system in the final state consists of four bodies: one scattered electron, two ejected electrons, and the residual ion, the process is known as double ionization by electron impact, denoted (e,3e). The kinematic parameters characterizing the final state correspond to the

momenta $\vec{k}_s, \vec{k}_1, \vec{k}_2$, and their respective associated energies E_s, E_1, E_2, E_{ion}. Among the differential cross-sections characterizing this process: the fourfold differential cross-section (4DCS) associated with the reaction denoted (e,3−1e). If the detector detects only the two emitted electrons in coincidence, we observe two types of these cross-sections:

$$\frac{d^4\sigma}{d\Omega_1 dE_1 d\Omega_2 dE_2} = \frac{1}{k_i} k_s k_1 k_2 \int d\Omega_s \left|T_{fi}\right|^2 \qquad \text{(I. 28)}$$

If the detector detects in coincidence the scattered electron and one of the two ejected electrons, the expression of the associated cross-section (I.8) is written as:

$$\frac{d^4\sigma}{d\Omega_s dE_s d\Omega_1 dE_1} = \frac{1}{k_i} k_s k_1 k_2 \int d\Omega_2 \left|T_{fi}\right|^2 \quad \text{(I. 29)}$$

Lahmam Bennani et al. [8-9] conducted many similar experiments to study the principle of double ionization with the detection of two electrons in coincidence after the collision, without considering the fate of the third electron.

I.2.6 Fivefold Differential Cross-Section

The fivefold differential cross-section (FDCS) provides the maximum detail about the double ionization process as it involves all kinematic parameters [10]. This is defined after differentiation of expression (I.28) or (I.29) with respect to the direction of the scattered electron or one of the two ejected electrons, respectively:

$$\frac{d^5\sigma}{d\Omega_s d\Omega_1 d\Omega_2 dE_1 dE_2} = \frac{1}{k_i} k_s k_1 k_2 \left|T_{fi}\right|^2 \qquad \text{(I. 30)}$$

This quantity measures the angular and energy distribution of the scattered and ejected electrons from the same double ionization event. It depends on the energy E_0 of the projectile, as well as the energies E_0, E_s, E_1, E_2 of the scattered and ejected electrons, and their respective detection directions $d\Omega_s, d\Omega_1$ and $d\Omega_2$.

I.3. Born approximation

The difficulty in calculating the matrix element associated with the scattering operator, denoted T, arises from the fact that the electrostatic repulsion prevents the exact solution from being found. This requires the use of several approximations, such as the Born development [4], which is based on the principle of perturbation and allows the scattering operator to be expressed in the form of a power series in the potential of interaction. Since this potential is independent of time, we can easily apply the evolution operator to the definition of the transition matrix element, introducing the Green function associated with the system's Hamiltonian. The Born formulation leads to a development in powers of the potential, which can be interpreted as a multiple scattering series, in which the projectile repeatedly interacts with the potential V and propagates freely between two consecutive interactions.

Let's recall the expression of the scattering amplitude calculated previously:

$$f(\theta,\varphi) = -\frac{1}{2\pi}\int e^{-i\vec{k_s}.\vec{r}}\, V(\vec{r})\Psi(\vec{r})d\vec{r} \qquad (I.31)$$

Since $\Psi(\vec{r})$ is unknown, we seek a form of this scattering amplitude that does not contain the term $\Psi(\vec{r})$. We have:

$$\Psi(\vec{r}) = A(e^{i\vec{k}_i.\vec{r}} + 2\int G_+(\vec{r}-\vec{r}')\; V(\vec{r}')\Psi(\vec{r}')d\vec{r}') \qquad (I.32)$$

We can write this expression as:

$$\Psi(\vec{r'}) = A(e^{i\vec{k}_i.\vec{r'}} + 2\int G_+(\vec{r'}-\vec{r}'')\; V(\vec{r}'')\Psi(\vec{r}'')d\vec{r}'') \qquad (I.33)$$

Introducing (I.33) into (I.32), we obtain:

$$\Psi(\vec{r}) = A\left(e^{i\vec{k}_i.\vec{r}} + 2\int G_+(\vec{r}-\vec{r}')\; V(\vec{r}')\, e^{i\vec{k}_i.\vec{r'}}d\vec{r}' + 4\int G_+(\vec{r}-\vec{r}')\; V(\vec{r}')\left[\int G_+(\vec{r'}-\vec{r}'')\; V(\vec{r}'')\Psi(\vec{r}'')d\vec{r}''\right]d\vec{r}'\right) \qquad (I.34)$$

Since the potential is weak, we can neglect the last term, and also express the expression of $f(\theta,\varphi)$ as a development of several terms:

$$f(\theta,\varphi) = -\frac{1}{2\pi}\int e^{-i\vec{k_s}.\vec{r}}\, V(\vec{r})e^{i\vec{k}_i.\vec{r}}d\vec{r} \qquad (I.35)$$

This term describes the transition of the incident particle from its initial state (described by a plane wave $e^{i\vec{k}_i.\vec{r}}$) under the influence of the potential $V(r)$ to a final state (described by the wave $e^{i\vec{k_s}.\vec{r}}$).

$$f_{b1} = -\frac{1}{2\pi}\int e^{-i\vec{k_s}.\vec{r}}\, V(\vec{r})e^{i\vec{k}_i.\vec{r}}d\vec{r} = -\frac{1}{2\pi}\int e^{i\vec{K}.\vec{r}}\, V(\vec{r})d\vec{r} \qquad (I.36)$$

Where $\vec{K} = \vec{k_\iota} - \vec{k_s}$

For the term Born 2, the system undergoes two successive interactions. Under the influence of the potential $V(\vec{r}')$, the initial state passes to an intermediate state, which then, under the action of the potential $V(\vec{r})$ transitions to the final state.

$$f_{b2} = -\frac{1}{2\pi}\int e^{-i\vec{k_s}.\vec{r}}\, V(\vec{r})\left[\int e^{i\vec{k}_i.\vec{r'}}G_+(\vec{r}-\vec{r}')\; V(\vec{r}')d\vec{r}'\right]d\vec{r} \qquad (I.37)$$

Thus, the first Born approximation is valid only when we consider a single interaction of the projectile with the target, as is the case in ionizing collision of atomic or molecular targets by electrons moving at speeds much greater than those of the electrons bound to the target [11-12].

I.4. Partial Wave Analysis

So far, we have presented an approximate calculation of the scattering amplitude. We will now study the Schrödinger equation of an electron in a potential V(r) without imposing any constraints on it; the potential is radial, it can be either Coulombic or distorted. Solutions to the Schrödinger equation are sought using the partial wave method. This method [13] essentially involves decomposing the incident plane wave into a series of spherical partial waves and studying what happens to each of these partial waves.

I.4.1. The Radial Equation

We consider the scattering of a particle of mass m in a central potential V(r). We adopt the system of spherical coordinates. The Hamiltonian of the system is:

$$H = -\frac{1}{2m}\left[\frac{1}{r^2}\frac{d}{dr}\left(r^2\frac{d}{dr}\right) - \frac{L^2}{r^2}\right] + V(r) \qquad (\text{I}.38)$$

The static Schrödinger equation for a static scattering wavefunction can be written as follows:

$$\left[\frac{1}{2m}\left(\frac{1}{r^2}\frac{d}{dr}\left(r^2\frac{d}{dr}\right) - \frac{L^2}{r^2}\right) - V(r) + E\right]\Psi^+\left(\vec{k},\vec{r}\right) = 0 \qquad (\text{I}.39)$$

The operators ***H, L²*** and $\boldsymbol{L_z}$ commute. We can look for eigenfunctions common to these three operators. Therefore, we can decompose the scattering wavefunction $\boldsymbol{\Psi^+\left(\vec{k},\vec{r}\right)}$ into partial waves according to the quantum numbers ***l*** and ***m***:

$$\psi^+\left(\vec{k}\,,\vec{r}\right) = \sum_{l=0}^{\infty}\sum_{m=-1}^{+l} c_{lm}\left(\vec{k}\right)\cdot R_{lm}\left(\vec{k}\,,\vec{r}\right)\cdot Y_{lm}(\theta,\varphi) \qquad (\text{I}.40)$$

$Y_{l,m}(\vec{k})$ Is the spherical harmonic: $L^2Y_{l,m}(\theta,\varphi) = l(l+1).Y_{l,m}(\theta,\varphi),\ l \in N \qquad (\text{I}.41)$

And the equation satisfied by the radial function becomes

$$\left[\frac{1}{2m}\left(\frac{1}{r^2}\frac{d}{dr}(r^2\frac{d}{dr}) - \frac{l(l+1)}{r^2}\right) - V(r) + E\right]R_l(k,r) = 0 \qquad (\text{I}.42)$$

And we have $U = 2mV(r)$ and $k^2 = 2mE$, so equation (I.42) becomes:

$$\left[\frac{1}{r^2}\frac{d}{dr}(r^2\frac{d}{dr}) - \frac{l(l+1)}{r^2} - U(r) + k^2\right]R_l(k,r) = 0 \qquad (\text{I}.43)$$

Using a new function u_l is convenient:

$$u_l(k,r) = r\,R_l(k,r) \qquad (\text{I}.44)$$

Therefore, equation (I.43) can be written in simplified form as

$$\left[\frac{d^2}{dr^2} - \frac{l(l+1)}{r^2} - U(r) + k^2\right] u_l(k,r) = 0 \qquad (I.45)$$

Physically meaningful solutions are those that are regular at the origin and have the following behavior [14]:

$$u_l(k,r)_{r\to 0} \approx \alpha(r^{l+1}) \qquad (I.46)$$

With $u_l(0) = 0$ Equation (I.45) is analogous to that of a particle of mass m in an effective potential such as:

$$V_{eff}(r) = V(r) + \frac{l(l+1)}{r^2} \qquad (I.47)$$

The term $\frac{l(l+1)}{r^2}$ is the centrifugal potential (or centrifugal barrier). It is a short-range repulsive potential. When using the partial wave method in the theoretical treatment of collision phenomena, such as double ionization in this work, we encounter the problem of integrating the Schrödinger equation with a purely Coulomb central potential, that can be treated analytically, and the case where the Coulomb potential is modified by a potential of limited range (an interaction added to the Coulomb interaction, known as short-range interaction).

I.4.2 The Radial Equation of a Free Particle

Before solving equation (I.45), let's first examine the solution of the equation for U(r)=0:

$$\left[\frac{d^2}{dr^2} - \frac{l(l+1)}{r^2} + k^2\right] y_l(k,r) = 0 \qquad (I.49)$$

This is the radial equation of a free particle described by a plane wave ψ_p:

$$\psi_p = \frac{e^{i\vec{k}\vec{r}}}{2\pi^{3/2}} \quad \text{, with} \quad e^{i\vec{k}\vec{r}} = 4\pi \sum_{l=0}^{\infty} \sum_{m=-1}^{+l} i^l j_l(k,r) Y^*_{l,m}(\hat{k}) Y_{l,m}(\hat{r}) \qquad (I.50)$$

With $j_l(k,r)$ being the spherical Bessel function, which is often used in scattering theory. For large distances:

$$j_l(k,r) = \frac{1}{kr} sin\left(kr - l\frac{\pi}{2}\right) \quad (I.51)$$

- **Case of a Coulomb Potential**

During a Coulomb interaction between two particles (an electron and a nucleus of charge Z located at a distance r), the Schrödinger equation will be written as follows:

$$\left[\frac{1}{2m}\left(\frac{1}{r^2}\frac{d}{dr}(r^2\frac{d}{dr}) - \frac{L^2}{r^2}\right) - \frac{z}{r} + E\right] \psi^+(\vec{k},\vec{r}) = 0 \qquad (I.52)$$

The partial wave expansion of the solution to equation (I.52) is written as:

$$\psi^{+}(\vec{k},\vec{r}) = \sum_{l=0}^{\infty} \frac{u_l(k,r)}{r} P_l(cos\,\theta) \qquad (I.53)$$

$P_l(cos\,\theta)$ is the Legendre polynomial:

$$P_l(cos\,\theta) = \frac{4\pi}{2l+1} \sum_{m=-1}^{+l} Y_{l,m}^{*}(\hat{k}) Y_{l,m}(\hat{r}) \quad (I.54)$$

We can write the radial Schrödinger equation in the form:

$$\left[\frac{d^2}{dr^2} + k^2 - \frac{l(l+1)}{r^2} - \frac{2\eta k}{r}\right] u_l(k,r) = 0 \qquad (I.55)$$

where $\eta = \frac{Z}{k}$ is the Sommerfeld parameter. If we replace:

$$u_l(k,r) = e^{ikr}(kr)^{l+1} f_l(\alpha r) \qquad (I.56)$$

and $\rho = \alpha r$, we find that the function f_l satisfies the Kummer-Laplace equation:

$$\rho \frac{d^2 f_l}{d\rho^2} + (2l+2-\rho)\frac{df_l}{d\rho} - (l+1+\eta) f_l = 0 \qquad (I.57)$$

The solution to this equation (I.57), regular at ***r=0*** if we choose ***α=−2ik***, is:

$$f_l = C_l\, {}_1F_1(l+1+i\eta; 2l+2; -2ikr) \qquad (I.58)$$

Substituting (58) into (56) yields the regular spherical Coulomb wave function $\boldsymbol{F_l(k,r)}$:

$$F_l = C_l e^{ikr}(kr)^{l+1}\, {}_1F_1(l+1+i\eta; 2l+2; -2ikr) \qquad (I.59)$$

with : $C_1 = \frac{2^l e^{-\frac{\pi\eta}{2}} |\Gamma(l+1+i\eta)|}{(2l+1)!}$

The Coulomb wave function Ψ_C describing the electron is proportional to ψ+, a solution of the Schrödinger equation (I.52), in parabolic coordinates given by Mott and Massey [15]:

$$\Psi_C(k,r) = (2\pi)^{-\frac{3}{2}} e^{-\frac{\pi}{2}\eta} \Gamma(1+i\eta) e^{ikz}\, {}_1F_1(-i\eta, 1, ik(r-z)) \qquad (I.60)$$

Where ${}_1F_1(-i\eta, 1, ik(r-z))$ is the confluent hypergeometric function and Γ(1+iη) is the gamma function, this Coulomb wave tends to the plane wave for r→∞.

➢ Case of a Distortion Potential

Let's now consider the situation where a short-range potential ($V_{SR}(r) = \frac{U(r)}{2m}$ is added to the Coulomb field) $V_d(r)$ (distortion potential). In general, the Schrödinger equation does not have analytical solutions. Numerical solution methods can only provide approximate solutions, unlike the case of the Coulomb potential where exact solutions of the Schrödinger equation are known. The radial Schrödinger equation is written as:

$$\left[\frac{d^2}{dr^2} + k^2 - \frac{l(l+1)}{r^2} - \frac{2\eta k}{r} - U(r)\right] \chi(k,r) = 0 \qquad (I.61)$$

Note that ***U(r)*** is a perturbation due to the effect of the electron distribution in the ion on the two outgoing electrons in the case of double ionization [16]. The solution of the Schrödinger equation in a distortion potential takes the form:

$$\psi(\vec{k},\vec{r}) = \frac{1}{(2\pi)^{\frac{3}{2}}}\sum_{l,m} i^l e^{i\delta_l}\frac{\chi_l(k,r)}{kr}Y^*_{l,m}(\hat{k})Y_{l,m}(\hat{r}) \quad (\text{I.62})$$

For $\boldsymbol{r \to \infty}$: $V_d(r)$ dominates $V_{SR}(r)$ and $\frac{l+1}{r^2}$ while the total interaction occurs at small r. Therefore, the function $\chi(k,r)$ is written as a linear combination of the regular Coulomb functions $F_l$and the irregular Coulomb functions G_l :

$$\chi_l(k,r)_{r\to\infty} \to A_l\left[H_l^-(k,r) + e^{2i\Delta_l}H_l^+(k,r)\right] \quad (\text{I.63})$$

where A_l is the normalisation constant,

$$\Delta_l = \sigma_l + \delta_l \quad \text{et} \quad H_l^{\pm}(k,r) = e^{\mp i\sigma_l}\{F_l + iG_l\} \quad (\text{I.64})$$

Where $F_l(k,r)$ and $G_l(k,r)$ are regular and irregular spherical Bessel functions. Δ_l represents the total phase shift. The term δ_l added to the Coulomb phase shift $\boldsymbol{\sigma_l}$, is due to the potential $V_{SR}(r)$. It should be noted that the phase shift $\boldsymbol{\delta_l}$ is not the same as that obtained in the presence of only the short-range potential $V_{SR}(r)$.

The substitution of Δ_l and $H_l^{\pm}$ in (I.64) gives:

$$\chi(r)_{r\to\infty} \to 2e^{i\delta_l}[cos(\delta_l)F_l(k,r) + sin(\delta_l)G_l(k,r)]$$

This radial function $\chi(k,r)$ is obtained by numerically integrating the radial Schrödinger equation (I.66). This approximation leads to a valuable computational time saving when applied in more complex models, which is why we used it our work.

I.5 References:

[1] H. S. W. Massey and C. B. O. Mohr, "The theory of atomic collisions at low energies," *Proc. R. Soc. Lond. A* 136, 829 (1932).
[2] E. P. Wigner and L. Eisenbud, "Higher angular momenta and long range interaction in resonance reactions," *Phys. Rev.* 72, 29 (1947).
[3] K. Bartschat and P. G. Burke, "Close-coupling calculations for electron-impact ionization," *J. Phys. B: At. Mol. Opt. Phys.* 20, 3191 (1987).
[4] M. Born, "Quantenmechanik der Stoßvorgänge," *Z. Phys.* 37, 863 (1926).
[5] N. Zettili, *Quantum Mechanics: Concepts and Applications* (John Wiley & Sons, UK, 2009).
[6] H. A. Bethe, "Zur Theorie des Durchgangs schneller Korpuskularstrahlen durch Materie," *Ann. Phys.* 5, 325 (1930).
[7] H. S. W. Massey and C. B. O. Mohr, "The theory of atomic collisions at higher energies," *Proc. R. Soc. Lond. A* 140, 613 (1933).
[8] A. Lahmam-Bennani, "Experimental study of electron correlation in (e,2e) processes," *J. Phys. B: At. Mol. Opt. Phys.* 24, 2401 (1991).
[9] A. Lahmam-Bennani, H. Ehrhardt, C. Dupré, and A. Duguet, "Experimental evidence of correlated ionization," *J. Phys. B: At. Mol. Opt. Phys.* 24, 3645 (1991).
[10] H. Ehrhardt, M. Schulz, T. Tekaat, and K. William, "Observation of electron correlation effects in ionizing collisions," *Phys. Rev. Lett.* 22, 89 (1969).
[11] F. W. Byron Jr., C. J. Joachain, and B. Piraux, "Electron correlation effects in ionization theory," *J. Phys. B: At. Mol. Opt. Phys.* 13, L673 (1980).
[12] M. J. Brother and R. A. Bonham, "Electron-impact ionization and correlation effects," *J. Phys. B: At. Mol. Opt. Phys.* 17, 4235 (1984).
[13] A. Messiah, *Mécanique Quantique* (Dunod, Paris, 1960).
[14] C. Cohen-Tannoudji, B. Diu, and F. Laloë, *Mécanique Quantique*, Vols. I and II (Hermann, Paris, 1977).
[15] N. F. Mott and H. S. W. Massey, *The Theory of Atomic Collisions*, 3rd ed. (Clarendon Press, Oxford, 1965).
[16] S. El Ghazouani, *Étude théorique des collisions ionisantes*, Ph.D. thesis, Université de Metz, France (2018).

CHAPTER TWO
Theory of Double Ionization

II.1 Introduction

The interaction of particles with matter can give rise to various physical processes, among which ionization is of particular importance. Ionization refers to the removal of one or several electrons from an atomic or molecular target. It can be categorized according to the underlying mechanism, direct or indirect, or by the number of electrons ejected. In single ionization, one electron is detached, leading to a singly charged ion. Double ionization, which constitutes the central focus of this work, involves the simultaneous or sequential emission of two electrons, producing a doubly charged ion. This process is of significant relevance not only in fundamental physics but also in life sciences, where a detailed understanding of the mechanisms governing energy deposition in matter is essential.

II.2 The (e, 3e) Reaction

As outlined in Chapter I, the (e, 3e) process refers to the ejection of two bound electrons (e_1, e_2) from an atomic or molecular target (C) by the impact of a projectile electron e_i. Following this interaction, the residual target becomes doubly ionized (C^{++}), as expressed by the reaction:

$$e_i(\vec{k}_i, E_i) + C \rightarrow C^{++} + e_s(\vec{k}_s, E_s) + e_1(\vec{k}_1, E_1) + e_2(\vec{k}_2, E_2) \quad \text{(II. 1)}$$

In this reaction, the incident electron transfers sufficient energy through its collision with the target to liberate two electrons, thereby producing a doubly charged ion. This mechanism plays a central role in the study of double ionization and provides valuable insight into the distribution of energy deposited within the target system.

The terminology (e,3e) arises from the composition of the initial and final states: one incoming projectile electron in the entrance channel, and three electrons detected in the exit channel (the scattered electron, typically carrying higher kinetic energy, together with two slower ejected electrons). Experimentally [1], such measurements are particularly demanding due to the very small magnitude of the associated double ionization cross section and the necessity of recording a triple-coincidence signal from all three outgoing electrons. To alleviate these difficulties, an alternative experimental scheme, denoted as (e,3-1e), is often employed, in which coincidence detection is limited to only two of the three final-state electrons.

The conservation laws of energy and momentum indicated in the first chapter ($E_i = \mathrm{E_f}$) and ($\mathrm{k}_i = \mathrm{k_f}$) can be written as follows:

$$E_0 + E_c = E_1 + E_2 + E_{c^{++}} + E_s + E_r \qquad \text{(II. 2)}$$

$$\vec{k}_i = \vec{k}_1 + \vec{k}_2 + \vec{k}_s + \vec{q} \qquad \text{(II. 3)}$$

Here, E_c and E_{c++} represent the energies of the ground state of the target C and any state of the doubly ionized residual ion C^{++}, respectively. $\vec{\boldsymbol{q}}$ denotes the recoil momentum transferred to the residual ion after the collision. Additionally, we define the momentum transfer $\vec{\boldsymbol{K}}$ as follows:

$$\vec{K} = \vec{k}_i - \vec{k}_s \qquad \text{(II. 4)}$$

$$\vec{q} = \vec{K} - (\vec{k}_1 + \vec{k}_2) \quad \text{(II. 5)}$$

If we denote the double ionization energy of the target as $I^{++} = E_{c^{++}} - E_c$, and knowing that the recoil energy of the ion is very small compared to the energies of the other particles due to the ion's large mass, equation (2) becomes:

$$E_0 = E_1 + E_2 + E_s + I^{++} \quad \text{(II. 6)}$$

It is important to note that if the value of the momentum transfer to the target k is small, we obtain information regarding the dynamics of the collision. Conversely, if k is large, we obtain information related to the structure of the target particle.

II.2.1 Geometries

The kinematical parameters of the ejected electrons, their energies ($\boldsymbol{E_1 and\ E_2}$) and momenta ($\overrightarrow{k_1} and\ \overrightarrow{k_2}$) determine the type of regime and geometry in which the ionization reaction can be studied. Broadly, experimental setups fall into two categories: coplanar and noncoplanar geometries. Each of these can be further classified as symmetric or asymmetric, depending on the relative energies and emission angles of the ejected electrons.

II.2.1-1Coplanar Geometries

In coplanar configurations, all vectors of interest (incident momentum $\overrightarrow{\boldsymbol{k_i}}$, scattered momentum $\overrightarrow{\boldsymbol{k_s}}$ and ejected momenta $\overrightarrow{\boldsymbol{k_1}}, \overrightarrow{\boldsymbol{k_2}}$) lie in the same collision plane. This setup simplifies the analysis of angular distributions and electron-electron correlations.

- **Symmetric Coplanar Geometry**

Both ejected electrons share similar energies ($E_1 \approx E_2$) and are detected at equal but opposite angles relative to the incident beam. This symmetry enhances the visibility of correlation effects and is frequently employed in benchmark experiments [1-3]

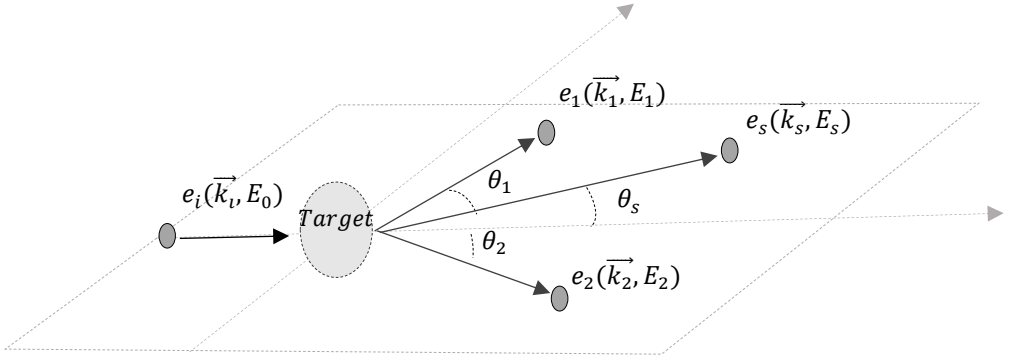

Figure2-1: Coplanar symmetric geometry

- **Asymmetric Coplanar Geometry**

In this case, one ejected electron carries significantly more energy than the other ($E_1 \neq E_2$). The scattered electron is typically fast and detected at a small angle ($\theta s < 1.5°$), while the slower electrons are measured at larger variable angles.
Two common experimental modes are used, fixed-angle mode where one electron angle is

fixed while the other is varied, allowing analysis of angular correlations [4]. And constant relative-angle mode with the relative angle $|\theta_1 - \theta_2|$ between the two electrons is held fixed while varying their emission angles. This approach has been applied in helium[5-7]

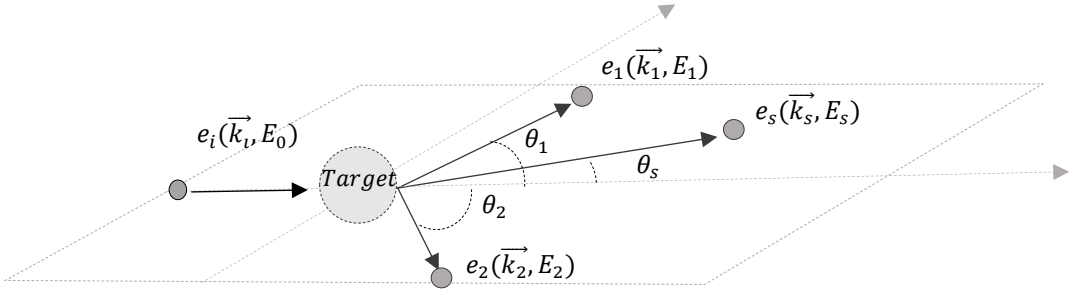

Figure2-1: Coplanar asymmetric geometry, $\boldsymbol{E_1 \neq E_2},\ \boldsymbol{\theta_1 \neq \theta_2}$

II.2.1.2 Non Coplanar Geometries

In non-coplanar setups, the ejected electrons are not restricted to the same collision plane as the incident and scattered projectiles. This configuration introduces an azimuthal degree of freedom, making the analysis more complex but also richer in information.

- **Symmetric Non-Coplanar Geometry**

The two electrons share equal energies and are detected outside the collision plane, often at symmetrical azimuthal positions. This geometry is particularly sensitive to electron–electron correlation effects and has been applied to helium ionization by N. Watanabe et al. [8].

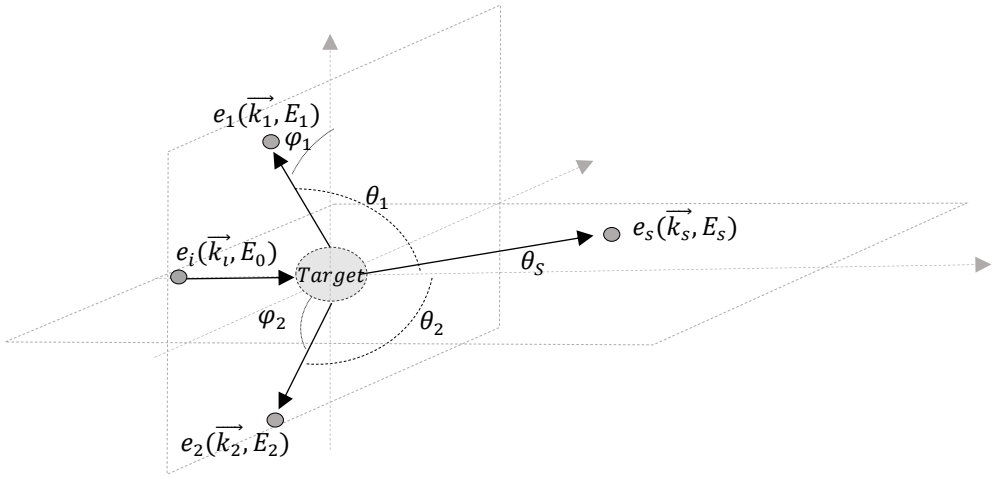

Figure2-3: Non-coplanar symmetric geometry, $E_1 = E_2$, $\theta_1 = 2\pi - \theta_2$

- **Asymmetric Non Coplanar Geometry**

Here, the ejected electrons have unequal energies and emission directions outside the collision plane. This geometry provides insight into multi body dynamics and recoil effects, though it is experimentally more challenging due to reduced coincidence detection rates.

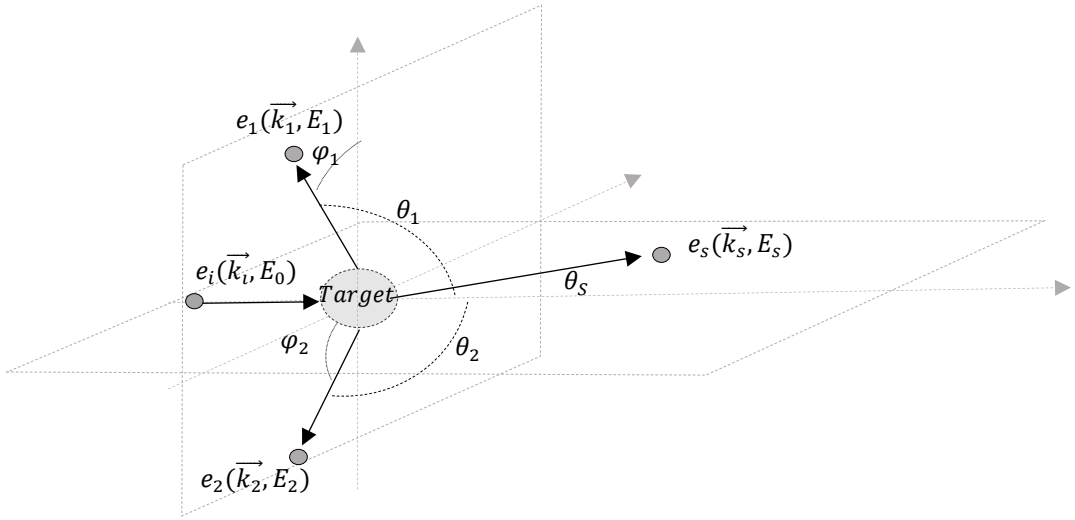

Figure 2-4: Non-coplanar asymmetric geometry, $E_1 \neq E_2$, $\theta_1 \neq \theta_2$

II.2.2 Experimental Relevance

➢ Each geometry provides access to different aspects of the ionization dynamics:

- **Coplanar symmetric:** highlights strong electron correlation and is a benchmark for testing theoretical models.
- **Coplanar asymmetric:** useful for studying kinematic dependencies and energy-sharing dynamics.
- **Non-coplanar symmetric:** emphasizes azimuthal correlations and three-body interactions.
- **Non-coplanar asymmetric:** probes recoil and momentum-transfer effects in complex scattering scenarios.

➢ **Symmetry and Asymmetry**

The symmetry or asymmetry of these geometries significantly impacts experimental results. In symmetric configurations, where all angles are equal or follow a specific pattern, one often observes more uniform distributions of ejected electrons. This uniformity can simplify theoretical modeling since symmetric systems tend to yield predictable patterns. Conversely, asymmetric configurations may lead to more complex distributions that reflect variations in electron dynamics. Asymmetry can arise from differences in energy sharing between ejected electrons or from external influences such as electric or magnetic fields during the experiment.

II.3 Double ionization mechanisms:

The (e,3e) reactions can be obtained through direct or indirect mechanism, the first work that successfully described the process was Tweed in 1992 [9] followed by Popov in 1994[10]. They were able to effectively study each mechanism and determine its impact only using plan wave functions to describe the electrons. For the moment, we have identified three principal mechanisms, The Shake-off (SO), Two step 1 (TS1) and Two step 2 (TS2)

II.3.1 The Shake-off process

The *Shake-Off* (SO) mechanism is one of the basic ways in which double ionization (DI) can happen in atoms. It was one of the first processes proposed to explain how a single fast projectile (such as an electron) can cause the emission of two electrons from a target atom [9]. The mechanism is described within first order perturbation theory, meaning the projectile interacts only once with the target. The process takes place in two steps, first ejection, where the incident electron collides with one of the target electrons (a binary collision), which is then knocked out of the atom. This step is very similar to ordinary single ionization. In the second ejection after the first electron is removed, the target potential changes suddenly because the nucleus is now less screened. The second electron instantly feels a stronger attraction from the nucleus. This change happens so quickly that the second electron cannot adapt its wavefunction smoothly, and instead it is forced out into the continuum.

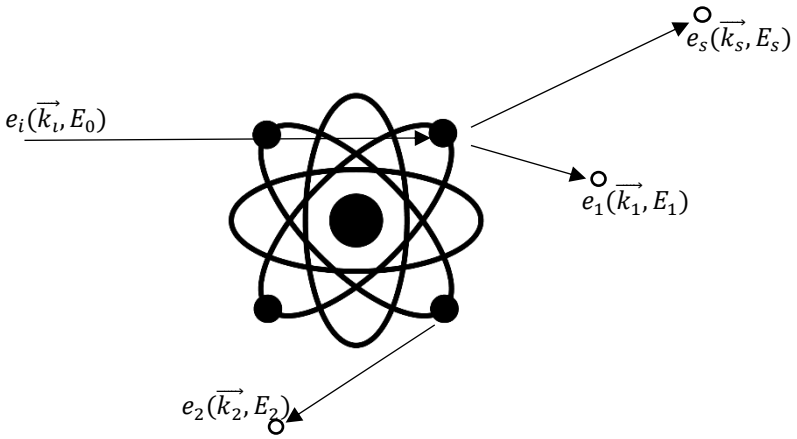

Figure 2-2: Shake off mechanism illustrated

Mathematically, the process is described in the first Born approximation, where the projectile target interaction is treated as a weak perturbation. The transition amplitude can be written as an overlap between the initial and final states of the system, with the interaction potential (V) acting between the projectile and the two active electrons. For helium, this amplitude has the form:

$$T_{SO} = -\frac{1}{2\pi}\left\langle \psi_f^-(\vec{k}_1, \vec{k}_2, \vec{r}_1, \vec{r}_2) e^{i\vec{k}_s.\vec{r}_0} \left| -\frac{2}{r_0} + \frac{1}{|\vec{r}_{01}|} + \frac{1}{|\vec{r}_{02}|} \right| \psi_i(\vec{r}_1, \vec{r}_2) e^{i\vec{k}_i.\vec{r}_0} \right\rangle \quad \text{(II. 7)}$$

The plane waves ($e^{i\vec{k}_i.\vec{r}_0}$ and $e^{i\vec{k}_s.\vec{r}_0}$) respectively represent the projectile and scattered electrons, as they move very rapidly [10]. V is the interaction potential between the projectile electron and two electrons of the target (two electrons due to the frozen core approximation where only active electrons are considered).

Two typical situations can occur, the binary collision SO, the projectile directly removes one electron, and the second electron is ejected because of the sudden change in potential and the excitation induced SO, the projectile excites the target, and the rapid rearrangement of the potential causes both electrons to be emitted together. In both cases, the two electrons are released almost at the same time, since the change in the potential is extremely fast. The essential idea is that the second electron does not leave because of a direct collision, but because it is shaken off by the abrupt change in its environment.

This mechanism explains an important part of the double ionization cross section, especially at high projectile energies where the Born approximation works well. It shows how electron-electron correlation and sudden changes in potential play a key role in multi-electron ionization processes

II.3.2 Two step1 (TS1)

The *Two-Step One* (TS1) mechanism describes double ionization as a sequential process involving two distinct stages. First step, the incident projectile collides with one of the two active electrons in the target. As a result, this electron is ejected, leaving the target singly ionized. The residual ion may remain in its ground state or be left in an excited state. The projectile, after this first collision, is scattered away. The second step, the first ejected electron, carrying some intermediate momentum, interacts with the second active electron. This secondary interaction provides enough energy to liberate the second electron, producing a doubly ionized target.

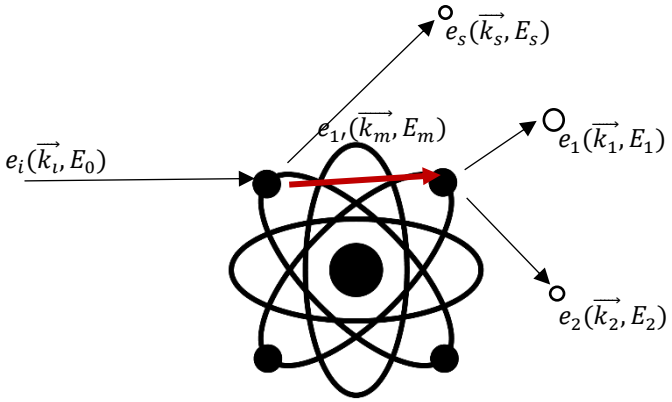

Figure2-3: Two step one-TS1 mechanism illustrated.

This process is represented mathematically by the second Born term, which accounts for two successive interactions: one between the projectile and the first active electron, and another between the two target electrons themselves [11].

$$\boldsymbol{T_{TS1}} = -\frac{1}{\pi}\sum_n \int \frac{d\vec{k}_m}{(2\pi)^3[k_i^2 - k_m^2 - k_s^2 - 2I_n]} \left\langle \psi_f^-(\vec{k}_1, \vec{k}_2, \vec{r}_1, \vec{r}_2) \right| \frac{1}{|\vec{r}_{12}|} \left| \psi_n^+(\vec{k}_m, \vec{r}_1, \vec{r}_2) \right\rangle$$
$$\left\langle \psi_n^-(\vec{k}_m, \vec{r}_1, \vec{r}_2) e^{i\vec{k}_s.\vec{r}_0} \right| -\frac{2}{r_0} + \frac{1}{|\vec{r}_{01}|} + \frac{1}{|\vec{r}_{02}|} \left| \psi_i(, \vec{r}_1, \vec{r}_2) e^{i\vec{k}_i.\vec{r}_0} \right\rangle \quad (\text{II}.8)$$

ψ_n^+ and ψ_n^-represent an intermediate state of the first ejected electron (incoming, outgoing) with wave vector $\vec{k}_m$. The summation over all possible intermediate states is noted by $\sum_n$.

$V_1 = -\frac{2}{r_0} + \frac{1}{|\vec{r}_{01}|} + \frac{1}{|\vec{r}_{02}|}$ is the interaction potential between the incident electron and the two ejected electrons, and $V_2 = \frac{1}{|\vec{r}_{12}|}$ represents the interaction potential between the two electrons of the second step.

A more detailed picture of the TS1 mechanism also includes the possibility of target recoil. In this case, the residual ion (the target nucleus plus remaining electrons) recoils during the collision. The first ejected electron then interacts with the second active electron either before or after experiencing the recoil of the target. This leads to variations of TS1 often referred to as *TS1 with recoil*. TS1 can still be interpreted as a first order interaction between the projectile and the target, because the projectile itself interacts with the target only once, while the second ejection is due to the subsequent electron-electron correlation. The mechanism is therefore well described within the plane-wave first Born approximation provided that electron-electron correlations in both the initial and final states are properly included [12].

In summary, TS1 emphasizes the role of electron-electron interactions in double ionization: the projectile initiates the process by removing one electron, and that electron then transfers part of its energy to eject the second one. This sequential picture is particularly useful for interpreting experiments where angular and energy correlations between the two ejected electrons are observed.

II.3.3 Two-Step 2 (TS2) mechanism

The Two-Step Two (TS2) mechanism is a second-order process in the Born expansion, meaning that the projectile interacts with the target twice. It represents a more complex pathway for double ionization than Shake Off or TS1. In the first interaction the incoming projectile collides with the target. This first step may result in a single ionization, leaving the target singly charge. And the second interaction, after the first collision, the same projectile undergoes a second collision with the already ionized target. In this step, the projectile transfers additional energy to a second bound electron, which is then ejected. The end result is a doubly ionized target.

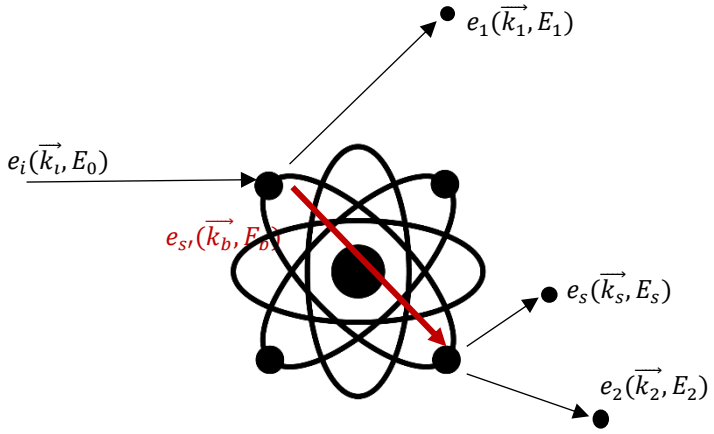

Figure2-7: Two step Two-TS2 mechanism illustrated.

Mathematically, the TS2 mechanism is described by the second Born approximation, in which the scattering amplitude explicitly contains two successive interactions between the projectile and the target electrons [13].

$$
\begin{aligned}
&\boldsymbol{T_{TS2}} \\
&= -\frac{1}{\pi}\sum_n \int \frac{d\vec{k}_b}{(2\pi)^3[k_i^2 - k_b^2 - k_1^2 - 2I_n]} \left\langle \psi_f^-(\vec{k}_2, \vec{r}_2) e^{i\vec{k}_s.\vec{r}_0} \left| \frac{1}{|\vec{r}_{02}|} \right| e^{i\vec{k}_b.\vec{r}_0} \psi_n(\vec{r}_2) \right\rangle \\
&\qquad x \left\langle \psi_n^-(\vec{k}_1, \vec{r}_1, \vec{r}_2) e^{i\vec{k}_b.\vec{r}_0} \left| -\frac{2}{r_0} + \frac{1}{|\vec{r}_{01}|} + \frac{1}{|\vec{r}_{02}|} \right| \psi_i(\vec{r}_1, \vec{r}_2) e^{i\vec{k}_i.\vec{r}_0} \right\rangle \\
&-\frac{1}{\pi}\sum_n \int \frac{d\vec{k}_b}{(2\pi)^3[k_i^2 - k_b^2 - k_2^2 - 2I_n]} \left\langle \psi_f^-(\vec{k}_1, \vec{r}_1) e^{i\vec{k}_s.\vec{r}_0} \left| \frac{1}{|\vec{r}_{01}|} \right| e^{i\vec{k}_b.\vec{r}_0} \psi_n(\vec{r}_1) \right\rangle \\
&\qquad x \left\langle \psi_n^-(\vec{k}_2, \vec{r}_1, \vec{r}_2) e^{i\vec{k}_b.\vec{r}_0} \left| -\frac{2}{r_0} + \frac{1}{|\vec{r}_{01}|} + \frac{1}{|\vec{r}_{02}|} \right| \psi_i(\vec{r}_1, \vec{r}_2) e^{i\vec{k}_i.\vec{r}_0} \right\rangle
\end{aligned}
\qquad \text{(II. 9)}
$$

A variant of TS2 also exists. In this case, the first interaction is not ionization but rather an elastic or inelastic collision with the target, which modifies the energy and momentum distribution of the system. The second step is then a double ionization triggered by the redistribution of this transferred energy and momentum.
Theoretically, the plane wave Born approximation (PWBA), which includes only SO and TS1, fails to reproduce these features. More sophisticated approaches such as the distorted wave Born approximation (DWBA) improve agreement by taking into account the continuous interaction of the scattered projectile with the residual ion. However, DWBA alone is not sufficient at low momentum transfer, where TS2 contributions become significant [14-15].

In summary, the TS2 mechanism highlights the importance of multiple projectile target interactions in double ionization. While less dominant than TS1 at high energies and small momentum transfer, TS2 plays a crucial role in explaining experimental results, particularly in regimes where angular distributions show deviations from simple symmetry. It also emphasizes that interference between SO, TS1, and TS2 must be considered to obtain a complete description of double ionization dynamics [10-13].

II.4. Electrons Correlation in Double Ionization Processes

The concept of *correlation* in atomic systems was first introduced in 1930 by Wigner and Seitz [16], who recognized that electrons in a many-body system cannot be treated as completely independent. Later, in 1959, Löwdin [17] provided a modern and more rigorous definition of correlation in the context of atomic physics. In general terms, correlation implies that any perturbation applied to one part of a system influences all other parts, reflecting the intrinsically collective nature of many electron dynamics [18]. In the study of atomic and molecular double ionization (DI), electron correlation plays a central role in both the initial and the final states of the process.

II.4.1 Correlation in the Initial State

A proper theoretical description of the initial state of the atom must account for inter-electronic correlations in order to provide accurate predictions of DI observables. In the ground state, electron correlation influences the spatial and spin arrangements of electrons, shaping the electronic cloud and its response to external perturbations. Neglecting such correlations often leads to significant discrepancies between theoretical models and experimental data, particularly in angular distributions and energy sharing spectra.

II.4.2 Correlation in the Final State

Following ionization, the situation becomes even more intricate. The two ejected electrons interact not only with the residual ion but also with each other, leading to final-state correlations. These include phenomena such as post collision interactions (PCI), where the trajectory and energy of one electron are altered by the Coulomb field of the other, even after the initial ionization event has taken place. Such correlations are responsible for subtle structures in angular distributions, energy sharing asymmetries, and interference effects observed in fully differential cross sections (FDCS).

II.4.3 Computational Treatment of Correlation

Accurately incorporating correlation into FDCS calculations requires advanced theoretical frameworks. The accurate treatment of **electron correlation** is fundamental to the theoretical description of **double ionization (DI)** processes in atoms and molecules. Since DI inherently involves the simultaneous participation of two electrons, the development of advanced correlation methods is essential to describe the interplay between their motions. Among the most widely used approaches in this context are the Interaction of Configuration (IC) method, Coupled-Cluster (CC) theory, Many-Body Perturbation Theory (MBPT), and Density Functional Theory (DFT) together with its time-dependent extension (TDDFT). Each method offers a distinct balance between accuracy and computational feasibility, allowing researchers to capture both static and dynamic correlation effects relevant to ionization phenomena.

- **Interaction Configuration (IC) method**

This method is one of the earliest and most intuitive techniques for including electron correlation in atomic and molecular systems. In IC, the total electronic wavefunction is expressed as a linear combination of multiple Slater determinants, each representing a different electron configuration. This allows the inclusion of both short range (dynamic) and long range (static) correlations. The inclusion of excited configurations enables IC to account for configuration mixing and electron-electron coupling effects, which are crucial for describing double ionization mechanisms namely SO and TS1. Although IC becomes computationally demanding for large systems, it provides a benchmark for smaller atomic and molecular targets, such as helium and the other noble gases, where detailed fully differential cross section (FDCS) calculations have been successfully compared with experimental data [18-20].

- **Coupled Cluster (CC) Theory**

The Coupled-Cluster (CC) method provides a more powerful and systematically improvable approach to electron correlation. In the context of DI and electron-impact ionization, CC theory yields accurate reference states and correlation amplitudes for use in scattering calculations and for benchmarking other approximate methods [21-23].

- **Many-Body Perturbation Theory (MBPT)**

The MBPT provides a systematic and conceptually clear framework to incorporate correlation corrections beyond the mean field approximation. It treats the residual electron-electron interaction as a perturbation to an independent particle model, expanding the total

wavefunction and energy in powers of the interaction potential. For double ionization, MBPT based methods provide essential corrections to the calculated FDCS, improving agreement with experimental observations at intermediate projectile energies where first-order treatments are insufficient [24–26].

- **Density Functional Theory (DFT) and Time-Dependent DFT (TDDFT)**

DFT reformulates the quantum many body problem in terms of the electron density according to the Hohenberg Kohn theorems. In collision physics, TDDFT enables time resolved simulations of correlated electron emission in atoms and molecules exposed to fast projectiles or intense laser fields. Despite its limitations in describing strong correlation and continuum couplings, TDDFT remains one of the most computationally efficient approaches for modeling ultrafast and strong field double ionization dynamics [27-30].

II.4.4 Structural Correlation in Double Ionization

One of the most fundamental types of correlation in collision studies is **structural correlation**, encompassing both electron-electron interactions within the target prior to ionization and correlations between the two continuum electrons after ejection. The importance of these effects has been extensively demonstrated. Early works by Byron and Joachain [31], Smirnov et al. [32], and Dal Cappello and Le Rouzo [33] highlighted the critical role of correlation in shaping angular distributions in electron-impact double ionization of helium. Their studies showed that while initial state correlation contributes to the overall dynamics, final state electron-electron correlation often dominates the observed experimental signatures. Understanding correlation effects is not only fundamental for testing quantum mechanical many-body theories but also has implications for other fields such as radiation biology and plasma physics. In particular, the way energy is redistributed among correlated electrons plays a decisive role in energy deposition mechanisms at the microscopic scale.

II.4.4.1 Structural Correlation- Interaction Configuration (IC) method

Interaction of Configuration (IC) is a quantum mechanical method developed to improve the accuracy of wave functions in multi-electron systems by explicitly accounting for electron correlation. Unlike the Hartree Fock (HF) approximation, which assumes that electrons move independently in an average potential, IC introduces the instantaneous Coulomb repulsion between electrons, which is crucial for processes like double ionization. In HF theory, the system's wave function is expressed as a single Slater determinant. This provides a mean-field description, where electrons move independently. While useful for many systems, HF neglects dynamic correlations and thus fails to describe strongly correlated processes such as DI, where the ejection of one electron is strongly coupled to the other.

- **Principle of IC method**

The IC method improves on HF by representing the total wave function as a linear superposition of multiple Slater determinants:

$$\phi(\vec{r}_1, \vec{r}_2) = \sum_{ij} C_{ij}(\phi_i, \phi_j) \quad \text{(II. 10)}$$

Where C_{ij} are variational coefficients chosen to minimize the energy, and $\phi(\vec{r}_1, \vec{r}_2)$ are anti symmetrized products of one electron orbitals. Each determinant corresponds to a different configuration (a distinct distribution of electrons among orbitals).

Initial state correlation**,** it allows the description of the correlated motion of electrons even before ionization. This correlation impacts cross sections, angular distributions, and energy-sharing spectra. The final state correlation**,** after ionization, the ejected electrons remain dynamically correlated due to mutual Coulomb repulsion and their interaction with the residual ion. The IC method provides a framework for describing post-collision interactions (PCIs), leading to more accurate predictions of fully differential cross sections (FDCSs). It gives a more realistic description of correlated ground and excited states and captures both short-range (exchange and Coulomb) and long-range correlations. It also improves the agreement between theoretical predictions and experimental data, while also serving as a foundation for more advanced methods.

II.5 Theoretical Models for double ionization

After having described the bound states of the target, we now turn to the representation of the final state of the system**,** which consists of a fast scattered electron and two relatively slow ejected electrons moving in the Coulomb field of the residual ion. This three-body Coulomb problem, commonly referred to as the double continuum electronic problem, remains one of the most fundamental yet unsolved challenges in atomic collision theory. Its inherent complexity arises from the long-range nature of the Coulomb interaction and the strong electron-electron correlation effects that govern the dynamics of double ionization (DI). To overcome these difficulties, different theoretical models have been developed, most of them within the Born approximation framework. The choice of a suitable model depends on several factors: the simplicity of the wave functions, computational feasibility, and the ability to reproduce experimental observables. In what follows, we summarize the most frequently employed models, emphasizing their assumptions, limitations, and the mathematical form of the final-state wave function.

II.5.1 Models under the First Born Approximation

Models based on the First Born approximation are most effective at high incident energies and small momentum transfers, where perturbative treatments are valid. In the FBA, both the incident and scattered electrons are approximated as plane waves, neglecting distortion effects due to the target's potential. These models provide reasonable agreement with experimental data under such conditions, but they are limited to describing first order processes, such as single ionization (SO) and the two-step (TS1) mechanism of double ionization. They fail, however, to accurately describe strong correlation or higher-order processes (TS2). The final state wave function is symmetrized to satisfy the Pauli principle:

$$\Phi_f(\vec{k}_1, \vec{r}_1; \vec{k}_2, \vec{r}_2) = \frac{1}{(2\pi)^3}\left[\frac{1}{\sqrt{2}}\left(e^{i(\vec{k}_1\vec{r}_1+\vec{k}_2\vec{r}_2)} + e^{i(\vec{k}_2\vec{r}_1+\vec{k}_1\vec{r}_2)}\right)\right] \quad \text{(II. 11)}$$

II.5.1.1Coulomb Wave Model

Introduced by Byron and Joachain [34], where the Coulomb interaction in the outgoing channel specifically between the ejected electrons and the residual ion, is taken into account, while the interaction between the two ejected electrons is neglected. Consequently, these electrons are represented by two uncorrelated Coulomb waves. Their wave functions, accounting for possible electron exchange, were written as follows:

$$\Phi_f(\vec{k}_1,\vec{r}_1;\vec{k}_2,\vec{r}_2) = \frac{1}{\sqrt{2}}\left[\varphi_c(\vec{k}_1,\vec{r}_1)\varphi_c(\vec{k}_2,\vec{r}_2) \pm \varphi_c(\vec{k}_1,\vec{r}_2)\varphi_c(\vec{k}_2,\vec{r}_1)\right] \quad \text{(II. 12)}$$

$$\varphi_c(\vec{k},\vec{r}) = (2\pi)^{-\frac{3}{2}} e^{-\frac{\pi}{2}\eta}\Gamma(1+i\eta)e^{i\vec{k}.\vec{r}}\ {}_1F_1\left(-i\alpha, 1, i(\vec{k}.\vec{r}-kr)\right) \quad \text{(II. 13)}$$

$\eta = z/k$, Γ et ${}_1F_1$ respectively denote the Gamma function and the confluent hypergeometric function.

This approximation simplifies the problem by focusing on the primary Coulomb forces between the electrons and the ion, while disregarding electron-electron interactions, allowing for a more tractable solution. However, it fails to fully capture the complexity of the correlation between the two ejected electrons.

A possible improvement of the model involves defining effective charges that account for the dynamic screening of the nucleus by the two electrons. These effective charges depend on the momenta of the two electrons and must satisfy Peterkop's equation [35]:

$$\frac{z_1}{k_1} + \frac{z_2}{k_2} = \frac{z}{k_1} + \frac{z}{k_2} - \frac{1}{|\vec{k}_1 - \vec{k}_2|} \quad \text{(II. 14)}$$

This adjustment helps refine the model by considering how the electron cloud shields the nucleus, which impacts the accuracy of the final state wave function, especially in scenarios involving multi-electron interactions.

II.5.1.2 Distorted Wave Born Approximation (DWBA) Model

further refines the description by incorporating distortion effects in both the entrance and exit channels. Here the electrons are not simple plane waves or independent Coulomb functions, but rather distorted waves, solutions of the Schrödinger equation with a potential that includes the long-range Coulomb interaction and a short-range correction representing exchange and polarization effects. Thus, the scattered and ejected electrons are described by distorted wave functions, symmetrized to respect electron indistinguishability. The DWBA is particularly effective in accounting for exchange effects and for kinematics where distortion of the trajectories due to the residual ion cannot be neglected. However, the computational effort is considerably higher than in FBA or CWM, making it less tractable for complex targets or large energy ranges.

$$\Phi_f(\vec{k}_1,\vec{r}_1;\vec{k}_2,\vec{r}_2) = \frac{1}{\sqrt{2}}\left[\varphi_{DW}(\vec{k}_1,\vec{r}_1)\varphi_{DW}(\vec{k}_2,\vec{r}_2) \pm \varphi_{DW}(\vec{k}_1,\vec{r}_2)\varphi_{DW}(\vec{k}_2,\vec{r}_1)\right] \quad \text{(II. 15)}$$

$$\varphi_{dw}(\vec{k},\vec{r}) = \frac{4\pi}{(2\pi)^{\frac{3}{2}}}\sum_{l,m} i^l\, e^{i\Delta_l}\frac{\chi_l(k,r)}{kr}Y^*_{l,m}(\hat{k})Y_{l,m}(\hat{r}) \quad \text{(II. 16)}$$

Δ_l represents the total phase shift, and $\chi_l(k,r)$ is the radial wave function.

In the DWBA framework, the distorted wave functions provide a more realistic description of electron motion in both the entrance and exit channels. They account for corrections arising from long range Coulomb forces as well as short range interactions, which makes the model particularly effective for capturing the complex electron dynamics involved in double ionization. Applications of the DWBA model have shown good agreement with experimental data at intermediate incident energies (below 1 keV), notably in the works of Bickert et al. [36] and Lohmann et al. [37]. Over the years, several adaptations of this approach have been proposed. For example, Bartschat and Burke [38] developed the hybrid DWBA-R model, while Kheifets et al. [39] introduced the DWBA-G variant. These extensions share the feature of incorporating interactions between the ion and the outgoing electrons but still only partially consider the electrostatic repulsion between the two ejected electrons. A more comprehensive treatment of this electron-electron interaction is necessary to further improve the theoretical description of such collision processes.

II.5.1.3 Brauner, Briggs, and Klar Model (BBK or 3C)

In order to incorporate electron-electron correlation effects more rigorously in the exit channel, Brauner, Briggs, and Klar (BBK) proposed in 1989 a theoretical framework originally designed for the single ionization of the hydrogen atom [40]. Their approach relies on an exact asymptotic description of the final state, where the correct long-range Coulomb behavior of all interacting particles is explicitly included. The final-state wave function is thus expressed as the product of three Coulomb waves: two of them describe the interactions of each ejected electron with the residual ion, while the third represents the post-collision interaction (PCI) between the two electrons themselves. This explicit treatment of PCI marked an important step forward compared to earlier models, which generally neglected or only approximated electron-electron coupling in the continuum.

An alternative formulation of the BBK model was later introduced in which the third Coulomb function, associated with electron-electron PCI, is replaced by unity, while the so-called Gamow factor is added to reproduce the effect of mutual Coulomb repulsion between the outgoing electrons. This adjustment simplified the formalism while still retaining the essential features of correlation in the asymptotic regime.

$$\Phi_f(\vec{k}_1,\vec{r}_1;\vec{k}_2,\vec{r}_2) = \frac{1}{\sqrt{2}}\begin{bmatrix}\varphi_c(\vec{k}_1,\vec{r}_1)\varphi_c(\vec{k}_2,\vec{r}_2)\mathrm{C}(\alpha_{12},\vec{k}_{12},\vec{r}_{12}) \pm \\ \varphi_c(\vec{k}_1,\vec{r}_2)\varphi_c(\vec{k}_2,\vec{r}_1)\mathrm{C}(\alpha_{12},\vec{k}_{12},\vec{r}_{12})\end{bmatrix} \quad \text{(II. 17)}$$

where $\varphi_c(\vec{k},\vec{r})$ represent the coulomb wavefunction and $\mathrm{C}(\alpha_{12},\vec{k}_{12},\vec{r}_{12})$ describe PCI.

$$\mathrm{C}(\alpha_{12},\vec{k}_{12},\vec{r}_{12}) = e^{-\frac{\pi}{2k_{12}}}\Gamma\left(1-\frac{i}{2k_{12}}\right){}_1F_1\left(-i\alpha_{12},1,-i\left(k_{12}r_{12}+\vec{k}_{12}\vec{r}_{12}\right)\right) \quad \text{(II. 18)}$$

with: $\vec{k}_{12} = \frac{(\vec{k}_1 - \vec{k}_2)}{2}$ et $\alpha_{12} = \frac{1}{2k_{12}}$

When applied within the First Born Approximation, both versions of the BBK model demonstrated a clear qualitative improvement in reproducing experimental observations. In particular, they captured more accurately the angular and energy correlations between the ejected electrons, features that are highly sensitive to electron–electron interactions. Studies of Joulakian et al. [20, 41], as well as Hda et al. [42], confirmed the enhanced predictive power of the BBK framework.

The success of the BBK model lies in its ability to reconcile mathematical tractability with a physically realistic representation of three-body Coulomb dynamics. By embedding the correct asymptotic behavior in the final state wave function, it provides a more reliable foundation for exploring double ionization and related many-body processes, where electron correlation plays a decisive role, but it has a significant drawback: the computational time required.

Several authors have employed simplified treatments of the post-collision interaction (PCI) to reduce the computational burden, making the approach more practical while still capturing the essential features of electron correlation in the exit channel. These simplifications help strike a balance between accuracy and efficiency, especially in complex systems where full calculations would be prohibitively time-consuming.

II.5.1.4 Approximate BBK Model-2CWGamow factor:

Dal Cappello and co-workers [32] $C(\alpha_{12}, \vec{k}_{12}, \vec{r}_{12})$ proposed a simplified version of the BBK model, often referred to as the two-Coulomb-wave Gamow (2CWG) model. The key idea is to normalize the function by arbitrarily setting the confluent hypergeometric term ${}_1F_1\left(-i\alpha_{12}, 1, -i\left(k_{12}r_{12} + \vec{k}_{12}.\vec{r}_{12}\right)\right)$ to unity. This reduces the mathematical complexity of the final-state wave function while retaining the essential Coulomb correlation between the two outgoing electrons. In this formulation, only the factor $\left(e^{-\frac{\pi}{2k_{12}}}\Gamma\left(1 - \frac{i}{2k_{12}}\right)\right)$ is preserved, as it adequately encodes the strong electron–electron correlation in the continuum. This factor is traditionally known as the Gamow factor, $F_G(k_{12})$ and is expressed as:

$$\boldsymbol{F_G(k_{12})} = \left|e^{-\frac{\pi}{2k_{12}}}\Gamma\left(1 - \frac{i}{2k_{12}}\right)\right|^2 = \frac{\pi}{k_{12}\left(e^{\frac{\pi}{k_{12}}} - 1\right)} \qquad \text{(II. 19)}$$

The Gamow factor originates from nuclear and atomic physics, where it was first introduced to describe tunneling probabilities and Coulomb barriers in low-energy charged-particle reactions. In the context of double ionization, it plays a crucial role in representing the mutual Coulomb repulsion between the two continuum electrons. One of its most remarkable features is its ability to suppress configurations where the ejected electrons leave the collision in nearly the same direction. This reflects the physical impossibility of two like-charged electrons propagating parallel at small separations without being strongly repelled.

The use of the Gamow factor in the 2CWG model offers several advantages. First, it considerably simplifies numerical calculations compared to the full BBK treatment, reducing computation time while retaining the essential physics of electron-electron interaction. Second, by enforcing the correct asymptotic behavior of the two-electron wave function, it provides a physically meaningful correction to the otherwise uncorrelated Coulomb approximation. However, this simplification is not without limitations. The 2CWG approach tends to underestimate the absolute value of the transition amplitude, leading to discrepancies in cross-section magnitudes, even though the qualitative features of angular correlations are well reproduced. Despite this, the model has been shown to provide reasonably good agreement with experimental data, particularly in studies of (e,3-1e) and (e,3e) processes in rare gases performed by the Orsay group [43-46].

II.5.1.5 Limitations of the First Born Approximation

The First Born Approximation (FBA), which treats the interaction between the projectile and the target in the framework of first-order perturbation theory, provides a simplified approach to analyzing scattering processes. In FBA, the projectile is assumed to interact weakly with the target, and higher-order interactions are neglected. While this approximation is often valid for high-energy collisions, experimental data frequently reveal limitations even in this regime, especially in cases involving complex interactions or lower momentum transfer. For example, in high-energy collisions, FBA assumes that the scattering event occurs over a very short time, minimizing the influence of higher-order effects such as multiple scattering or exchange interactions. However, this approach can fail to accurately describe the physical reality when electron correlation effects, nuclear recoil, or strong Coulomb interactions between the projectile and the target are significant.

In the low-energy regime, where the interaction time between the projectile and the target increases, these higher-order effects become more prominent. Experimental observations have shown discrepancies between FBA predictions and measured cross-sections, especially in cases of double ionization or complex multi-electron targets. Therefore, a more sophisticated theoretical treatment is required to capture these additional effects.

II.5.2 The second Born approximation treatment

The Second Born Approximation (SBA) addresses the limitations of the first Born approximation by incorporating higher-order terms in the perturbation expansion. This approximation considers the successive interactions of the incoming electron with the two target electrons, accounting for more complex interactions between the projectile and target. By including these higher-order terms, SBA captures the dynamic exchange of momentum and energy between the particles. It takes into account multiple scattering events and correlations between particles, providing a more accurate description of the collision process. This is particularly important in the low energy regime, where interactions cannot be simplified as single events. These interactions are responsible for secondary effects in the cross sections, notably symmetry breaking around the direction of momentum transfer, which is manifested by the presence of the TS2 mechanism. The SBA allows for the inclusion of

post-collision interactions (PCI), which are crucial when studying processes like double ionization. The interaction between ejected electrons can significantly alter the outcome of collisions.

The fivefold differential cross section "FDCS" based on the second Born approximation "SBA" is given by:

$$\frac{d^5\sigma}{d\Omega_s d\Omega_1 d\Omega_2 dE_1 dE_2} = \frac{1}{k_i} k_s k_1 k_2 |f_{b1} + f_{b2}|^2 \quad \text{(II. 20)}$$

Experiments show a certain inadequacy of the treatment involving the FBA, both at low and high incident energies, hence the need for the second Born approximation, for extension of the projectile-target interaction to higher orders. It accounts for the contribution of two-step mechanisms in the angular distribution of the fivefold differential cross section (FDCS).
The second Born term in the FDCS expression, is expressed in the following form [47-48]:

$$f_{B2} = \frac{1}{8\pi^4} \sum_n \int \frac{d\vec{q}}{q^2 + k_n^2 - i\varepsilon} \left\langle e^{i\vec{k_s}\vec{r_0}} \Psi_f(k_1, r_1, k_2, r_2) \middle| V \middle| e^{i\vec{q}\vec{r_0}} \Phi_n(r_1, r_2) \right\rangle \times \left\langle e^{i\vec{q}\vec{r_0}} \Phi_n(r_1, r_2) \middle| V \middle| e^{i\vec{k_i}\vec{r_0}} \Phi_i(r_1, r_2) \right\rangle \quad \text{(II. 21)}$$

With $\varepsilon \to 0^+$ and k_n is given by:

$$\frac{k_n^2}{2} = \frac{k_i^2}{2} - (E_n - E_i) \quad \text{(II. 22)}$$

This second Born term will be explicitly developed in chapter 3.

II.5.2.1 Computational Considerations

The use of SBA in studying reactions such as (e, 3e) requires significant attention and a long computation time. Consequently, studies conducted so far on atomic and molecular targets have utilized the 2CWG model to help reduce computation time. It is also noteworthy that calculations involving the BBK model up to the second term of Born, developed by Ancarani [49] showed slight differences from those conducted under the first Born approximation.

II.5.3 The 6C Approach

The 6C approach represents an advanced method that goes beyond the first Born approximation (FBA) by considering all possible mutual interactions among the various particles in the final state of a scattering event the scattered electron (the two ejected electrons, and the residual ion) [50]. The method utilizes a sophisticated final wave function as a product of six Coulomb waves, which accounts for the different Coulomb interactions involved. Implementing the 6C wave function requires considerable computational resources due to the necessity of numerically evaluating a nine-dimensional integral in the continuum. This complexity arises from the need to accurately depict all interactions between particles, making it a computationally intensive task. Despite these challenges, comparisons between the 6C model results and experimental data demonstrate excellent agreement, validating its effectiveness in accurately modeling scattering processes.

II.5.3.1 Simplification to A6C

To mitigate the extensive computation time associated with the full 6C approach, Elazzouzi et al [51] proposed an alternative termed A6C (approximated 6C). This method simplifies calculations by replacing the three wave functions that describe electron-electron repulsion with three Gamow factors. The A6C approach is implemented in two scenarios: one with variable charges and another within the framework of the second Born approximation. Both versions yield good agreement with experimental data, particularly for specific experimental conditions involving incident electron energies of 601 eV, although some discrepancies remain for other scenarios.

II.6. Chapter overview: Theory of Double Ionization (DI)

This chapter, is dedicated to the theory of double ionization (DI), where we begin by describing the reactions (e, 3e) and (e-3-1e), followed by an exploration of the associated geometries and kinematics. The various mechanisms involved in the DI process due to electron impact, specifically Shake off (SO), Two step1 (TS1), and Two step2 (TS2), are outlined. The second part of this chapter is devoted to examining bound states and the continuum in two-electron atomic systems. This section emphasizes the concept and significance of electron correlation**,** which plays a crucial role in understanding the interactions within these systems. Finally, we explore various theoretical models that have been used to study and represent the double ionization reaction.

References:

[1] A. Lahmam-Bennani, I. Taouil, A. Duguet, M. Lecas, L. Avaldi, and J. Berakdar, "Evidence for electron correlation effects in (e,2e) ionization of helium," *Phys. Rev. A* 59, 3548 (1999).
[2] C. D. Schröter, R. El Marji, A. Lahmam-Bennani, A. Duguet, M. Lecas, and L. Spielberger, "Fully differential cross sections for electron-impact ionization of helium," *J. Phys. B: At. Mol. Opt. Phys.* 31, 131 (1998).
[3] A. S. Kheifets, I. Bray, A. Lahmam-Bennani, A. Duguet, and I. Taouil, "Theory of electron correlation effects in (e,2e) ionization," *J. Phys. B: At. Mol. Opt. Phys.* 32, 5047 (1999).
[4] B. El Marji, C. Schröter, A. Duguet, A. Lahmam-Bennani, and M. Lecas, "Angular distributions in electron-impact ionization of helium," *J. Phys. B: At. Mol. Opt. Phys.* 30, 3677 (1997).
[5] A. Dorn, R. Moshammer, C. D. Schröter, T. J. M. Zouros, W. Schmitt, H. Kollmus, and R. Mann, "Strong correlation effects in electron-impact ionization," *Phys. Rev. Lett.* 82, 2496 (1999).
[6] R. Choubisa, G. Porohit, and K. K. Sud, "Electron correlation in ionization of atomic targets," *J. Phys. B: At. Mol. Opt. Phys.* 36, 1731 (2003).
[7] N. Watanabe, Y. Khajuria, M. Takahashi, Y. Udagawa, P. S. Vinitsky, Yu. V. Popov, O. Chuluunbaatar, and K. A. Kouzakov, "Electron-impact ionization of helium: Correlation effects," *Phys. Rev. A* 72, 032705 (2005).
[8] R. Tweed, "Electron correlation in ionization processes," *Z. Phys. D* 23, 109 (1992).
[9] Yu. V. Popov, C. Dal Cappello, B. Joulakian, and N. M. Kuzmina, "Post-collision interaction effects in electron-impact ionization," *J. Phys. B: At. Mol. Opt. Phys.* 27, 995 (1994).
[10] H. Nebdi, G. K. Lagmago, and B. Piraux, "Electron correlation effects in atomic ionization," *J. Physique IV* 9, 105 (1999).
[11] M. Grin, C. Dal Cappello, R. El Mkhanter, and J. Rasch, "Theoretical study of electron-impact double ionization," *J. Phys. B: At. Mol. Opt. Phys.* 33, 131 (2000).
[12] C. Dal Cappello, R. El Mkhanter, and P. A. Hervieux, "Correlation effects in (e,2e) ionization," *Phys. Rev. A* 57, R693 (1998).
[13] R. El Mkhanter and C. Dal Cappello, "Theoretical description of correlated ionization," *J. Phys. B: At. Mol. Opt. Phys.* 31, 301 (1998).
[14] J. W. Cooper and R. W. Van Boeyen, "Correlation effects in electron-impact ionization," *J. Phys. B: At. Mol. Opt. Phys.* 37, L77 (2004).
[15] J. H. McGuire, *Introduction to Dynamic Correlation in Atomic Collisions* (Cambridge University Press, Cambridge, 1997).
[16] P.-O. Löwdin, "Correlation problem in many-electron quantum mechanics I: Review of different approaches and discussion of some current ideas," *Adv. Chem. Phys.* 2, 207 (1959).
[17] F. Catoire, *Étude des corrélations électroniques dans les collisions ionisantes*, Ph.D. thesis, Université Paris-Sud XI (2006).
[18] A. Szabo and N. S. Ostlund, *Modern Quantum Chemistry: Introduction to Advanced Electronic Structure Theory* (Dover, New York, 1996).
[19] I. Shavitt and R. J. Bartlett, *Many-Body Methods in Chemistry and Physics: MBPT and Coupled-Cluster Theory* (Cambridge University Press, Cambridge, 2009).
[20] B. Joulakian and C. Dal Cappello, "Electron correlation in ionization processes," *J. Phys. B: At. Mol. Opt. Phys.* 26, 2257 (1993).
[21] R. J. Bartlett and M. Musiał, "Coupled-cluster theory in quantum chemistry," *Rev. Mod. Phys.* 79, 291 (2007).
[22] T. D. Crawford and H. F. Schaefer, "An introduction to coupled cluster theory," *Rev. Comput. Chem.* 14, 33 (2000).
[23] M. Kállay and P. R. Surján, "Higher excitations in coupled-cluster theory," *J. Chem. Phys.* 115, 2945 (2001).
[24] I. Lindgren and J. Morrison, *Atomic Many-Body Theory* (Springer-Verlag, Berlin, 1986).
[25] B. H. Bransden and C. J. Joachain, *Physics of Atoms and Molecules*, 2nd ed. (Prentice Hall, 2003).
[26] I. Shavitt and R. J. Bartlett, *Many-Body Methods in Chemistry and Physics: MBPT and Coupled-Cluster Theory* (Cambridge University Press, Cambridge, 2009).
[27] R. G. Parr and W. Yang, *Density-Functional Theory of Atoms and Molecules* (Oxford University Press, Oxford, 1994).

[28] E. Runge and E. K. U. Gross, "Density-functional theory for time-dependent systems," *Phys. Rev. Lett.* 52, 997 (1984).
[29] M. A. L. Marques, N. T. Maitra, F. M. S. Nogueira, E. K. U. Gross, and A. Rubio, *Fundamentals of Time-Dependent Density Functional Theory* (Springer, Berlin, 2012).
[30] M. Petersilka, U. J. Gossmann, and E. K. U. Gross, "Excitation energies from time-dependent density-functional theory," *Phys. Rev. Lett.* 76, 1212 (1996).
[31] F. W. Byron Jr. and C. J. Joachain, "Electron correlation in ionization theory," *Phys. Rev.* 164, 1 (1967).
[32] Yu. F. Smirnov, A. V. Pavlitchenkov, V. G. Levin, and V. G. Neudatchin, "Correlation effects in atomic collisions," *J. Phys. B: At. Mol. Opt. Phys.* 11, 20 (1978).
[33] V. G. Neudatchin, Yu. F. Smirnov, and A. V. Pavlitchenkov, "Few-body correlation effects," *Phys. Lett. A* 64, 31 (1977).
[34] F. W. Byron Jr. and C. J. Joachain, "Electron correlation in ionization processes," *Phys. Rev. Lett.* 16, 1139 (1966).
[35] R. K. Peterkop, "Energy correlations in ionization," *Opt. Spectrosc.* 13, 87 (1962).
[36] P. Bickert, W. Hink, C. Dal Cappello, and A. Lahmam-Bennani, "Experimental study of correlated ionization," *J. Phys. B: At. Mol. Opt. Phys.* 24, 4603 (1991).
[37] B. Lohmann, S. Cavanagh, M. A. Haynes, I. Taouil, and A. Lahmam-Bennani, "Correlation effects in electron-impact ionization," *Aust. J. Phys.* 51, 679 (1998).
[38] K. Bartschat and P. G. Burke, "Close-coupling calculations for electron-impact ionization," *J. Phys. B: At. Mol. Opt. Phys.* 20, 3191 (1987).
[39] A. S. Kheifets, A. Naja, E. M. Staicu-Casagrande, and A. Lahmam-Bennani, "Fully differential cross sections for helium ionization," *J. Phys. B: At. Mol. Opt. Phys.* 41, 145201 (2008).
[40] M. Brauner, J. S. Briggs, and H. Klar, "Triple differential cross sections for electron-impact ionization," *J. Phys. B: At. Mol. Opt. Phys.* 22, 2265 (1989).
[41] B. Joulakian, C. Dal Cappello, and M. Brauner, "Correlation effects in ionization processes," *J. Phys. B: At. Mol. Opt. Phys.* 25, 2863 (1992).
[42] H. Hda, C. Dal Cappello, and J. Langlois, "Theoretical study of correlated ionization," *Z. Phys. D* 29, 25 (1994).
[43] C. Dal Cappello, B. Joulakian, and J. Langlois, "Electron correlation in ionizing collisions," *J. Phys.* 3, 125 (1993).
[44] A. Lahmam-Bennani, C. Dupré, and A. Duguet, "Observation of strong electron correlation effects," *Phys. Rev. Lett.* 63, 1582 (1989).
[45] A. Lahmam-Bennani, H. Ehrhardt, C. Dupré, and A. Duguet, "Experimental evidence of correlated ionization," *J. Phys. B: At. Mol. Opt. Phys.* 24, 3645 (1991).
[46] A. Lahmam-Bennani, A. Duguet, A. M. Grisogono, and M. Lecas, "Electron correlation in (e,2e) ionization," *J. Phys. B: At. Mol. Opt. Phys.* 25, 2873 (1992).
[47] C. J. Joachain, *Quantum Collision Theory* (Université Libre de Bruxelles, 1983).
[48] M. Grin, C. Dal Cappello, R. El Mkhanter, and J. Rasch, "Theoretical study of electron-impact ionization," *J. Phys. B: At. Mol. Opt. Phys.* 33, 131 (2000).
[49] L. U. Ancarani, T. Montagnese, and C. Dal Cappello, "Correlation effects in electron and photon impact ionization," Proc. Int. Conf. on Electron and Photon Impact Ionization (IOP Publishing, 2005).
[50] S. Jones and D. H. Madison, "Fully differential cross sections for electron-impact ionization," *Phys. Rev. Lett.* 91, 073201 (2003).
[51] S. El Azzouzi, C. Dal Cappello, A. Lahmam-Bennani, and F. Catoire, "Correlation effects in electron-impact ionization of helium," *J. Phys. B: At. Mol. Opt. Phys.* 38, 1391 (2005).

CHAPTER THREE

Application to Noble Gases and Molecules

III.1 Introduction:

In this chapter; consolidating the theoretical developments presented in earlier chapters and identifying pathways for future adjustments; we aim to test the predictive capabilities of the proposed models against experimental FDCS by evaluating the extent to which the consideration of correlation and second order effects improves agreement with experimental data. By doing so, the study provides a more comprehensive understanding of the competing mechanisms that drive DI and will highlight a comparison of the correlation contributions for atomic noble gases and that of second Born term in the case of a molecular system (CH_4).

Through this dual application to noble gases and methane, the present chapter links the gap between reference atomic systems and realistic many electron molecular environments, reinforcing the central role of DI studies in advancing both the experimental and theoretical understanding of correlated electron dynamics.

III.2 Description of the double ionization of noble gases

The (e,3e) process represents one of the most complete experimental methods for studying double ionization (DI) of atoms and molecules by electron impact. In this reaction, a fast incident electron of kinetic energy E_0 and momentum $\vec{k}_i$ collides with a target atom or molecule, leading to the ejection of two electrons into the continuum. The incident electron is scattered with energy E_s and momentum $\vec{k}_s$ while the two ejected electrons are detected in coincidence, characterized by their energies $E_1$and E_2 momenta $\vec{k}_1$, $\vec{k}_2$ and emission directions (θ_1, φ_1) , (θ_2, φ_2) . The process can be summarized as:

$$e_i(\vec{k}_i, E_0) + C \rightarrow \ C^{++} + e_s(\vec{k}_s, E_s) + e_1(\vec{k}_1, E_1) + e_2(\vec{k}_2, E_2) \quad \text{(III.1)}$$

Given that the mass of the incident electron is negligible compared to that of the target, the transfer of kinetic energy from the incident electron to the target is considered negligible. This allows for the establishment of conservation equations for energy and momentum:

$$\frac{k_i^2}{2} = \frac{k_s^2}{2} + \frac{k_1^2}{2} + \frac{k_2^2}{2} + I^{++} \quad \text{et} \quad \vec{k}_i = \vec{k}_s + \vec{k}_1 + \vec{k}_2 + \vec{q} \quad \text{(III.2)}$$

Where I^{++} represent the energy needed to ejected the two electrons and $\vec{q}$ the recoil momenta of the ionized target.

III.2.1 FDCS in First Born Approximation (FBA)

The FDCS provides the most detailed information available about the underlying dynamics of double ionization, it retains the complete angular and energy dependence of the process. This richness makes FDCS an indispensable tool for probing both initial state correlation (the entanglement of bound electrons before to ionization) and final state correlation (the Coulomb interaction between the ejected electrons and the residual ion). Experimentally, FDCS measurements were pioneered by Lahmam-Bennani and collaborators in the 1990s, who used electron-electron coincidence spectroscopy to perform the first (e,3e) experiments on rare gases

[1]. Their work demonstrated how FDCS maps reveal distinct ionization depending on energy sharing conditions and detection geometry. Other high-resolution FDCS experiments by Schröter et al. [2] and Avaldi et al.[3-4] extended these studies to heavier noble gases, emphasizing the persistent role of correlation even in large closed shell systems.
In the FBA, the scattering amplitude is expressed as a single interaction between the incoming projectile and the target electrons. The incident electron is typically described by a plane wave, while the two ejected electrons are represented by Coulomb functions or distorted wave functions to represent their motion in the field of the residual ion. As such, final state electron-electron correlations are only partially accounted for, and long-range interactions are often neglected or treated approximately. Despite these limitations, the FBA captures essential first-order processes such as shake off and two step oneTS1 mechanisms. Both of these processes are accessible within the FBA formalism and contribute significantly to the FDCS.

We consider the following situation where the incident and scattered electrons are fast, allowing us to study the process within the first Born approximation (FBA). The differential fivefold cross section associated with this reaction is given by:

$$\frac{d^5\sigma}{d\Omega_d d\Omega_1 d\Omega_2 dE_1 dE_2} = \frac{1}{k_i} k_s k_1 k_2 |f_{B1}|^2 \quad \text{(III.3)}$$

Here, the matrix element f_{B1} represents the transition from the initial state $\boldsymbol{\Psi_i}$ to the final state $\boldsymbol{\Psi_f}$ under the influence of a potential $\boldsymbol{V}$. This first term is expressed as:

$$f_{B1} = -\frac{1}{2\pi}\langle \Psi_f | V | \Psi_i \rangle \quad \text{(III. 4)}$$

The FDCS calculated under the FBA framework varies sensitively with the scattering angles of the outgoing electrons and with their kinetic energies.

III.2.2 Interaction Potential

The interaction potential between the projectile and the atomic target depends solely on the electric charges and the distances between them. Its form is defined as follows:

$$V = -\frac{z}{r_0} + \sum_i \frac{1}{r_{0i}} \quad \text{(III. 5)}$$

where z is the charge of the nucleus, and $r_{0i} = |\vec{r}_0 - \vec{r}_i|$.
This potential will be simplified by use of the well-known frozen-core approximation which allows as to reduce the N-body problem (10-electrons of the target) to a helium like system with only two electrons [5] which interact with the projectile and will be ejected in the ion continuum. In these conditions, it is reasonable to assume that the remaining electrons of the doubly charged ion core are unaffected by the ionization process itself [6].
This potential is then written as:

$$V(\vec{r}_0, \vec{r}_1, \vec{r}_2) = -\frac{2}{r_0} + \frac{1}{r_{01}} + \frac{1}{r_{02}} \quad \text{(III. 6)}$$

The integration over the projectile coordinates r_0 can be performed analytically using Bethe's relation [7]:

$$\int \frac{e^{i\vec{K}\vec{r}_0}}{|\vec{r}_i - \vec{r}_0|} d\vec{r_0} = \frac{4\pi}{K^2} e^{i\vec{K}\vec{r}_i} \qquad \text{(III. 7)}$$

Thus, the first Born term for the scattering amplitude takes the form:

$$f_{B1} = -\frac{2}{K^2}\left\langle \Phi_f(\vec{k}_1, \vec{r}_1; \vec{k}_2, \vec{r}_2)\middle| -2 + e^{i\vec{K}\vec{r}_1} + e^{i\vec{K}\vec{r}_2}\middle|\varphi_i(\vec{r}_1, \vec{r}_2)\right\rangle \quad \text{(III. 8)}$$

Alternatively, this can be expressed as:

$$f_{B1} = -\frac{2}{K^2}\left(f_{e_1} + f_{e_2} - 2.f_N\right) \quad \text{(III. 9)}$$

where:

$$\begin{cases} f_{e_1} = \left\langle \Phi_f(\vec{k}_1, \vec{r}_1; \vec{k}_2, \vec{r}_2)\middle| e^{i\vec{K}\vec{r}_1}\middle|\varphi_i(\vec{r}_1, \vec{r}_2)\right\rangle \\ f_{e_2} = \left\langle \Phi_f(\vec{k}_1, \vec{r}_1; \vec{k}_2, \vec{r}_2)\middle| e^{i\vec{K}\vec{r}_2}\middle|\varphi_i(\vec{r}_1, \vec{r}_2)\right\rangle \\ f_N = \left\langle \Phi_f(\vec{k}_1, \vec{r}_1; \vec{k}_2, \vec{r}_2)\middle|\varphi_i(\vec{r}_1, \vec{r}_2)\right\rangle \end{cases} \quad \text{(III. 10)}$$

An analytical expression can be obtained for each term f_{e_1} , f_{e_2}, and f_N in the case of a Slater-type wave function. Calculations for this element have been performed in several theses [8-9].

III.2.3 Description of the Initial State

The initial state of the projectile-target system is expressed as follows:

$$|\Psi_i\rangle = \left|\phi_i(\vec{k}_{0,}\vec{r}_0)\varphi_i(\vec{r}_1, \vec{r}_2, \ldots \vec{r}_N)\right\rangle \quad \text{(III. 11)}$$

Here, $\phi_i(\vec{k}_{0,}\vec{r}_0)$ represents a plane wave describing the incident electron, and $\vec{r}_0$ denotes the position vector of the incident electron. The function $\varphi_i(\vec{r}_1, \vec{r}_2, \ldots \vec{r}_N)$ represents the wave function for the ground state of the target, with $\vec{r}_i = 1,2, \ldots, N$ indicating the position vectors of the target's electrons. The N electron target problem can be simplified to a two active electron problem [5] using the frozen-core approximation, assuming that the other electrons in the target are not affected by the collision process:

$$|\varphi_i(\vec{r}_1, \vec{r}_2, \ldots \vec{r}_N)\rangle \approx |\varphi_i(\vec{r}_1, \vec{r}_2)\rangle \quad \text{(III. 12)}$$

➢ **Wave Function of the Target**

The wave function of the target (Neon and Krypton) is represented as a Slater determinant that must be an eigenfunction of the operators L^2 and S^2. In this work, to describe the two active electrons of the target (np^6), we will use a Hartree Fock wave function from Clementi and Roetti [8]:

$$\varphi_i(\vec{r}_1, \vec{r}_2) = \phi(\vec{r}_1)\phi(\vec{r}_2) \qquad \text{(III. 13)}$$

The function $\phi(\vec{r}_i)$is expressed as:

$$\phi_i(\vec{r}_j) = Y_l^m(\vec{r}_j) \sum_i \xi_i^{3/2} \alpha_i r_j^{n_i - 1} e^{\xi_i r_j} \qquad \text{(III. 14)}$$

The parameters $(n_i, l, m, \xi_i, \alpha_i)$ for neon ($2p^6$) are provided in Tables (III.1) and (III.2) below for neon and krypton This comprehensive description establishes a framework for understanding how double ionization processes can be modeled and analyzed within this theoretical context. By utilizing these foundational wave functions and approximations, we aim to explore various aspects of electron interactions during ionization events.

Table III.1: Parametres of the Hartree-Fock of Clementi and Roetty for Neon $2p^6$

n_i	l	M	ξ_i	α_i
				2p
2	1	M	1.4700	0.22430
2	1	M	2.3717	0.51826
2	1	M	4.4545	0.33902
2	1	M	9.4550	0.01765

Table III.2: Parametres of the Hartree-Fock of Clementi and Roetty for Krypton $4p^6$

n_i	l	m	ξ_i	α_i
				4p
2	1	m	16.3363	0.09018
2	1	m	24.8543	0.00779
3	1	m	15.4451	0.03172
3	1	m	9.18326	-0.08481
3	1	m	6.4205	-0.26625
4	1	m	5.25899	0.0349
4	1	m	3.07835	0.54322
4	1	m	1.9621	0.40037
4	1	m	1.422	0.16488

In order to account for correlation effects in the initial state, we will use correlated wave function calculated through configuration interaction [9] expressed as follows:

$$\phi_i^j(\vec{r}_1, \vec{r}_2) = \sum_{j=1}^{k} C_j(\phi_1, \phi_2) \quad \text{(III. 15)}$$

where the coefficients C_j are the coefficients of the linear combination of the products of single-electron orbitals. Two possible cases of double ionization of neon [10] and argon [11] have been studied:

First Case: Both electrons are ejected from the outer shell (np^6); thus, we need to consider the 15 possible combinations ($k = C_6^2 = 15$) under LS coupling: 9 for the $C^{2+}(np^4)$ ^3P, 5 state for the $C^{2+}(np^4)$ ^1D state, and one for the ionic state $C^{2+}(np^4)$ ^1S. This approach allows us to explore the intricacies of electron correlations during the double ionization process, providing a more accurate representation of the interactions involved in ionizing (Ne and Kr) atoms. By incorporating configuration interaction into our models, we aim to improve our understanding of how these correlations influence the outcomes of double ionization events.
All the eigenfunctions for the first case are presented in Table III.3 with n=2 for Neon and for Krypton n=4.

Table III.3: Eigenfunctions and double ionization (I^{++}) energies of the first case for Ne and Kr:

J	stats	m_l	m_s	$\phi_i^j(\vec{r}_1, \vec{r}_2)$	I^{++}
1	**^{3}P**	+1	+1	$\lvert np_1 np_0 \rvert$	
2	**^{3}P**	+1	-1	$\lvert np_1 \bar{np}_0 \rvert$	$Ne^{2+}(2p^4)$: 62.6 eV
3	**^{3}P**	0	+1	$\lvert np_1 np_{-1} \rvert$	
4	**^{3}P**	0	-1	$\lvert np_1 \bar{np}_{-1} \rvert$	$Kr^{2+}(4p^4)$: 38.4 eV
5	**^{3}P**	-1	+1	$\lvert np_{-1} np_0 \rvert$	
6	**^{3}P**	-1	-1	$\lvert \bar{np}_{-1} \bar{np}_0 \rvert$	
7	**^{3}P**	1	0	$^1/_{\sqrt{2}}(\lvert np_1 \bar{np}_0 \rvert + \lvert \bar{np}_1 np_0 \rvert)$	
8	**^{3}P**	0	0	$^1/_{\sqrt{2}}(\lvert np_1 \bar{np}_{-1} \rvert + \lvert \bar{np}_1 np_{-1} \rvert)$	
9	**^{3}P**	-1	0	$^1/_{\sqrt{2}}(\lvert np_{-1} \bar{np}_0 \rvert + \lvert \bar{np}_{-1} np_0 \rvert)$	
10	**^{1}D**	2	0	$\lvert np_1 \bar{np}_1 \rvert$	$Ne^{2+}(2p^4)$: 65.3 eV
11	**^{1}D**	-2	0	$\lvert np_{-1} \bar{np}_{-1} \rvert$	
12	**^{1}D**	+1	0	$^1/_{\sqrt{2}}(\lvert np_1 \bar{np}_0 \rvert - \lvert \bar{np}_1 np_0 \rvert)$	$Kr^{2+}(4p^4)$: 42.1 eV
13	**^{1}D**	-1	0	$^1/_{\sqrt{2}}(\lvert np_0 \bar{np}_{-1} \rvert - \lvert \bar{np}_0 np_{-1} \rvert)$	
14	**^{1}D**	0	0	$\frac{1}{\sqrt{6}}(\lvert np_1 \bar{np}_{-1} \rvert - \lvert \bar{np}_1 np_{-1} \rvert + 2\lvert np_0 \bar{np}_0 \rvert)$	
15	**^{1}S**	0	0	$\frac{1}{\sqrt{3}}(-\lvert np_1 \bar{np}_{-1} \rvert + \lvert \bar{np}_1 np_{-1} \rvert + \lvert np_0 \bar{np}_0 \rvert)$	$Ne^{2+}(2p^4)$: 69.3 Ev $Kr^{2+}(4p^4)$: 40.7 eV

Second Case : In the second case, the ejected electrons originate from the outer shells (ns^2np^6). Here, we have in LS coupling the 9 possible ion final states corresponding to a part of the 12 possibilities of leaving two electrons in the ($2s^22p^6$) shells of the neon atom, nine possible combinations (k = 9) for the ionic state Ne^{++} ($2s^12p^5$) ^3P and three other for the ion state $Ne^{++}(2s^12p^5)(^1P)$) which is neglected here because the corresponding threshold is too high; (Table III.4 for neon). This analysis of the second case allows [10-11] us to further explore the dynamics of double ionization processes and the specific configurations that arise when electrons are ejected from different electron shells. By examining these combinations and their corresponding states, we can gain deeper insights into the mechanisms governing electron interactions during ionization events.

Table III.4: IC-Eigenfunctions and double ionization energies (I^{++}) of Ne in the second case:

j	États	M_L	M_S	$\phi_i^j(\vec{r}_1, \vec{r}_2)$	I^{++}
1	^3P	0	+1	$\lvert nsnp_0\rvert$	$Ne^{2+}(2s^12p^5)$: *87.8 eV*
2	^3P	0	-1	$\lvert n\bar{s}n\bar{p}_0\rvert$	
3	^3P	+1	+1	$\lvert nsnp_1\rvert$	
4	^3P	+1	-1	$\lvert n\bar{s}n\bar{p}_1\rvert$	
5	^3P	-1	+1	$\lvert nsnp_{-1}\rvert$	
6	^3P	-1	-1	$\lvert n\bar{s}n\bar{p}_{-1}\rvert$	
7	^3P	0	0	$^1/_{\sqrt{2}}(\lvert nsn\bar{p}_0\rvert + \lvert n\bar{s}np_0\rvert)$	
8	^3P	+1	0	$^1/_{\sqrt{2}}(\lvert nsn\bar{p}_{-1}\rvert + \lvert n\bar{s}np_1\rvert)$	
9	^3P	-1	0	$^1/_{\sqrt{2}}(\lvert nsn\bar{p}_{-1}\rvert + \lvert n\bar{s}np_{-1}\rvert)$	

III.2.4 Description of the Final State

The final state is expressed as follows:

$$\left|\Psi_f\left(\vec{k}_s, \vec{r}_0; \vec{k}_1, \vec{r}_1; \vec{k}_2, \vec{r}_2\right)\right\rangle = \left|\phi_s\left(\vec{k}_{s,}\vec{r}_0\right)\Phi_f\left(\vec{k}_1, \vec{r}_1; \vec{k}_2, \vec{r}_2\right)\right\rangle \quad \text{(III. 16)}$$

Where the wave function $\phi_s\left(\vec{k}_{s,}\vec{r}_0\right)$ is a plane wave representing the scattered electron:

$$\phi_s\left(\vec{k}_{s,}\vec{r}_0\right) = \frac{1}{(2\pi)^{3/2}} e^{i\vec{k}_s\vec{r}_0} \qquad \text{(III. 17)}$$

And the function $\Phi_f\left(\vec{k}_1, \vec{r}_1; \vec{k}_2, \vec{r}_2\right)$) represents the wave function of the two ejected electrons in the outgoing channel, depending on the choice of theoretical model to use.

In our study we have used different models in order to show the role of the final state correlation in improving the agreement with experiment.

III.2.4.1 The BBK Model

In the framework of the BBK model. the final state is represented by a product of three Coulomb waves:

$$\Phi_f(\vec{k}_1,\vec{r}_1;\vec{k}_2,\vec{r}_2) = \frac{1}{\sqrt{2}}\left[\varphi_c(\vec{k}_1,\vec{r}_1)\varphi_c(\vec{k}_2,\vec{r}_2) \pm \varphi_c(\vec{k}_1,\vec{r}_2)\varphi_c(\vec{k}_2,\vec{r}_1)\right]C(\alpha_{12},\vec{k}_{12},\vec{r}_{12}) \quad \text{(III. 18)}$$

The plus sign in the equation (III.12) corresponds to a symmetric function for the spatial part (for states ^{1}D and ^{1}S), while the minus sign corresponds to an antisymmetric function (for ^{3}P state).
The Coulomb wave function is given by:

$$\varphi_c(\vec{k}_j,\vec{r}_j) = \frac{1}{(2\pi)^{3/2}} e^{i\vec{k}_j\vec{r}_j} C(\alpha_j,\vec{k}_j,\vec{r}_j) \qquad (j = 1,2.) \qquad \text{(III. 19)}$$

$$C(\alpha_j,\vec{k}_j,\vec{r}_j) = e^{-\frac{\pi\alpha_j}{2}}\Gamma(1+i\alpha_j)\ {}_1F_1\left(-i\alpha_j, 1, -i(k_j r_j + \vec{k}_j\vec{r}_j)\right) \quad \text{(III. 20)}$$

and : $\alpha_i = -\frac{z}{k_j}$, $z = 2$

The third wave function $C(\vec{k}_{12},\vec{r}_{12})$ represents the post-collision interaction between the two ejected electrons in the continuum of residual ions and it is defined for:

$\alpha_{12} = \frac{1}{2k_{12}}$, $\vec{k}_{12} = \frac{1}{2}(\vec{k}_1 - \vec{k}_2)$,

The expressions ${}_1F_1(a,b,z)$ and $\Gamma(z)$ refer to the confluent hypergeometric function and the Euler gamma function, respectively:

$${}_1F_1(a,b,z) = \sum_{n=0}^{\infty} \frac{(a)_n}{(b)_n}\frac{z^n}{n!}; (a)_0 = 1 \quad et \quad (a)_n = a(a+1)\dots(a+n-1) \quad \text{(III. 21)}$$

It can be noted that for *Z=0*, the distortion factor becomes a plane wave. The calculation of the matrix element f_{B1} in this model is quite challenging and time-consuming due to the evaluation of a six-dimensional integral. To address this issue, we utilize an approximate version of this model introduced by Miraglia et al. [12], which employs Fourier transforms to reduce the six dimensional integral to a three dimensional one. Let us recall the property of the double Fourier transform: This approach significantly simplifies calculations while retaining essential physical information about the interactions involved in electron scattering and ionization processes.

the double Fourier transform is defined by:

$$f(\vec{r}) = \frac{1}{(2\pi)^3}\int e^{i\vec{p}\vec{r}}d\vec{p}\int e^{-i\vec{p}\vec{r'}}f(r')d\vec{r'} \qquad \text{(III. 22)}$$

The application of this property to the function $C(\alpha_{12},\vec{k}_{12},\vec{r}_{12})$gives:

$$C(\alpha_{12},\vec{k}_{12},\vec{r}_{12}) = \frac{1}{(2\pi)^3}\int e^{i\vec{p}\vec{r}_{12}}d\vec{p}\int e^{-i\vec{p}\vec{r}_{12}}C(\alpha_{12},\vec{k}_{12},\vec{r}_{12})d\vec{r}_{12} \quad \text{(III. 23)}$$

The scattering amplitude within the framework of the frozen-core approximation for this model is written as follow:

$$f_{B1} = -\frac{1}{2\pi}\left\langle \phi_s(\vec{k}_{s,}\vec{r}_0)\varphi_c(\vec{k}_1,\vec{r}_1)\varphi_c(\vec{k}_2,\vec{r}_2)C(\alpha_{12},\vec{k}_{12},\vec{r}_{12})\right|-\frac{2}{r_0}+\frac{1}{r_{01}}+\frac{1}{r_{02}}\left|\phi_i(\vec{k}_{0,}\vec{r}_0)\,\varphi_i(\vec{r}_1,\vec{r}_2)\right\rangle \quad \text{(III. 24)}$$

Using Bethe's relation, this expression becomes:

$$f_{B1} = -\frac{2}{k^2}\left\langle \varphi_c(\vec{k}_1,\vec{r}_1)\varphi_c(\vec{k}_2,\vec{r}_2)C(\alpha_{12},\vec{k}_{12},\vec{r}_{12})\right|-2+e^{i\vec{k}\vec{r}_1}+e^{i\vec{k}\vec{r}_2}\left|\,\varphi_i(\vec{r}_1,\vec{r}_2)\right\rangle \quad \text{(III. 25)}$$

Inserting (III.47) into (III.49) gives:

$$f_{B1} = -\frac{1}{(2k)^2\pi^3}\int\left(-2.I_0(\vec{p})+I_1(\vec{p})+I_2(\vec{p})\right)d\vec{p} \quad \text{(III. 26)}$$

Where

$$\begin{cases} I_0 = \iint \varphi_c{}^*(\vec{k}_1,\vec{r}_1)\varphi_c{}^*(\vec{k}_2,\vec{r}_2)e^{i\vec{p}\vec{r}_{12}}\,\varphi_i(\vec{r}_1,\vec{r}_2)d\vec{r}_1d\vec{r}_2\int e^{-i\vec{p}\vec{r}_{12}}C(\alpha_{12},\vec{k}_{12},\vec{r}_{12})d\vec{r}_{12} \\ I_1 = \iint \varphi_c{}^*(\vec{k}_1,\vec{r}_1)\varphi_c{}^*(\vec{k}_2,\vec{r}_2)e^{i\vec{p}\vec{r}_{12}}e^{i\vec{k}\vec{r}_1}\,\varphi_i(\vec{r}_1,\vec{r}_2)d\vec{r}_1d\vec{r}_2\int e^{-i\vec{p}\vec{r}_{12}}C(\alpha_{12},\vec{k}_{12},\vec{r}_{12})d\vec{r}_{12} \\ I_2 = \iint \varphi_c{}^*(\vec{k}_1,\vec{r}_1)\varphi_c{}^*(\vec{k}_2,\vec{r}_2)e^{i\vec{p}\vec{r}_{12}}\,e^{i\vec{k}\vec{r}_2}\varphi_i(\vec{r}_1,\vec{r}_2)d\vec{r}_1d\vec{r}_2\int e^{-i\vec{p}\vec{r}_{12}}C(\alpha_{12},\vec{k}_{12},\vec{r}_{12})d\vec{r}_{12} \end{cases} \quad \text{(III. 27)}$$

These expression can also be written as:

$$\begin{aligned} I_0 &= \lim_{\beta\to0}\int e^{-\beta\vec{r}_{12}}e^{-i\vec{p}\vec{r}_{12}}C(\alpha_{12},\vec{k}_{12},\vec{r}_{12})d\vec{r}_{12}\int\varphi_c{}^*(\vec{k}_1,\vec{r}_1)e^{i\vec{p}\vec{r}_1}\,\varphi_i(\vec{r}_1,\vec{r}_2)d\vec{r}_1 \\ &\qquad \int\varphi_c{}^*(\vec{k}_2,\vec{r}_2)\,e^{-i\vec{p}\vec{r}_2}\varphi_i(\vec{r}_1,\vec{r}_2)d\vec{r}_2 \\ I_1 &= \lim_{\beta\to0}\int e^{-\beta\vec{r}_{12}}e^{-i\vec{p}\vec{r}_{12}}C(\alpha_{12},\vec{k}_{12},\vec{r}_{12})d\vec{r}_{12}\int\varphi_c{}^*(\vec{k}_1,\vec{r}_1)e^{i(\vec{k}+\vec{p})\vec{r}_1}\,\varphi_i(\vec{r}_1,\vec{r}_2)d\vec{r}_1 \\ &\qquad \int\varphi_c{}^*(\vec{k}_2,\vec{r}_2)\,e^{-i\vec{p}\vec{r}_2}\varphi_i(\vec{r}_1,\vec{r}_2)d\vec{r}_2 \\ I_2 &= \lim_{\beta\to0}\int e^{-\beta\vec{r}_{12}}e^{-i\vec{p}\vec{r}_{12}}C(\alpha_{12},\vec{k}_{12},\vec{r}_{12})d\vec{r}_{12}\int\varphi_c{}^*(\vec{k}_1,\vec{r}_1)e^{i\vec{p}\vec{r}_1}\,\varphi_i(\vec{r}_1,\vec{r}_2)d\vec{r}_1 \\ &\qquad \int\varphi_c{}^*(\vec{k}_2,\vec{r}_2)\,e^{i(k-\vec{p})\vec{r}_2}\varphi_i(\vec{r}_1,\vec{r}_2)d\vec{r}_2 \end{aligned} \quad \text{(III. 28)}$$

Where β is a parameter close to 0. These three-dimensional integrals require many integration points. We found perfect agreement with the results from the method used by Joulakian et al.

[13] in the case of double ionization of argon for β=0.005, but with a very large number of integration points.

This formulation helps in deriving the scattering amplitude by breaking down the contributions from different interactions and integrating over the relevant variables. The use of Fourier transforms simplifies the calculations involved in evaluating the scattering processes, particularly in complex systems where multiple interactions occur simultaneously.

This BBK method requires significant computational time due to the third Coulomb function $C(\alpha_{12}, \vec{k}_{12}, \vec{r}_{12})$that describes the repulsion between the two ejected electrons [14]. To reduce the computation time for the FDCS, we have approximated this function $C(\alpha_{12}, \vec{k}_{12}, \vec{r}_{12})$using two factors mentioned in Chapter II. This approach allows us to efficiently model the final state in double ionization processes while still accounting for essential interactions between ejected electrons, and to facilitate a more manageable computation without sacrificing accuracy in our results.

III.2.4.2 The 2CWGamow model

As shown in chapter 2 (section II-2-6), The third Coulomb function of the BBK model $C(\alpha_{12}, \vec{k}_{12}, \vec{r}_{12})$ is simplified to the Gamow factor which is capable of explaining the repulsion that exists between slow electrons with similar velocities. It depends solely on the electronic momentum k_i $(i = 1\ or\ 2)$ of the ejected electrons and is defined by the expression:

$$\boldsymbol{F_G(k_{12})} = \left| e^{-\frac{\pi}{2k_{12}}} \Gamma\left(1 - \frac{i}{2k_{12}}\right) \right|^2 = \frac{\pi}{k_{12}\left(e^{\frac{\pi}{k_{12}}} - 1\right)} \qquad \text{(III. 29)}$$

III.2.4.3 The 2DWG Model (Distortion Effect)

This model is a new version of the old BBK model [11,15], where the distortion of the two ejected electrons in the final continuum is taken into account by including the variable ion charge in the Coulomb wave function. The 2DWG model is introduced as a significant correction to the 2CWG model, retaining the initial state and the interaction potential while modifying how the interaction between the ejected electrons and the residual target is described. This adjustment allows us to capture the complexities of electron behavior during double ionization.

- **Final State Representation**

In the 2DW model, the final state of the system is expressed as follows:

$$\Phi_f(\vec{k}_1, \vec{r}_1; \vec{k}_2, \vec{r}_2) =$$

$$= \frac{1}{\sqrt{2}}\left[\varphi_{DW}(\vec{k}_1, \vec{r}_1)\varphi_{DW}(\vec{k}_2, \vec{r}_2) \pm \varphi_{DW}(\vec{k}_1, \vec{r}_2)\varphi_{DW}(\vec{k}_2, \vec{r}_1)\right] F_G(\alpha_{12}, \vec{k}_{12}, \vec{r}_{12}) \qquad \text{(III. 30)}$$

Here $F_G(\alpha_{12}, \vec{k}_{12}, \vec{r}_{12})$ represents either the Gamow factor in the context of the 2DWG model. This distinction is crucial as it influences how we account for electron repulsion in our calculations.

➢ **The distorted wave**

In this approach, each ejected electron is represented by an approximate distorted wave that incorporates the effects of its interaction with the residual target. Specifically, this wave consists of a Coulomb wave modified by a variable charge Z(r) that each ejected electron perceives. This representation acknowledges that as an electron moves away from the nucleus, it experiences a changing effective charge due to its distance from the residual ion. The mathematical form of the distorted wave for each ejected electron is given by:

$$\varphi_{DW}(\vec{k}_j, \vec{r}_j) = \frac{1}{(2\pi)^{3/2}} e^{i\vec{k}_j\vec{r}_j}\, e^{-\frac{\pi z(r_j)}{2k_j}}\, \Gamma\left(1 + i\frac{z(r_j)}{k_j}\right)\, {}_1F_1\left(-i\frac{z(r_j)}{k_j}, 1, -i\left(k_j r_j + \vec{k}_j\vec{r}_j\right)\right) \quad \text{(III.31)}$$

In this equation ($e^{i\vec{k}_j\vec{r}_j}$) represents a plane wave associated with the momentum of the ejected electron and the exponential term $e^{-\frac{\pi z(r_j)}{2k_j}}$ accounts for the distortion due to Coulomb attraction from the residual ion.

The Gamma function and hypergeometric function provide additional corrections that account for the complex interactions as electrons move through space.

➢ **Charge Perception**

Each ejected electron perceives a nuclear charge Z at $r = 0$ (with$Z(0) = Z$), and this charge approaches Z=2 as ***r*** goes to infinity. If we assume a constant effective charge perceived by each ejected electron (Z(r)=2), then the 2DW model simplifies to the 2CW model [11].

This simplification highlights how our model can transition between different levels of complexity depending on how we choose to represent electron interactions.

➢ **Computational Efficiency**

One of the main advantages of using this distorted wave approach is that it can be highly computationally efficient. By employing analytical calculations rather than relying solely on numerical methods, we can intensely reduce computation time while still capturing essential physical effects. It is important to note that:

$$\begin{cases} \varphi_{DW}(\vec{r}) = \varphi_{DW}(\vec{r}) & r \le d \\ \varphi_{DW}(\vec{r}) = \varphi_c(\vec{r}) & r > d \end{cases} \quad \text{(III. 32)}$$

In this expression, ***d*** represents the range of the potential. For noble gases atoms and in cases of double ionization, this range is typically around 6 atomic units.

The scattering amplitude derived from this model can be expressed accordingly, allowing us to analyze how distortion effects influence double ionization outcomes.

$$f_{B1} = -\frac{2}{K^2}\left\langle \Phi_{DW}(\vec{k}_1, \vec{r}_1; \vec{k}_2, \vec{r}_2)\middle| -2 + e^{i\vec{K}\vec{r}_1} + e^{i\vec{K}\vec{r}_2}\middle|\varphi_i(\vec{r}_1, \vec{r}_2)\right\rangle \quad \text{(III. 33)}$$

Taking the term f_{e_1} as an example (the other two terms $f_{e_2} and\ f_N$ are calculated in a similar manner):

$$f_{e_1} = \left\langle \Phi_{DW}(\vec{k}_1, \vec{r}_1; \vec{k}_2, \vec{r}_2) \middle| e^{i\vec{K}\vec{r}_1} \middle| \varphi_i(\vec{r}_1, \vec{r}_2) \right\rangle \quad \text{(III. 34)}$$

Using the property from the previous equation we can express f_{e_1} as follows:

$$f_{e_1} = \frac{2}{K^2}\left(\int \int_0^d \varphi_{DW}^*(\vec{r}_1, \vec{r}_2) e^{i\vec{K}\vec{r}_1} \varphi_i(\vec{r}_1, \vec{r}_2) r_1^2 dr_1 d\Omega + \int \int_d^\infty \varphi_c^*(\vec{r}_1, \vec{r}_2) e^{i\vec{K}\vec{r}_1} \varphi_i(\vec{r}_1, \vec{r}_2) r_1^2 dr_1 d\Omega \right) \quad \text{(III. 35)}$$

We can rewrite the second term I_2 as the following form:

$$I_2 = \int \int_0^\infty \varphi_c^*(\vec{r}_1, \vec{r}_2) e^{i\vec{K}\vec{r}_1} \varphi_i(\vec{r}_1, \vec{r}_2) r_1^2 dr_1 d\Omega - \int \int_0^d \varphi_c^*(\vec{r}_1, \vec{r}_2) e^{i\vec{K}\vec{r}_1} \varphi_i(\vec{r}_1, \vec{r}_2) r_1^2 dr_1 d\Omega \quad \text{(III. 36)}$$

So the f_{e_1} becomes:

$$f_{e_1} = \left(\int \int_0^\infty \varphi_c^*(\vec{r}_1, \vec{r}_2) e^{i\vec{K}\vec{r}_1} \varphi_i(\vec{r}_1, \vec{r}_2)\, r_1^2 dr_1 d\Omega + \int \int_0^d \left(\varphi_{DW}^*(\vec{r}_1, \vec{r}_2) - \varphi_c^*(\vec{r}_1, \vec{r}_2) \right) e^{i\vec{K}\vec{r}_1} \varphi_i(\vec{r}_1, \vec{r}_2) r_1^2 dr_1 d\Omega \right) \quad \text{(III. 37)}$$

In this expression, the first term is calculated analytically (as in the case of the previous 2CW model), while the second term is computed using a standard integration method (such as Gauss-Legendre) over the interval $(0 \leq r \leq d)$.

This approach allows us to evaluate efficiently the contributions to the scattering amplitude from both the Coulomb wave and the distorted wave components. By separating these contributions and applying appropriate integration techniques, we can achieve accurate results while minimizing computational complexity.

III.2.4.4 Calculation of the Variable Charge

To calculate the variable charge Z(r), we use the static potential V_{stat} of the target as perceived by the ejected electron. In the case of atoms, the potential V_{stat} is given by:

$$V_{stat}(\vec{r}_j) = -\frac{z}{r_j} + \sum_{i=1}^{N_0} N_i \int \frac{|\varphi_i(\vec{r})|^2}{|\vec{r} - \vec{r}_j|} d\vec{r} = -\frac{z(r_j)}{r_j} \quad \text{(III. 38)}$$

Where: j=1,2 and i≠j.

Z is the charge of the nucleus.

N_0 is the number of atomic orbitals of the target.

N_i is the number of electrons in orbital i.

$\varphi_i(\vec{r})$ represents the wave function of the bound electron.

It is important to note that $V_{stat}(\vec{r}_j)$ is an anisotropic potential that can be complex to handle. To simplify this, we use a more practical potential known as the averaged radial potential $U_m(r_j)$.

$$U_m(r_j) = \frac{1}{4\pi}\int V_{stat}(\vec{r}_j)d\Omega_j = -\frac{z(r_j)}{r_j} \qquad \text{(III. 39)}$$

This averaged potential provides a more manageable approach to calculating interactions in systems where electrons are influenced by varying effective charges as they move away from the nucleus. By averaging over contributions from all relevant orbitals, we can derive a more straightforward expression for the variable charge experienced by an ejected electron. The calculation of Z(r) allows for a better understanding of how electrons interact with atomic targets during processes such as ionization. This understanding is crucial for accurately modeling and predicting outcomes in quantum mechanical scattering experiments and other related phenomena in atomic physics.

The static potential $V_{stat}(r)$ for the double ionization (DI) of the 2p orbital of Neon can be expressed as follows:

$$U_{2p}(r_j) = \frac{1}{4\pi}\int\left(-\frac{10}{r_j}+\sum_{i=1}^{3}N_i\int\frac{|\varphi_i(\vec{r})|^2}{|\vec{r}-\vec{r}_j|}d\vec{r}\right)d\Omega_j = -\frac{z(r_j)}{r_j} \qquad \text{(III..40)}$$

Alternatively, this can be written as:

$$U_{2p}(r_j) = \frac{1}{4\pi}\int\left(-\frac{10}{r_j}+2\int\frac{|\varphi_{1s}(\vec{r})|^2}{|\vec{r}-\vec{r}_j|}\,d\vec{r}+2\int\frac{|\varphi_{2s}(\vec{r})|^2}{|\vec{r}-\vec{r}_j|}\,d\vec{r}+4\int\frac{|\varphi_{2p}(\vec{r})|^2}{|\vec{r}-\vec{r}_j|}\,d\vec{r}\right)d\Omega_j \qquad \text{(III. 41)}$$

From this, we can derive:

$$U_{2p}(r_j) = -\frac{10}{r_j}+2\frac{z_{1s}}{r_j}+2\frac{z_{2s}}{r_j}+4\frac{z_{2p}}{r_j} = -\frac{z(r_j)}{r_j} \qquad \text{(III. 42)}$$

The variable charge can then be expressed as:

$$z(r_j) = 10 - 2.z_{1s} - 2.z_{2s} - 4.z_{2p} \qquad \text{(III. 43)}$$

Where:

$$Z_{nl} = \int\frac{|\varphi_{nl}(\vec{r})|^2}{|\vec{r}-\vec{r}_j|}d\vec{r} \qquad \text{(III. 44)}$$

The variable charge is calculated analytically using multipole expansion, which is given by:

$$\frac{1}{\mathrm{r}_{ij}} = \sum_{l,m} \frac{4\pi}{2l+1} \frac{r^{l}_{<}}{r_{>}^{l+1}} Y^{*}_{l,m}(\Omega_i) Y_{l,m}(\Omega_j) \qquad \text{(III. 45)}$$

By the same principle, the static potential $V_{stat}(r)$ for the double ionization (DI) of the 4p orbital of Krypton can be expressed as follows:

$$U_{4p}(r_j) = \frac{1}{4\pi} \int \left(-\frac{36}{r_j} + \sum_{i=1}^{6} N_i \int \frac{|\varphi_i(\vec{r})|^2}{|\vec{r} - \vec{r}_j|} d\vec{r} \right) d\Omega_j = -\frac{z(r_j)}{r_j} \qquad \text{(III. 46)}$$

Alternatively, this can be written as:

$$U_{4p}(r_j) = \frac{1}{4\pi} \int \left(-\frac{36}{r_j} + 2\int \frac{|\varphi_{1s}(\vec{r})|^2}{|\vec{r}-\vec{r}_j|}\, d\vec{r} + 2\int \frac{|\varphi_{2s}(\vec{r})|^2}{|\vec{r}-\vec{r}_j|}\, d\vec{r} + 2\int \frac{|\varphi_{3s}(\vec{r})|^2}{|\vec{r}-\vec{r}_j|} d\vec{r} + \right.$$
$$+ 2\int \frac{|\varphi_{4s}(\vec{r})|^2}{|\vec{r}-\vec{r}_j|} d\vec{r} + 6\int \frac{|\varphi_{2p}(\vec{r})|^2}{|\vec{r}-\vec{r}_j|}\, d\vec{r} + 6\int \frac{|\varphi_{3p}(\vec{r})|^2}{|\vec{r}-\vec{r}_j|}\, d\vec{r} + 10\int \frac{|\varphi_{3d}(\vec{r})|^2}{|\vec{r}-\vec{r}_j|}\, d\vec{r} +$$
$$\left. + 4\int \frac{|\varphi_{4p}(\vec{r})|^2}{|\vec{r}-\vec{r}_j|}\, d\vec{r} \right) d\Omega_j \qquad \text{(III.47)}$$

From this, we can derive:

$$U_{4p}(r_j) = -\frac{36}{r_j} + 2\frac{z_{1s}}{r_j} + 2\frac{z_{2s}}{r_j} + 2\frac{z_{3s}}{r_j} + 2\frac{z_{4s}}{r_j} + 6\frac{z_{2p}}{r_j} + 6\frac{z_{3p}}{r_j} + 10\frac{z_{3d}}{r_j} + 4\frac{z_{4p}}{r_j}$$
$$= -\frac{z(r_j)}{r_j} \qquad \text{(III. 48)}$$

The variable charge can then be expressed as:

$$z(r_j) = 36 - 2.z_{1s} - 2.z_{2s} - 2.z_{3s} - 2.z_{4s} - 6.z_{2p} - 6.z_{3p} - 10.z_{3d} - 6.z_{4p} \qquad \text{(III. 49)}$$

The variable charge is calculated analytically using multipole expansion, which is given by:

$$\frac{1}{\mathrm{r}_{ij}} = \sum_{l,m} \frac{4\pi}{2l+1} \frac{r^{l}_{<}}{r_{>}^{l+1}} Y^{*}_{l,m}(\Omega_i) Y_{l,m}(\Omega_j) \qquad \text{(III. 50)}$$

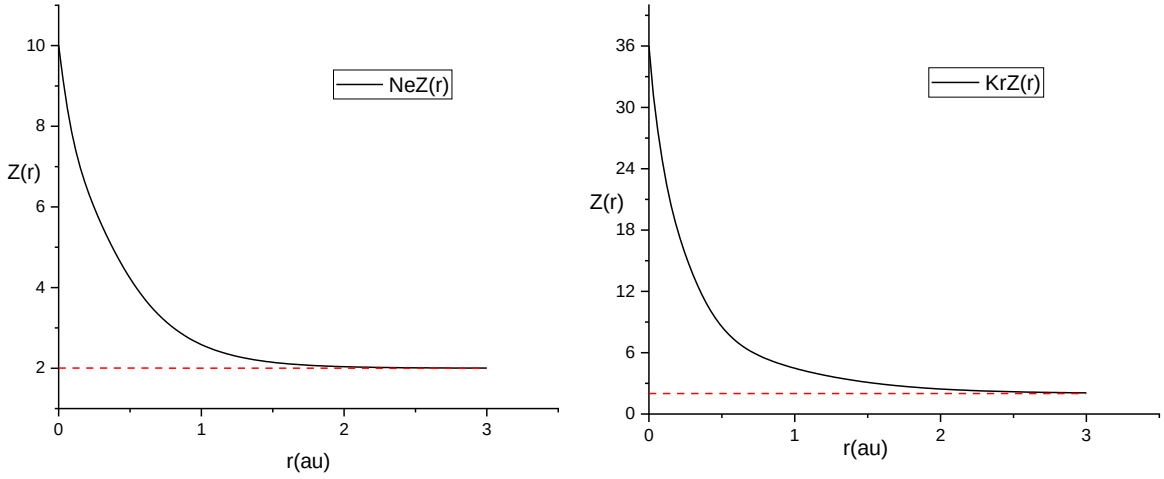

Figure 3-1: Neon and Krypton variable charge

III.2.4.5 The 2CWSR Model (Short-Range Potential Effect)

A second correction to the 2CW model is the 2CWSR model [11], where the initial and final states remain unchanged. In the 2CW model, the interaction between the projectile and the target is considered to be purely Coulomb interaction, represented by a Coulomb potential (VC(r)). However, in reality, there exists an additional short-range potential (VSR(r)) that arises from the effects of the electronic distribution in the target on the incident electron. We can express the interaction potential between the projectile and the remaining electrons in the target in the case of two active electrons as:

$$V = \frac{1}{r_{01}} + \frac{1}{r_{02}} + U_m(r_0) \quad \text{(III. 51)}$$

Where: $r_{0j} = \left|\vec{r}_0 - \vec{r}_j\right|$ is the distance between the projectile and one of the two active electrons. And:

$$U_m(r_0) = \frac{1}{4\pi}\int\left(-\frac{z}{r_0} + \sum_{\substack{i=1 \\ i\neq j}}^{N_0} N_i \int \frac{|\varphi_i(\vec{r})|^2}{|\vec{r}_0 - \vec{r}|} d\vec{r}\right) d\Omega_0 = -\frac{z(r_0)}{r_0} \qquad \text{(III. 52)}$$

This $\boldsymbol{V}$ potential is similar to the static potential V_{stat} used in the previous model; however, for the 2DW model, the final expression of the potential depends on the interaction distance between one of the two ejected electrons and the residual ion $\boldsymbol{r_j}$, while for this 2CWSR model, it depends on the interaction distance between the projectile and the target $\boldsymbol{r_0}$. This adjustment allows for a more accurate representation of interactions during double ionization processes by accounting for short-range effects that are not captured by a purely Coulomb approach. The inclusion of this short-range potential is crucial for improving predictions related to scattering amplitudes and cross sections in experimental setups involving electron impact ionization.

The short-range potential is calculated in a way that is similar to the approach used in the 2DW model. This potential is expressed as follows:

$$U_m(r_0) = -\frac{2}{r_0} + V_{SR} \qquad \text{(III. 53)}$$

With :

$$V_{SR} = \sum_{m=1}^{8} e^{-a_m r_0}\left[\frac{A_m}{r_0} + B_m + C_m r_0 + D_m {r_0}^2 + E_m {r_0}^3\right] \; for \; \boldsymbol{Ne} \qquad \text{(III. 54)}$$

Where $A_m, B_m, C_m, D_m, E_m,$ and a_m are obtained from the Roothaan Hartree Fock wave function of Clementi and Roetti or from the correlated wave function calculated by configuration interaction [10-16].

The interaction potential between the projectile and the target becomes:

$$V = -\frac{2}{r_0} + \frac{1}{r_{01}} + \frac{1}{r_{02}} + V_{SR} \qquad \text{(III. 55)}$$

And the scattering amplitude is:

$$f_{B1} = -\frac{1}{2\pi}\left\langle \phi_d(\vec{k}_d, \vec{r}_0)\Phi_C(\vec{k}_1, \vec{r}_1; \vec{k}_2, \vec{r}_2)\right|-\frac{2}{r_0} + \frac{1}{r_{01}} + \frac{1}{r_{02}} + V_{SR}(r_0)\left|\phi_i(\vec{k}_0, \vec{r}_0)\varphi_i(\vec{r}_1, \vec{r}_2)\right\rangle \text{ (III. 56)}$$

After applying Bethe's relation we get:

$$f_{B1} = -\frac{2}{K^2}\left(\left\langle \Phi_C(\vec{k}_1, \vec{r}_1; \vec{k}_2, \vec{r}_2)\right|-2 + e^{i\vec{K}\vec{r}_1} + e^{i\vec{K}\vec{r}_2}\left|\varphi_i(\vec{r}_1, \vec{r}_2)\right\rangle + \frac{K^2}{4\pi}\left\langle \Phi_C(\vec{k}_1, \vec{r}_1; \vec{k}_2, \vec{r}_2)\middle|\varphi_i(\vec{r}_1, \vec{r}_2)\right\rangle \int e^{i\vec{K}\vec{r}_0} V_{SR}(r_0) d\vec{r}_0\right) \text{ (III. 57)}$$

III.2.4.6 The 2DWSR Model (Distortion and Short-Range Potential Effect)

In this correction, the initial state remains unchanged. It is an extension of the 2CWSR model, where the interaction between the projectile and the target is no longer Coulomb interaction but also includes a short-range potential. Additionally, the distortion effects of the two ejected electrons are taken into account through two approximate distorted waves. Thus, the scattering amplitude for this model is expressed as follows:

$$f_{B1} = -\frac{1}{2\pi}\left\langle \phi_d(\vec{k}_d, \vec{r}_0)\Phi_{DW}(\vec{k}_1, \vec{r}_1; \vec{k}_2, \vec{r}_2)\right|-\frac{2}{r_0} + \frac{1}{r_{01}} + \frac{1}{r_{02}} + V_{SR}(r_0)\left|\phi_p(\vec{k}_0, \vec{r}_0)\varphi_i(\vec{r}_1, \vec{r}_2)\right\rangle \text{ (III. 58)}$$

This approach allows for a more comprehensive understanding of the interactions involved in double ionization processes by incorporating both distortion effects and short-range potentials.

We can also write:

$$f_{B1} = -\frac{2}{K^2}\left(\left\langle \Phi_{DW}(\vec{k}_1,\vec{r}_1;\vec{k}_2,\vec{r}_2)\right|-2+e^{i\vec{K}\vec{r}_1}+e^{i\vec{K}\vec{r}_2}\left|\varphi_i(\vec{r}_1,\vec{r}_2)\right\rangle + \frac{K^2}{4\pi}\left\langle \Phi_{DW}(\vec{k}_1,\vec{r}_1;\vec{k}_2,\vec{r}_2)\right|\varphi_i(\vec{r}_1,\vec{r}_2)\rangle \int e^{i\vec{K}\vec{r}_0}V_{SR}(r_0)d\vec{r}_0\right) \quad \text{(III. 59)}$$

This model requires a substantial amount of computational time due to the inclusion of both distortion effects and the short-range potential. To alleviate this challenge, as mentioned earlier, we carry out the calculations for these two potentials analytically, which allows us to significantly reduce the computation time.

III.3 Double ionization of Methane molecule

As previously mentioned, various theoretical and experimental studies on the double ionization of atomic targets have been conducted, but such studies remain scarce for molecular targets due to the complex structure of molecules, which presents numerous challenges both experimentally and theoretically [17]. In this work, we propose to investigate the double ionization of methane (CH_4). The choice of this target is motivated by its relevance in various fields such as astrophysics and environmental science; moreover, this molecule has been very little studied theoretically due to the lack of experimental data. Our Calculation for the five differential cross section (FDCS) of the double ionization of methane by fast electron impact is performed within the first and second Born approximation using the approximate 3C model with the usual Gamow factor then with the Ward and Macek factor [18-19] as a corrected version. The study allows to identify and analyze the different mechanisms for specific kinematic conditions [20].

III.3.1 FDCS in second Born approximation

We consider the (e, 3e) reaction of the methane molecule:

$$e^- + CH_4 \rightarrow 3e^- + CH_4^{++}$$

In the second order Born approximation the DI-FDCS is given by:

$$\sigma^5 = \frac{k_1 k_2 k_s}{k_i}|f_{B1}+f_{B2}|^2 \quad \text{(III.60)}$$

This FDCS is calculated for a special molecular orientation obtained by integrating the six-fold cross section (6DCS) over the solid angle of Euler ($d\Omega_{Euler} = \sin\beta\, d\beta\, d\alpha\, d\gamma$).

$$\sigma^5 = \frac{d^5\sigma}{d\Omega_s d\Omega_1 d\Omega_2 dE_1 dE_2} = \frac{1}{8\pi^2}\iiint \sin\beta\, d\beta d\alpha d\gamma \frac{d^6\sigma}{d\Omega_{Euler} d\Omega_s d\Omega_1 d\Omega_2 dE_1 dE_2} \quad \text{(III.61)}$$

- The first Born term f_{B1} of the 5DCS in equation (III.60) is written as previously (sectionIII.2.1):

$$f_{B1} = \frac{-1}{2\pi}\left\langle e^{(i\vec{k_s}.\vec{r_0})}\Psi_f(\vec{k}_1,\vec{k}_2,\vec{r}_1,\dots\vec{r}_{10})\right|V\left|e^{(i\vec{k_i}.\vec{r_0})}\Psi_i(\vec{r}_1,\vec{r}_2,\dots\vec{r}_{10})\right\rangle \quad \text{(III.62)}$$

Where:

The plane waves $\boldsymbol{e^{(i\overrightarrow{k_{i,s}}.\overrightarrow{r_0})}}$ describe the fast incident and scattered electrons, $\boldsymbol{\Psi_i(\vec{r}_1,\vec{r}_2,\dots\vec{r}_{10})}$ is the wave function of the initial state of CH_4 target and $\boldsymbol{\Psi_f(\vec{k}_1,\vec{k}_2,\vec{r}_1,\dots\vec{r}_{10})}$ represents the wave function of the double continuum state of the residual ion.
The Coulomb interaction potential between the incoming electron and the CH_4 molecule is of the form:

$$V=-\frac{6}{r_0}-\frac{1}{|\vec{r}_0-\vec{R}_1|}-\frac{1}{|\vec{r}_0-\vec{R}_2|}-\frac{1}{|\vec{r}_0-\vec{R}_3|}-\frac{1}{|\vec{r}_0-\vec{R}_4|}+\sum_{i=1}^{10}\frac{1}{|\vec{r}_{0i}|} \qquad \text{(III.63)}$$

With : $\boldsymbol{R_1=R_2=R_3=R_4=R_{CH}=2.080\ au}$ [21] denotes the length of CH link,
$\boldsymbol{r_0}$ is the coordinate of the incident particle and $\boldsymbol{\vec{r}_i}$ is the position vector of the i^{th} target-bound electron by respect to the center of the molecule placed on the carbon atom (C) nucleus with: $\boldsymbol{\vec{r}_{0i}=\vec{r}_0-\vec{r}_i}$.
This potential can be simplified by use of the well-known frozen-core approximation [5-6] justifying the fact that our interest is closed to the ejection of electrons from any valence shells (1t2x, 1t2y, 1t2z). The potential *V* is then given by:

$$V(\vec{r}_0,\vec{r}_1,\vec{r}_2)=-\frac{2}{r_0}+\frac{1}{r_{01}}+\frac{1}{r_{02}} \qquad \text{(III. 64)}$$

This being the case, it is reasonable to assume that the rest of the electrons in the doubly charged ionic nucleus are not affected by the ionization process itself. This allows to write the initial wave function describing the two active electrons and their final wave function as:

$$\Psi_i(\vec{r}_1,\vec{r}_2,\dots\vec{r}_{10})\equiv\psi_i(\vec{r}_1,\vec{r}_2),\qquad \Psi_f(\vec{k}_1,\vec{k}_2,\vec{r}_1,\dots\vec{r}_{10})\equiv\psi_f(\vec{k}_1,\vec{k}_2,\vec{r}_1,\vec{r}_2)$$

- The second Born approximation term is given by:

$$\acute{f}_{B2}=\frac{1}{8\pi^4}\sum_n\int\frac{d\vec{q}}{q^2-k^2-i\varepsilon}\left\langle e^{(i\overrightarrow{k_s}.\overrightarrow{r_0})}\psi_f(\vec{k}_1,\vec{r}_1,\vec{k}_2,\vec{r}_2)\middle|V\middle|e^{(i\vec{q}.\overrightarrow{r_0})}\psi_n(\vec{r}_1,\vec{r}_2)\right\rangle \left\langle e^{(i\vec{q}.\overrightarrow{r_0})}\psi_n(\vec{r}_1,\vec{r}_2)\middle|V\middle|e^{(i\overrightarrow{k_i}.\overrightarrow{r_0})}\psi_i(\vec{r}_1,\vec{r}_2)\right\rangle \qquad \text{(III.65)}$$

Where the summation over *n* means that we take into account all the contributions of the *n* discrete states and those of the continuum states of the methane. This term shows the twice interaction of the incident electron with the target which is explained by the well known two step 2 mechanism (TS2) [22]. The final expression of the second Born term is obtained by the integration over $\vec{r}_0$ and by applying the closure approximation [23].

$$f_{B2}=\frac{2}{\pi^2}\int\frac{d\vec{q}}{q^2-p^2-i\varepsilon}\frac{1}{K_i^2K_f^2}\langle\Psi_f(\vec{k}_1,\vec{r}_1,\vec{k}_2,\vec{r}_2)|\left(e^{(i\overrightarrow{K_f}.\overrightarrow{r_1})}+e^{(i\overrightarrow{K_f}.\overrightarrow{r_2})}-2\right)\left(e^{(i\overrightarrow{K_i}.\overrightarrow{r_1})}+e^{(i\overrightarrow{K_i}.\overrightarrow{r_2})}-2\right)|\psi_i(\vec{r}_1,\vec{r}_2)\rangle \qquad \text{(III.66)}$$

Where
$\vec{K}_i=\vec{k}_i-\vec{q}$ and $\vec{K}_f=\vec{q}-\vec{k}_s$ are the momentum transfer in the first and the second step.
$\vec{K}=\vec{K}_i+\vec{K}_f=\vec{k}_i-\vec{k}_s$ the final momentum transfer of the collision interaction.
It is necessary to note that:

$$\frac{p^2}{2}=\frac{k_i^2}{2}-\overline{\omega} \qquad \text{(III.67)}$$

where $\overline{\omega}$ refers to the average excitation energy.

III.3.1.1 Initial state of Methane (CH_4) target- Physical Description

Methane (CH_4) is a molecule of type XH_4, formed from one heavy carbon atom and four hydrogen atoms. It possesses a tetrahedral geometry, with bond angles of approximately 109.5°. The length of the carbon-hydrogen bond is about 1.09 angstroms (Å). This molecular structure contributes to methane's properties as a stable hydrocarbon and its role as a significant component of natural gas. Understanding the double ionization processes in methane is crucial for elucidating its behavior in various chemical reactions and its impact on atmospheric chemistry.

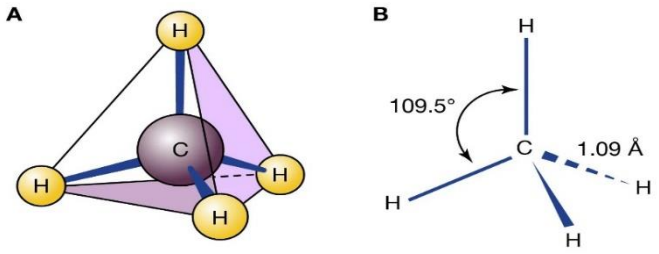

FigureError! No text of specified style in document.**3-2:** Molecular structure of CH4

In the case of methane (CH_4), the molecular structure is determined by the hybridization of atomic orbitals. The carbon atom, which has an electronic configuration of $1s^2\ 2s^2\ 2p^2$, undergoes sp^3 hybridization. This means that the 2s orbital mixes with the three 2p orbitals ($2p_x$, $2p_y$, and $2pz$) to form four equivalent sp^3 hybrid orbitals. Each of these hybrid orbitals is occupied by a valence electron from carbon, allowing for the formation of four identical covalent bonds with hydrogen atoms. This gives the CH_4 the following electronic configuration: $\mathbf{1a_1^2\ 2a_1^2\ 1t_2^6}$. the orbital $\mathbf{1t_2^6}$ is written as: $\mathbf{1t_{2x}^2\ 1t_{2y}^2\ 1t_{2z}^2}$.

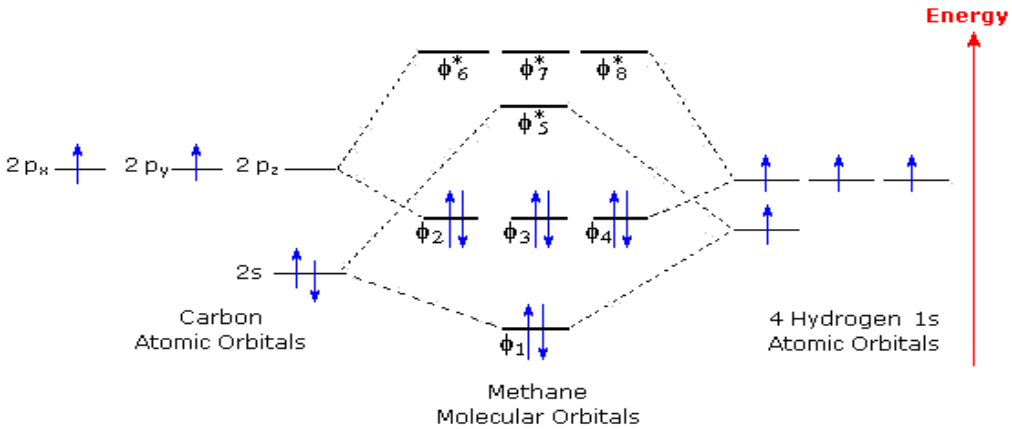

Figure3-3: Molecular orbitals of CH_4

One of the real challenges is the multicentric nature of molecules, which makes calculations very difficult and sometimes impossible. Moccia [21] proposes a tool capable of simplifying calculations while maintaining the accuracy of the theoretical model, where the multicentric molecular wave function is reduced to a monocentric wave function. Another difficulty arises in the theoretical treatment due to the random orientation of the molecule, necessitating a triple integration over all orientations of the molecule in space. Despite these challenges, there has been a growing interest in studying molecular targets in recent years.

In Moccia's [21] monocentric approach, these molecular orbitals are expressed using Slater-type wave functions centered on a common center (the heaviest atom: X). They take the following form:

$$\varphi_i\left(\vec{r}\right) = \sum_{k=1}^{N_i} a_{ik}\, \Phi^{\xi_{ik}}_{n_{ik},l_{ik},m_{ik}}\left(\vec{r}\right) \qquad \text{(III. 68)}$$

With: $\Phi^{\xi_{ik}}_{n_{ik},l_{ik},m_{ik}}\left(\vec{r}\right) = R^{\xi_{ik}}_{n_{ik}}(r) S_{l_{ik},m_{ik}}(\hat{r}) \quad and \quad R^{\xi_{ik}}_{n_{ik}}(r) = \frac{(2\xi_{ik})^{n_{ik}+\frac{1}{2}}}{\sqrt{2n_{ik}!}} r^{n_{ik}-1} e^{-\xi_{ik} r}$

Where $S_{lm}(\Omega)$ are the real spherical harmonics, and they are given by:

$$S_{l_{ik},m_{ik}}(\hat{r}) = \begin{cases} \left(\frac{2|m|}{m}\right)^{1/2} \left(Y_{l-|m|}(\hat{r}) + (-1)^m \frac{m}{|m|} Y_{l|m|}(\hat{r})\right) \text{ if } m \neq 0 \\ Y_{l0}(\Omega) \text{ if } m = 0 \end{cases} \qquad \text{(III. 69)}$$

Table III.5: Parameters of Moccia's wave functions and ionization energies of the molecular orbitals of the CH_4 molecule.

N	*l*	*M*	e_{ik}	a_{ik}				
				1a₁	***2a₁***	***1tx***	***1t$_y$***	***1t$_z$***
1	**0**	**0**	9.500	0.00877	0.05838			
1	**0**	**0**	5.500	-0.21248	0.93837			
2	**0**	**0**	1.500	0.98204	0.07150			
4	**0**	**0**	2.000	0.05076	-0.03310			
4	**0**	**0**	3.000	-0.01799	-0.03118			
7	**3**	**-2**	2.900	0.14254	0.00039			
2	**1**	**1**	1.373			1.25996		
3	**1**	**1**	2.950			-0.05760		
4	**1**	**1**	2.950			-0.26740		
7	**1**	**1**	2.900			0.05331		
7	**3**	**3**	2.900			-0.06875		
4	**3**	**-1**	2.400			-0.06694		
4	**2**	**-1**	1.900			0.32784		
2	**1**	**-1**	1.373				1.25996	
3	**1**	**-1**	2.950				-0.05760	

4	**1**	**-1**	2.950			-0.26740	
7	**3**	**-1**	2.900			0.05331	
7	**3**	**-3**	2.900			-0.06875	
4	**2**	**1**	2.400			-0.06694	
4	**2**	**1**	1.900			0.032784	
2	**1**	**0**	1.373				1.25998
3	**1**	**0**	2.950				-0.05762
4	**1**	**0**	2.950				-0.26738
7	**3**	**0**	2.900				-0.08695
4	**2**	**-2**	2.400				-0.06691
4	**2**	**-2**	1.900				0.32775
double ionization E(ev)				11.1949	0.9204	0.5042	

III.3.1.2 Final state description

The wave function $\psi_f(\vec{k}_1,\vec{r}_1;\vec{k}_2,\vec{r}_2)$ representing the two ejected electrons in the doubly ion continuum is firstly represented by the 2CWG model [5] described in the case of atoms, and then by a correction version of this model knowing by 2CWWM model.

- **The 2CW Ward and Macek model**

This model, considered as a second approximate version of the BBK model, is based on evaluating the function $C(\alpha_{12},\vec{k}_{12},\vec{r}_{12})$ at a fixed distance, between the two ejected electrons when leaving the interaction zone. The Ward and Macek factor [18] depends on the electronic momentum $\boldsymbol{k}_i$ (i=1,2) and on the average distance separating the two outgoing electrons during the repulsion interaction. This factor is defined by:

$$F_{WM}(|\vec{k}_1-\vec{k}_2|)=exp\left(\frac{-\pi\alpha_{12}}{2}\right)\Gamma(1-i\alpha_{12})_1F_1(i\alpha_{12},1,-ik_{12}\bar{r}_{12}) \qquad \text{(III. 70)}$$

The first term represents the Gamow factor, while the second term denotes the hypergeometric function at an average distance $\bar{r}_{12}$depending on the ejected electrons energies as:

$$\bar{r}_{12}=\frac{\pi^2}{16\varepsilon}\left[1+\frac{0.627}{\pi}\sqrt{\varepsilon}\,ln\varepsilon\right]^2 k_{12} \qquad \text{(III.71)}$$

and $\varepsilon = (k_1^2 + k_2^2)/2$ is the total energy of the two electrons.

III.4 References

[1] A. Lahmam-Bennani, H. Ehrhardt, C. Dupré, and A. Duguet, "Experimental evidence of correlated ionization," *J. Phys. B: At. Mol. Opt. Phys.* 24, 3645 (1991).
[2] C. D. Schröter, R. El Marji, A. Lahmam-Bennani, A. Duguet, M. Lecas, and L. Spielberger, "Fully differential cross sections for electron-impact ionization of helium," *J. Phys. B: At. Mol. Opt. Phys.* 36, 2591 (2003).
[3] L. Avaldi and G. Dawber, "Photoionization of atoms and molecules: Angular distributions," *Rep. Prog. Phys.* 59, 1571 (1996).
[4] L. Avaldi and A. Huetz, "Angular distributions in photoionization," *J. Phys. B: At. Mol. Opt. Phys.* 38, S861 (2005).
[5] H. Hda, C. Dal Cappello, and J. Langlois, "Theoretical study of correlated ionization," *Z. Phys. D* 29, 25 (1994).
[6] B. Joulakian, C. Dal Cappello, and M. Brauner, "Correlation effects in electron-impact ionization," *J. Phys. B: At. Mol. Opt. Phys.* 25, 2863 (1992).
[7] H. A. Bethe, "Zur Theorie des Durchgangs schneller Korpuskularstrahlen durch Materie," *Ann. Phys. (Leipzig)* 5, 325 (1930).
[8] E. Clementi and C. Roetti, "Roothaan–Hartree–Fock atomic wavefunctions," *At. Data Nucl. Data Tables* 14, 177 (1974).
[9] C. Dal Cappello, J. Langlois, M. C. Dal Cappello, B. Joulakian, A. Lahmam-Bennani, A. Duguet, and R. Tweed, "Electron correlation effects in ionizing collisions," *Z. Phys. D* 23, 389 (1992).
[10] I. Kada, C. Dal Cappello, and A. Mansouri, "Electron-impact ionization of atomic targets," *Eur. Phys. J. D* 71, 41 (2017).
[11] A. Herbadji, I. Kada, A. Mansouri, and C. Dal Cappello, "Fully differential cross sections for electron-impact ionization," *J. Phys. B: At. Mol. Opt. Phys.* 54, 215201 (2021).
[12] M. A. Kornberg and J. Miraglia, "Double ionization of helium by electron impact," *Phys. Rev. A* 48, 3714 (1989).
[13] B. Joulakian and C. Dal Cappello, "Electron correlation effects in atomic ionization," *Phys. Rev. A* 47, 3788 (1993).
[14] B. Joulakian, C. Dal Cappello, and M. Brauner, "Correlation effects in electron-impact ionization," *J. Phys. B: At. Mol. Opt. Phys.* 25, 2863 (1992).
[15] M. Chinoune, *Étude théorique des processus d'ionisation électronique*, Ph.D. thesis, Université Houari Boumediene, Algiers (2017).
[16] A. Herbadji, *Étude théorique des collisions ionisantes*, Ph.D. thesis, Université de Sétif-1, Algeria (2023).
[17] I. Kada, A. Mansouri, C. Dal Cappello, P. A. Hervieux, and A. C. Roy, "Electron-impact ionization dynamics," *J. Phys. B: At. Mol. Opt. Phys.* 42, 025201 (2009).
[18] S. J. Ward and J. H. Macek, "Electron-impact double ionization of helium," *Phys. Rev. A* 49, 1049 (1994).
[19] R. El Mir, E. M. Staicu Casagrande, A. Naja, C. Dal Cappello, S. Houamer, and F. El Omar, "Correlation effects in electron-impact ionization," *J. Phys. B: At. Mol. Opt. Phys.* 48, 175202 (2015).
[20] E. M. Staicu Casagrande, C. Li, A. Lahmam-Bennani, and C. Dal Cappello, "Electron correlation effects in (e,2e) ionization," *J. Phys. B: At. Mol. Opt. Phys.* 47, 115203 (2014).
[21] R. Moccia, "Configuration interaction in atomic systems," *J. Chem. Phys.* 40, 2176 (1964).
[22] T. A. Carlson and M. O. Krause, "Inner-shell ionization by electron impact," *Phys. Rev.* 140, 1057 (1965).
[23] M. Grin, C. Dal Cappello, R. El Mkhanter, and J. Rasch, "Theoretical study of electron-impact ionization," *J. Phys. B: At. Mol. Opt. Phys.* 33, 131 (2000).

CHAPTER FOUR

Results and discussions

IV.1 Introduction

In this chapter we represent our results about the double ionization of neon, krypton and methane. The main goal of this study is to validate the role of the initial and final states correlation description. In the calculation of the FDCS for the DI of neon and krypton, based on the first Born approximation, the correlation effects both in initial and final states are considered through the targets Interaction Configuration wave functions and post collision within distortion contributions models.

In the case of methane, the second order extension of the Born approximation is used to more explain and understand the influence of high order DI interaction. The final state correlations in the continuum is included under two versions of the approximate 3C model in order to assume the most appropriate description. In this model, each ejected electron is described by a Coulomb wave function. However, the mutual repulsion between these two electrons varies across the three BBK (3C) versions used here (2CWG) and (2CWWM).

IV.2 Results of electron impact double ionization of Neon

Recent studies have been realized on Neon [1-3] and compared with the experimental study of Schroter et al [4], which presents a groundbreaking experimental investigation of neon's double ionization (DI) dynamics under 5.5 keV electron impact. It should be noted that the experimental data are relative, and the ejection angles were measured with an uncertainty of $\Delta\theta = \pm 8°$. This significant remark will be considered when analyzing the FDCS maxima positions and identifying the DI mechanisms.

In 2017 Kada et al. [1] studied the double ionization (DI) of neon by fast electron impact (5582.6 eV) using the First Born Approximation (FBA) and the 3C model for all possible ion states ($2p^{++}$)-(^{3}P, ^{1}D, ^{1}S), and ($2s^{-1}2p^{-5}$)-(^{3}P). The authors show that initial state description didn't strongly affect the FDCS distribution for neon, unlike in previous studies on argon and krypton. While the 3C model broadly matches experimental trends, it underestimates certain peaks, suggesting the need for improved final-state descriptions using distorted waves.

After that Herbadji et al.[2-3] investigates the double ionization (DI) of argon by fast electron impact (~5500 eV) using the First Born Approximation (FBA)**,** and various theoretical models: BBK model**,** 2CWG/2CWGSR and 2DWG/2DWGSR (distorted waves with Gamow factor ± short-range potential). The latter model, incorporating partial electron correlation in both initial (via Hartree-Fock and configuration interaction wave functions) and final states (via Gamow factor), provided the best agreement with experimental data. The study underscores the importance of distorted-wave models and initial-state correlation for accurately describing DI in complex targets, suggesting further refinements for better predictive power.

In this part, we study the (e,3e)-Ne by high electron impact at 5.5 keV, in a symmetric regime (E_1=E_2=10 eV), and coplanar geometry under the first Born approximation by use of different models including both correlation and distortion effects.

We focus some interesting ejection situations:

- One ejection is along the direction of the momentum transfer (here it is closed to $\theta_{-K} = 134°$ and$\theta_{+K} = 314°$). These cases are important because of the symmetric shape around the momentum transfer owing to the first Born term contribution. Indeed, when this symmetry is broken it is usually needed to take the second Born approximation term [5-6] into account.
- One electron is ejected either 110◦, or 150◦ or 330◦. These specific choices let us to analyze the behavior of the angular distribution of the FDCS if one electron is ejected in the different intervals: $[O°, -\vec{K}]$; $[-\vec{K}, +\vec{K}]$; $[+\vec{K}; 360°]$.

Firstly, we present our results obtained by the BBK model for various ejection angles of one of the two outgoing electrons. Then we show results of the 2DWG model in the same previous conditions.

Figure 4-1 represents the five differential cross section of (e,3e)-Ne($2p^6$) as function of θ_2 for $\theta_1 = 134°$and $\theta_1 = 150°$.

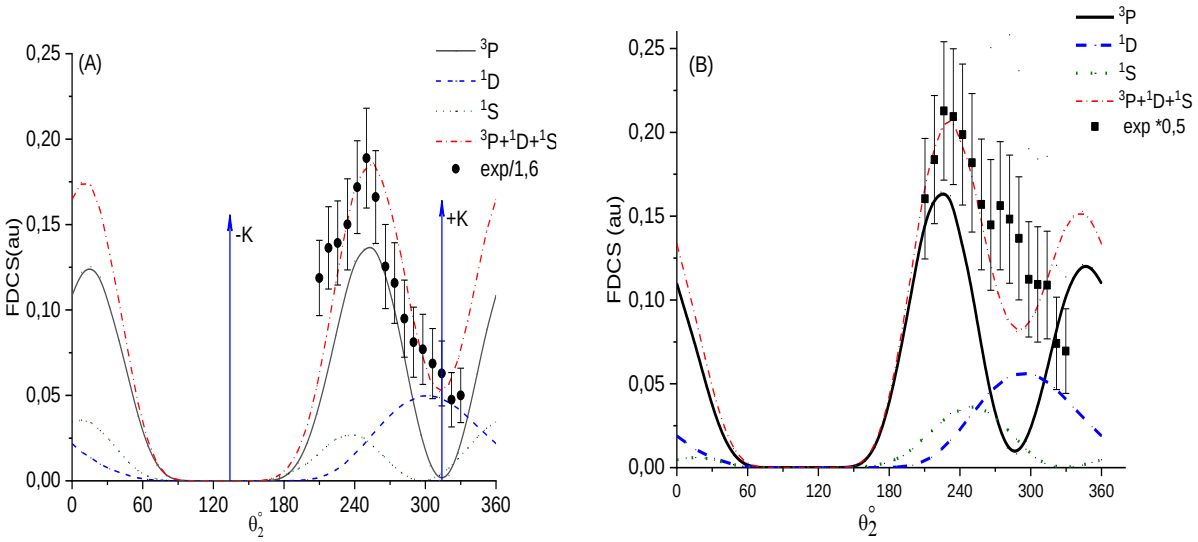

Figure 4-1: FDCS for DI of Neon with the BBK and interaction configuration model. Es=5500eV, $E_1 = E_2 = 10$eV, θs=0.45° θ_2 is variable and $\theta_1 = \theta_{-K} = 134°$ in (A) and $\theta_1 = 110°$ in (B),. Ion states-contribution: ^{3}P in full black line; ^{1}D in bleu dashed line; ^{1}S in green dotted line and the sum(^{3}P+^{1}D+^{1}S) in red dash-dotted line. The experimental data [4] in squares are normalized to the sum curve. The arrows are the transfer momentum and its opposite directions.

The FDCS distribution for θ_1=134°(**Fig4-1(A)**) reveals important key angular features: a symmetric form about the opposite moment transfer direction θ_{-K}=134°which constitute the main observation when using FBA, accompanied by a large minimum going around this direction due to the strong repulsion between the two ejected electrons having the same energy. The ^{3}P state exhibits two meaningful peaks: a forward peak at 20° and a second one at 250°, which result in a forward and a backward TS1 process respectively. We remark no significant structure at θ_K=314° indicating the absence of the back to back emission of the SO mechanism in this situation. The ^{1}D state dominates through a single peak at θ_2=300° maintaining the shape of the experience points in this region, where the ^{3}P curve shows a zero magnitude minimum. This ^{1}D maximum is due to the SO mechanism since $\Delta\theta = 170°(\approx 180°$ with back to back emission if we consider the measures uncertainty). However the ^{1}S state contributes only baseline enhancements at 20°and 240° as it was mentioned previously

[1]. The most important observation is that the sum curve confides with the experience peak both in position and magnitude. The two maxima can be attributed to TS1 mechanism with forward emission for the first peak located at θ_2=20° and backward emission for the second one at θ_2=250°. In this two-step reaction the fast projectile interacts once time with an active electron of the target which will collides with the neighbor one and ejects it when leaving the target.

This FDCS analysis for θ_1=110° **(**Figure 4-1(B)) reveals how the combined contributions of the Ne($2p^{++}$)-(^{3}P, ^{1}D,^{1}S) states reproduce the experimental data with varying degrees of success. The summed theoretical prediction shows excellent agreement with experiment between 200°–270°, where the ^{3}P's 220° peak and the ^{1}D's rising contribution create a near-perfect match to the measured data. The ^{1}S state plays a crucial bridging role, adding subtle but important intensity that smooths the transition between the dominant peaks, its broad enhancement at 245° accounts for half of the residual forward-angle emission, though it still underestimates the experimental values. The ^{1}D peak is located at 290°, with an amplitude that slightly overpredicts the measurements. The analysis of this peak separately expects an ejection near the transfer direction explained by a back to back emission of the SO mechanism.

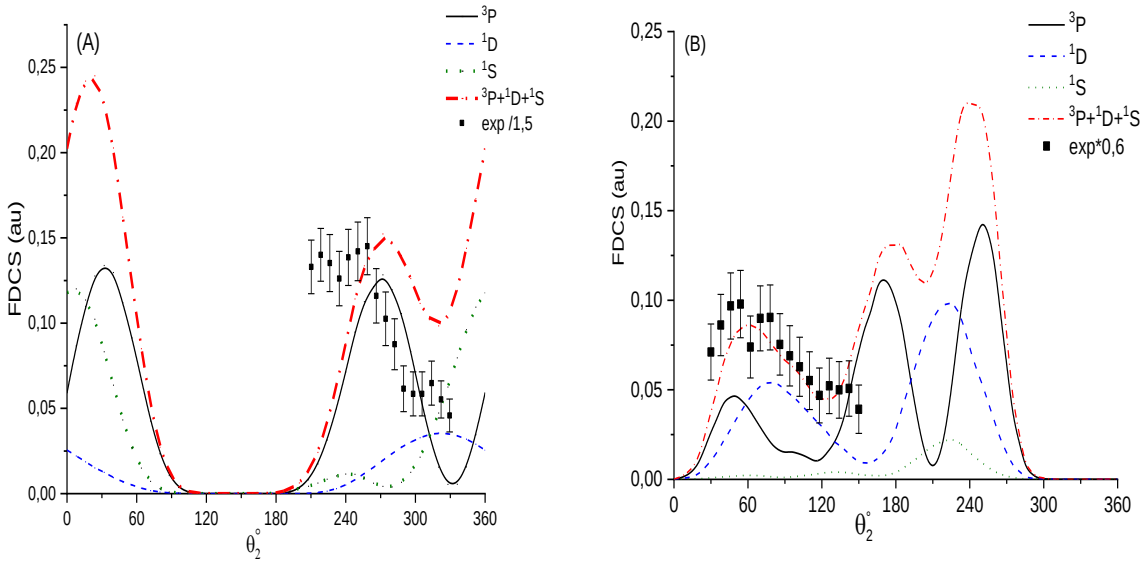

Figure 4-2: Same as figure 4-1 for the detection angle (A) θ_1=150° and (B) θ_1=330°

Figure4-2 (A) illustrates the FDCS in the case of θ_1=150° for the same conditions as in figure 4-1(A) through the BBK model framework. The plot discloses main insights into the underlying mechanisms and total ion state contributions when analyzed the symmetric low-energy ejection (E_1=E_2=10 eV) at high incident energy (5500 eV) strongly suggests shake-off (SO) as the dominant mechanism. In contrast, the first peak can't be characterized by expected SO emission since the mutual angle is about 130° (θ_2=20° relative to θ_1=150°) which is explained by the TS1 forward detection as provided by Schroter et al [4]. The theoretical angular distribution shows a second peak given by the sum of all ion states contribution (^{3}P+^{1}D+^{1}S) at θ_1=270° in good agreement with the experience. This maximum is due to a backward emission of the TS1 reaction. In other we distinct signatures from different Ne^{++} residual ion states: the ^{3}P state provides the dominant broad maxima in the both regions, the ^{1}D state enhances intensity near

momentum transfer direction (θ_K=314°), while the minor ^{1}S state contributes to background features by displaying an important maximum at 350°du to the SO contribution.

In this case θ_1=330°, the FDCS makes crucial angular dependencies through distinct theoretical contributions. The global FDCS (^{3}P+^{1}D+^{1}S) reproduce the experimental hump from θ_2=30° to θ_2=120°; containing the peak situated at 60° which can be due to a TS1 forward emission such as $\Delta\theta_{12} = 270°$. The second peak; at 177°; in this distribution should results from an interference process of the SO and TS1 mechanisms, while the third one situated at242° can be attributed to a backward ejection of the TS1 reaction. In a separating contribution analyze, the ^{3}P state (black line) displays a many-peak structure at θ_2 =47°, θ_2 =170° and θ_2 = 250° that suggests back to back emission, SO -TS1 interferences and TS1 backward ejection respectively. Meanwhile, the ^{1}D state (dashed line) shows stronger participation to both first and third peaks of the global ion contribution. The ^{1}S state (dotted line) contributes more diffusely, with a broad 135° maximum. When combined, these predictions (dot-dashed line) show good agreement with the experimental data. The enhanced 76° peak and the shallow 150° dip of a SO ejection are not captured by the theory. This may indicate limitations in the BBK model's treatment of angular correlations, or it may suggest that there are minor contributions from unaccounted mechanisms. While the overall angular patterns confirm shake-off as the dominant process, these persistent differences highlight the need for more sophisticated treatments of electron-electron interactions, particularly at intermediate angles where the current model shows reduced accuracy.

We conclude that the BBK model shows a good agreement with experimental data, particularly by the angular distribution of all ion state contributions. We can see the important contribution of the ^{3}P state in the process, the other might have a lesser impact but are nonetheless significant as they consider the electron-electron correlation, though potential refinements using distorted wave approaches could further improve accuracy, particularly in reproducing finer angular distribution details. The higher-energy $2s^{-1}2p^{-1}$ ^{3}P state, though less prominent, may introduce subtle modifications to the minima and maxima characteristics. These observations align with Kada et al.'s [1] findings that comprehensive agreement with experimental data requires summing contributions from all accessible ion states.

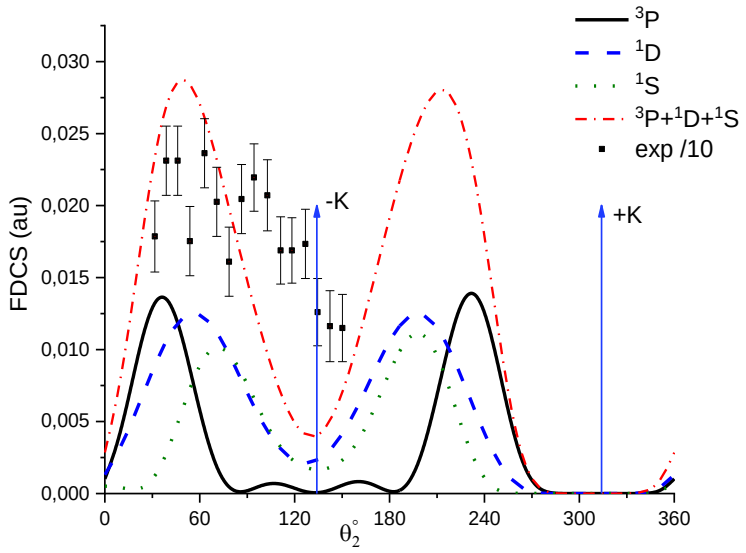

Figure 4-3: The FDCS for the double ionization of Neon with the 2DWG and interaction of configuration model. Es=5500eV, E_1 and E_2=10eV, θs=0.45°, θ_1= θ_K=314°, the other one is detected at variable angle. Contribution of: ^{3}P in black full line; ^{1}D in blue dashed line, ^{1}S in green dotted line (^{3}P+^{1}D+^{1}S) in red dash-dotted line. The experimental data [4] in squares are normalized to the global contribution curve. The arrows are the transfer momentum and its opposite directions.

In figure 4-3 we represent the FDCS-Ne($2P^{++}$) obtained with the 2DWG-IC model when one ejected electron is detected along the transfer momentum direction. The first attractive remark in this plot is the decreasing of the FDCS magnitude (max amplitude 0.03 au) which reveals nuanced reasons in neon's double ionization. The observation of the angular distributions shows a saved symmetric shape over the transfer direction, owing to the FBA use, in all curves displays. The global contribution curve aligns the experimental one just in the form but not in the position and magnitude. Separating each ion state FDCS, ^{3}P state (solid line) contribution maintains perfectly symmetric peaks at 36° and 230°, both 0.013au du to a shake off emission. Each one of ^{1}D (dashed line) and ^{1}S (dotted line) states contribute with defined two peaks (θ_2=55°, θ_2=196°) and (θ_2=75°, θ_2=196°) respectively where the first ones are resulting by a forward emission and the second ones with backward emission.

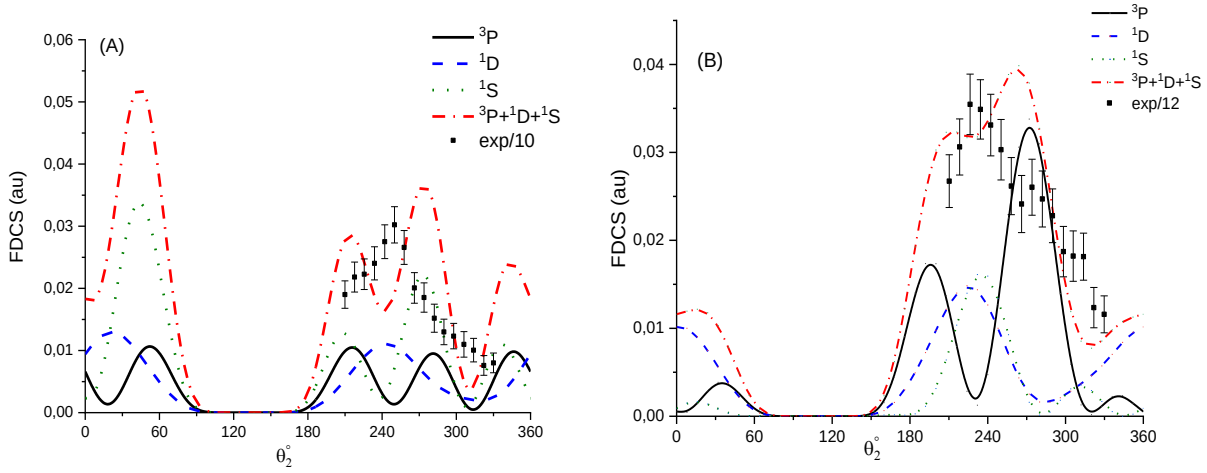

Figure4-4: same as figure 4-3 except for the detection angles: (A) θ_1=134° and (B) θ_1=110°

The 2DWG model calculation for neon($2P^{++}$) double ionization when θ_1 fixed at 134° exposes distinct angular distributions. The ^3P, ^1D, ^1S valence contributions show a pronounced many-peaks structure, which allows to a combined theoretical curve ($^3P+^1D+^1S$) slightly matching the experimental data with an important primary maximum at 43° resulting from a forward TS1 reaction. The others peaks located between-***K*** and ***+K*** (at 214°, 273°, 344°) are of less magnitude where the first and the third ones are described by a SO process while the middle one should be resulting from the interferences of SO and TS1.

For the FDCS with a fixed detection angle of θ_1=110°, reveals distinct angular dependencies in the ionization dynamics. The global ($^3P+^1D+^1S$) FDCS curve follows almost similar behavior but with reduced intensity. A significant discrepancy is produced in this situation between experimental data, scaled down by a factor of 12, and the theoretical curves. This suggests potential limitations in the model's treatment of post-collision interactions or experimental resolution effects. The 2DW model's Gamow factor approximation for PCI may inadequately capture the full electron-electron repulsion at the low ejection energy of 10 eV, but with an overestimation of both the maximums magnitude and positions.

If comparing with figure 4-1 we can deduce the differences included by the 2DWG model but overestimates its magnitude, requiring a 10× experimental scaling factor. This scaling suggests either an overestimation in the theoretical cross-section or potential experimental normalization issues. The model successfully reproduces the angular distribution's shape but appears to exaggerate contributions from certain ionization channels. Notably, the absence of the $2s^{-1}2p^{-1}$ ^3P state contribution in this analysis - which was found to improve agreement in Kada's 3C model study - might explain remaining discrepancies.

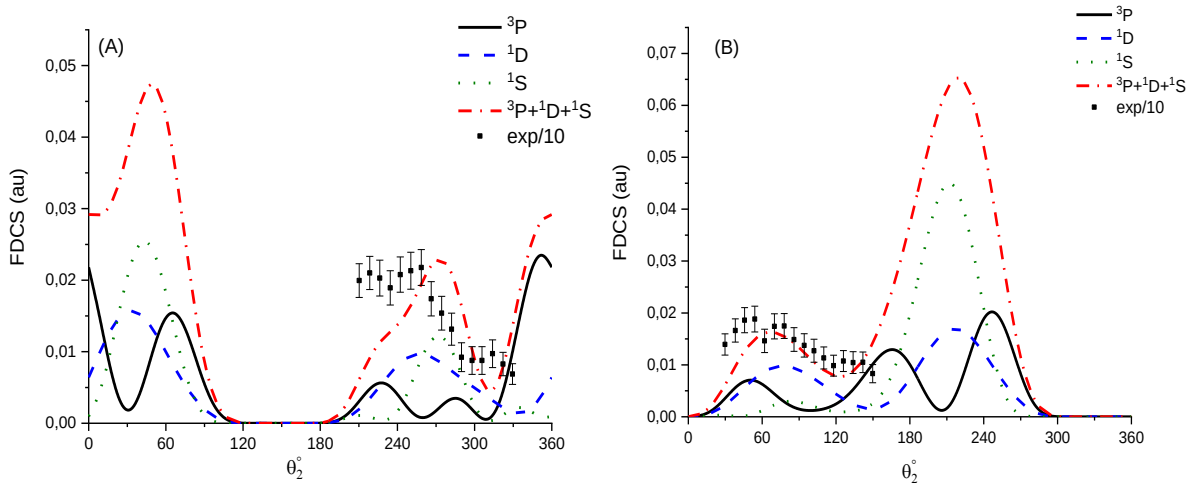

Figure 4-5: same as figure 4-3 except for the detection angle: (A) θ_1=150°, (B) θ_1=330°

The FDCS plot for neon double ionization at 5500 eV with fixed detection angle θ_1=150° demonstrates several key features of the ionization dynamics. We note discrepancies of the second global peak position(at272°), being previously in good agreement with experimental data fig4-2(A). In other, new maxima appear on the ^3P theoretical graphs with various magnitude showing the possibility of new DI reaction for ejection angles between ***-K*** and ***+K*** directions. The ^3P contribution (solid line) exhibits a dominant peak at 350° with secondary maxima at 64° and two others with less magnitude at 225° and 285°. Three of these maximums

(those seen at 64° 225°, and 350°) are well represented by SO process such as $\Delta\theta_{12} \leq 90°$, and $130° \leq \Delta\theta_{12}$ while the smallest one (285°) results in a TS1emission. However the ^{1}D state shows a pronounced twoTS1 peaks at 32° and 262°. Another interesting remark consist on the ^{1}S contribution which exposes two displaced peaks (about fig4-2) situated at 43° and 271° indicating TS1-forward and backward emission respectively.

The last case in this series is the FDCS plot for fixed detection angle θ_1=330°. The theoretical distribution of the global ion contribution discloses an important agreement with experience shape and maxima. We remark the disappearance of second peak observing in the FDCS within BBK model (fig4-2), but the theoretical curve successfully reproduces the experimental data structure, though with some positional shifts and amplitude discrepancies. The required 10× experimental scaling factor, consistent across all detection angles studied, suggests either a systematic overestimation in the theoretical cross-section magnitude or potential experimental normalization issues.

Notably, the 2DWG model fails to capture the experimental feature at some situation, suggesting missing physics in either the initial-state correlations or final-state interactions. The ^{3}P state's strong contribution accompanied by an important participation of the ^{1}S state, help align the theoretical peak position with experiment, though the amplitude discrepancy persists.

IV.3 Double ionization of Krypton by electron impact

In 1994, Hda et al [7] proposed a study in which they calculated the fivefold differential cross sections for the reaction (e,3e) of Krypton at 5 keV under the first Born approximation. The model incorporates both initial-state correlation via multi-configuration wavefunctions and final-state electrons correlations using an approximate BBK wavefunction for the ejected electrons. The model included the Gamow factor to describe the repulsion between the two ejected electrons. Key findings show the dominant contribution of the ^{3}P ionic state and the critical role of the $4d^2$ configuration (Langlois function not published) in the initial state. The results demonstrate good agreement with early experimental data, highlighting the importance of correlation effects and final state interactions in describing the angular distributions of ejected electrons. The work underscores the necessity of beyond Hartree-Fock methods for accurate modeling of double ionization dynamics.

In this section we present our results about the DI-Krypton using the first Born approximation and two version of the BBK model: 2CWG and 2DWG and by representing the initial state of krypton atom by an interaction of configuration of the Clementi-HF wave function. The calculation is realized under different kinematic conditions of Lahmam Bennani et al [8] experience.

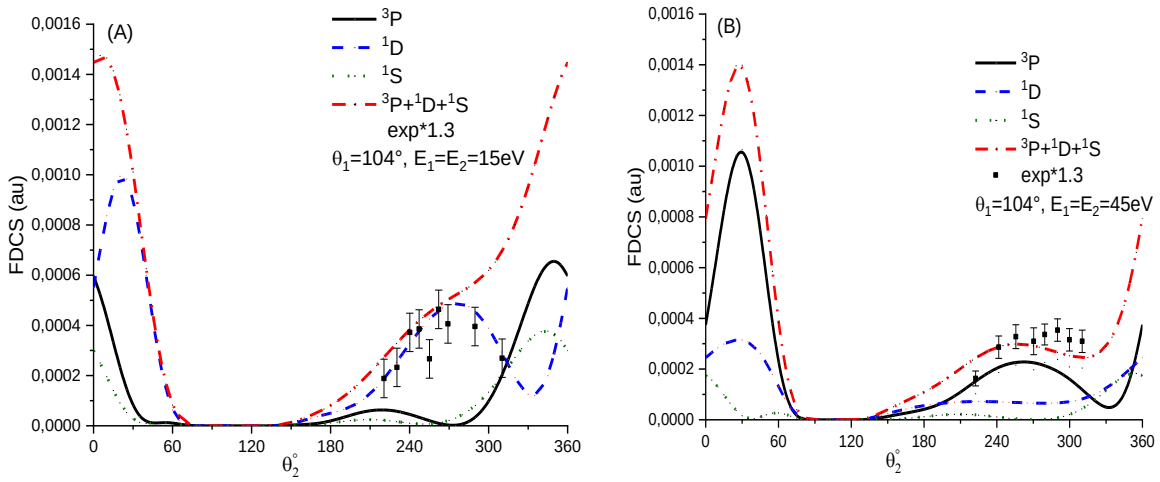

Figure4-6: FDCS for double ionization of Kr with 2CWG and interaction configuration model. Es=5,5KeV, $\theta_s = -1°$ and $\theta_1 = 104°$, the other one is detected at variable angle, in (A) E_1= E_2=15eV, in (B) E_1= E_2=45eV. Contribution of: ^{3}P in black full line; ^{1}D in blue dashed line, ^{1}S in green dotted line (^{3}P+^{1}D+^{1}S) in red dash-dotted line. The experimental data [8] in squares are normalized to the global contribution curve.

The **figure 4-6(A)** shows the FDCS for DI of krypton at a high incident energy of about 5,6KeV in coplanar geometry and symmetric regime E_1=E_2=15eV when one electron is detected at 104°. The angular distribution of the global contribution exhibits a strong peak at $\theta_1 = 6°$ by a forward emission of the TS1process.The minimum extended from 70° to 150° shows the role of the Gamow factor in introducing the repulsion of the ejected electrons with a significant over estimation of the FDCS magnitude [7]. In this case the ^{1}D contribution dominate the FDCS maximum comparing with ^{3}P state, while the ^{1}S influence remains weak that make it negligible.

The observations likely due to the limited configuration space and the neglect of post collision interaction and experimental resolution effects. Overall, the calculation captures the essential physics of the process and reproduces the experimental behavior in the measured angular region.

In the case of the second quasi sharing energy (45ev for each ejected electron) the structure of the FDCS distribution has roughly the same shape of the 15ev sharing case, but dominated by a strong peak comes mainly from the ^{3}P channel, while the ^{1}D and ^{1}S contributions stay small at almost all angles. The first maximum on the sum curve seeing at 27° as combination of ^{3}P and ^{1}D maxima can be explained by a shake off ejection where the fast projectile collides with one of the active electrons of the krypton atom and ejects it along 104°. The second ejected electron leaves the target in its potential reorganization. A broad maximum appears between 240° and 270°located at 256°, close to the region of the experimental data, is due to interferences between SO and TS1processes. The theory gives slightly higher values than the measurements even after applying the 1.3 scaling.

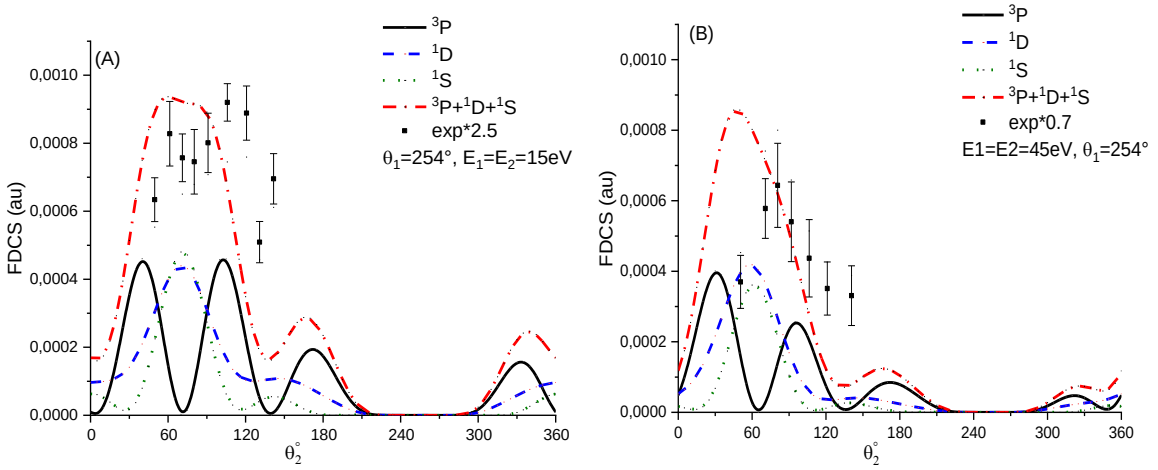

Figure 4-7: same as figure 4-6 except the fixed detection angle is $\boldsymbol{\theta_1 = 254°}$

In this Figure4-7(A-B), the FDCS shows two main changes: a decreasing of the maxima magnitudes for all states (^{3}P, ^{1}D and the sum) except for those of ^{1}S contribution which increase and confides here with the ^{1}D curve. The second remark is apparition of many peaks structure in the ^{3}P and the global distributions. In the case(A) $\theta_1 = 254°$and E_1=E_2= 15eV; The (^{3}P+^{1}D+^{1}S) graph aligns just the first maximum of the experience located at 61°. This latest looks as a back to back emission of the SO process. The two other maxima exposed at: $\theta_1 = 166°$and $\theta_1 = 340°$ are due to a pure backward TS1 and a back to back shake off ejection (close to $\Delta\theta_{12} = 180°$) respectively. In figure(B) we observe a significant discrepancy in both position and magnitude of the global ion contribution maximum (at 47°) over the experimental peak situated at $\theta_1 = 80°$. These peaks correspond to the Shake off mechanism.
Individually, the ^{3}P, ^{1}D, and ^{1}S channels each contribute with different shapes and intensities. The ^{3}P channel dominates and determines the overall double–peak structure, while the ^{1}D and ^{1}S channels add high side contributions when that of the ^{3}P is minimum (first maximum confused with the ^{3}P minimum).

Overall, the agreement confirms that the main ionization mechanism here is shake-off assisted by electron-electron repulsion, where the sudden removal of one electron perturbs the system strongly enough to release the second electron ejection, with observed forward and backward lobes arising from the underlying binary recoil scattering dynamics.

The last part in the study of double ionization of noble gases contains our results about the (e,3e) reaction on krypton under the first Born approximation using the 2DWG model. In this model each ejected electron is represented by a coulomb wave function with a variable charge Z(r). Both correlation in the initial state and in the final state are included trough the interaction of configuration wave function of the ionic target Kr($4p^{++}$) and the distorted wave function of the ejected electrons adding to the post collision repulsion introduced by the Gamow factor.

We limit our calculation to previous cases studied within the 2CWG in order to validate the role of correlation, distortion and post collision effects on the behavior of the FDCS.

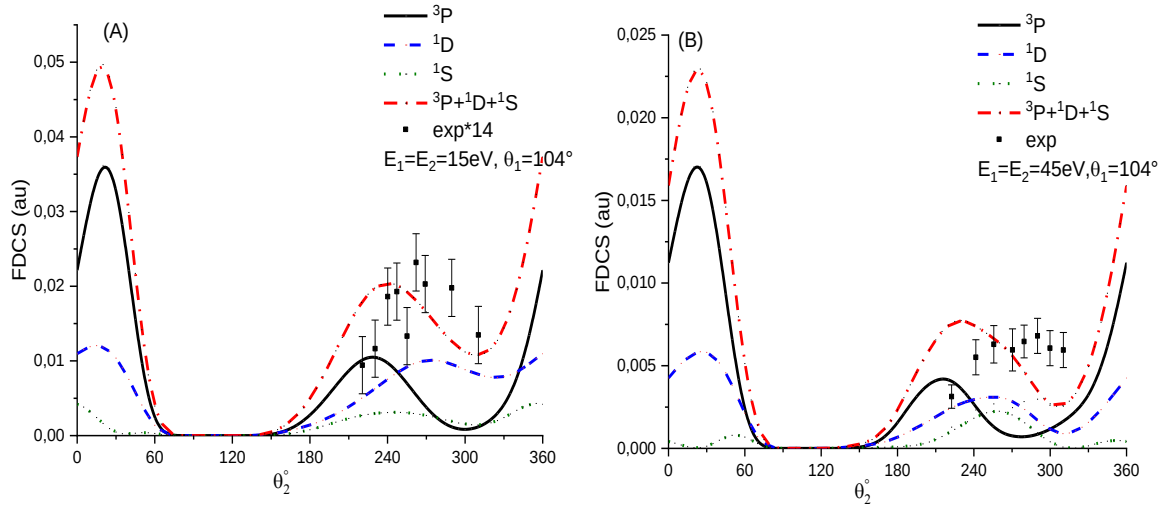

Figure4-8: FDCS for double ionization of Kr with 2DWG and interaction configuration model. Es=5,5KeV, $\theta_s = -1°$ and $\theta_1 = 104°$, the other one is detected at variable angle, in (A) E_1= E_2=15eV, in (B) E_1= E_2=45eV. Contribution of: ^{3}P in black full line; ^{1}D in blue dashed line, ^{1}S in green dotted line (^{3}P+^{1}D+^{1}S) in red dash-dotted line. The experimental data [8] in squares are normalized to the global contribution curve.

In figure4-8(A), the FDCS distribution of the coherent sum (^{3}P+^{1}D +^{1}S), shows a double peak structure containing a very strong peak at small ejection angle $\theta_2 = 19°$ and a broad secondary maximum at $\theta_2 = 240°$ which is almost in good agreement with the experimental points. The first peak can be attributed to a SO process although it checks out a mutual angle ($\Delta\theta_{12} = 85°$) roughly due to TS1 emission. However, the second maximum corresponds to a backward ejection of TS1 mechanism according to Shroter et al [4]. In the analyze of partial ion state contribution the ^{3}P state dominate largely the sum curve peaks both in position and in magnitude. The ^{1}D adds noticeable strength in the mid/back region, and the ^{1}S contribution is small throughout; therefore, these contributions set the overall envelope and raise the peak heights through summation. The calculation reproduces the experimental peak positions reasonably well but tends to overshoot the magnitudes this is likely because the IC is limited to a few configurations.

In the case of energy sharing 45eV(fig4-8B) the FDCS shows almost the same shape of the previous FDCS in the case of 15eV ejected electrons and of the corresponding experimental data especially at large ejection angles, despite the discrepancy of the second peak position.

The ^{3}P individual participation (black curve) is the main contributor and sets the SO dominance. The ^{1}D (dashed line) adds strength in the mid/back region, and the ^{1}S (green line) is negligible. The calculation reproduces the general shape but somewhat overestimates the peak heights and positions.

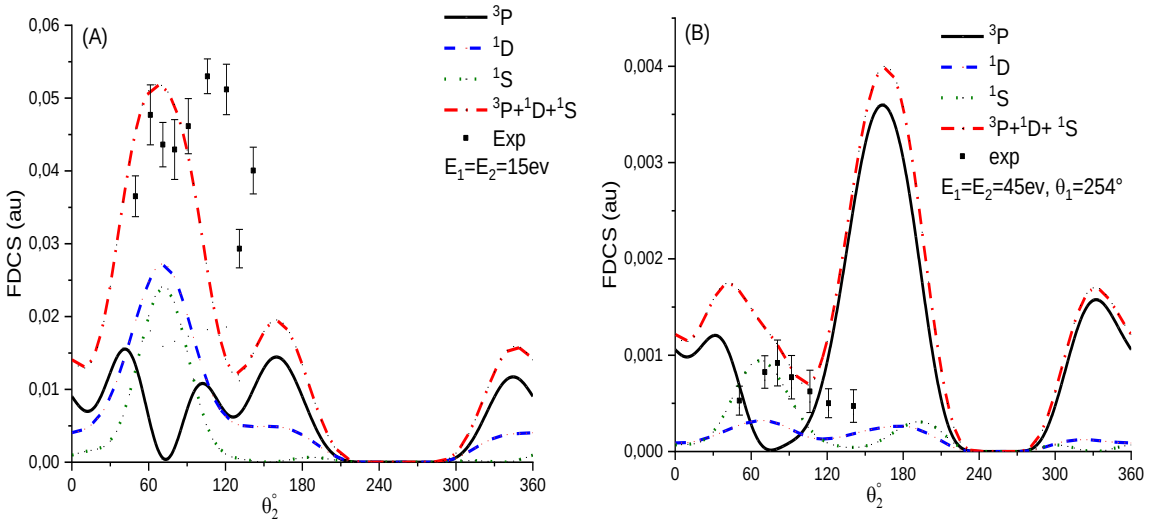

Figure4-9: same as figure 4-8 except the fixed detection angle is $\boldsymbol{\theta_1 = 254°}$

The plotted theoretical curve in figure 4-9(A) accurately predicts the shape and position of the main lobe, which appears around 70°, and it closely aligns with the experimental data in this angular range. The magnitude of the FDCS is here increasing when comparing with that obtained within the 2CWG model (known by its underestimation of FDCS magnitude). This strong agreement validates the 2DWG model's aptitude to account for the complex final-state interactions, including the repulsion between the two low-energy ejected electrons. The graph also decomposes the total FDCS into contributions from the three final states of the Kr^{+2} ion ^{3}P, ^{1}D, and ^{1}S showing that the ^{3}P ground state is the most probable outcome. However, a noticeable discrepancy exists in the secondary lobe at angles greater than 120°, where the theoretical model slightly underestimates the magnitude of the experimental results. This indicates that while the 2DWG model is highly effective, it may not fully capture all the intricacies of the electron-electron or electron-ion interactions in this specific configuration, pointing toward the need for further theoretical refinement.

the 2DWG FDCS in the (B) figure shows: a large central peak centered around 170°, a smaller maximum at 41°**,** and a modest feature around 330°. The black (^{3}P) curve is the main contributor and sets the shape of the large central peak, while the ^{1}D (blue-dashed) and ^{1}S (green-dotted) contributions are much weaker. The full sum graph lies slightly above the ^{3}P line because of constructive interference. The experimental data fall under the theoretical results, so the calculation reproduces the general angular pattern but overestimates the absolute height of the main peak. The angular pattern is consistent with a shake-off process for the first and third peaks however the central large peak looks almost due to TS1backward emission precisely if considering the uncertainty of the measured points.

Across the different FDCS graphs, the results show that the 3p contribution dominates the double ionization process, while the 1d and 1s channels remain comparatively weak. The summed (^{3}P+^{1}D+^{1}S) curves generally reproduce the main features of the measured data, but the theoretical peaks are often sharper and higher, mainly because experimental resolution and post collision effects are not fully accounted for. Overall, the comparison highlights a good qualitative agreement. The angular positions and general shapes are consistent with experiment, yet a quantitative discrepancy persists, underlining the need for improved theoretical treatments and resolution folding to better match experimental observations.

IV.4 Application to double ionization of Methane-CH4

This section is dedicated to a new study of the double ionization of molecules that play an important role in many areas of physics. Recently, researchers in both experimental [9] and theoretical [10–12] investigations have been attracted to the double ionization of methane molecules. Staicu et al. [9] compared (e,3-1e) measurements for the neon atom and the methane molecule as iso- electronic systems. This study confirmed the hypothesis that the TS2 mechanism is involved in the double ionization process at intermediate impact energies (below 1 keV), as observed in the case of helium atom [13] and water molecule [14]. El Mir et al. [10] compared the CH_4(e,3-1e) reaction experimental results with the those of the approximate 3C model using the first Born approximation and two repulsion factors: the standard Gamow factor [7] and its corrected version of Ward and Macek [15]. The authors concluded that the theory could only align part of the fourfold differential cross section (4DCS) which is related to the first Born order contribution: the shake-off and TS1 reactions. The study reveals discrepancies between the experience and theories used here, in cases of asymmetric energy sharing (37 eV and 12 eV), due to apparition of new structures in the measured 4DCS, but absent in the theoretical distribution, indicating the existence of the TS2 reaction, and so needs the application of the second Born approximation. More recently, the results obtained for the double ionization of oriented methane molecule [11-12] demonstrate the significant role of target orientation when examining the contributions of the SO and TS1 mechanisms in isolation.

We present new findings on the five-differential cross section (FDCS) of (e,3e) reaction on methane molecule by fast electrons. Our calculation was performed within second Born approximation extension. The main goal of this study is to identify the different mechanisms responsible of the double ionization process and to isolate, if possible the contribution of the second order interaction. In the initial state the target is described by the old function of Moccia [9] which represent a good background of a single-center XHn-molecules wave functions. The final state is represented using to versions of the approximate 3C model: 2CWG model with the Gamow factor, then 2CWWM with the Ward and Macek factor as a corrected version. The findings are obtained for specific kinematic conditions [9-10].

Figure 4-10 shows a surface plot of the FDCS angular distribution of (e,3e)-CH_4 reaction as function of the ejection angles (θ_1, θ_2) at intermediate electron impact of 612eV, for two ejection energies sharing: **(a)** 12-37eV and **(b)** 37-37eV. The scattered electron is detected at -6°. The calculation is performed under the first Born approximation by use of the 2CWG model.

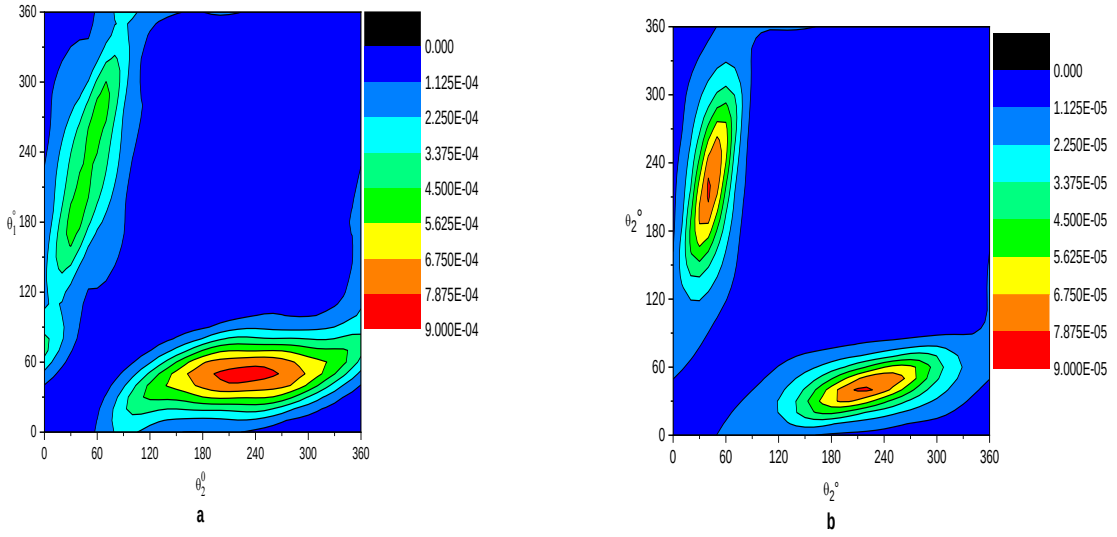

Figure 4-10: Fivefold differential cross section (FDCS) for the double ionization of methane molecular orbital t2z as a function($\boldsymbol{\theta_1, \theta_2}$). The scattered angle $\boldsymbol{\theta_s = -6°}$, the incident electron energy is$\boldsymbol{E_i}$ =612eV. In (a): E_1=12eV , E_2=37eV, in (b): $E_1 = E_2$=37eV. **The FDCS is obtained with the first Born approximation and the 2CWG model.**

The angular distribution is limited to two lobes in the region$\theta_1 = 60° \rightarrow 360°(\theta_2 = 0° \rightarrow 70°)$ and. $\theta_1 = 0° \rightarrow 90°(\theta_2 = 80° \rightarrow 360°)$ The maximum is located on the first hill. $(\theta_1; \theta_2) = (50°, 225°)$. Assuming that the TS1 is the responsible process, the interaction we can propose here consists of the first electron ejection in the direction of $-\vec{K}$ $(\theta_{-K} = 230°, \theta_{+K} = 50°)$, This will then collide with and eject another electron from the target, forming the second step of TS1. In our case, it is the slower electron that is ejected at $\theta_1 = \theta_{+K} \cong 50°$and The faster one is emitted along $\theta_2 = \theta_{-K} \cong 230°$ such as $|\theta_1 - \theta_2| \approx 180°$ This means that the TS1 is not the dominant mechanism, but this result can be attributed to the SO process, which dominates due to back-to-back emission.

In Figure 4-10(b); same as fig-4-10(a) but for E_1 = E_2=37eV; We observe two large symmetrical hills extended form $\theta_1 = 0° \rightarrow 80°(\theta_2 = 50° \rightarrow 360°)$ and from $\theta_1 = 50° \rightarrow 350°(\theta_2 = 0° \rightarrow 80°)$ where the maxima are localized at $(\theta_1, \theta_2) = (40°, 220°)$ and symmetrically at $(\theta_1, \theta_2) = (220°, 40°)$ such as $|\theta_1 - \theta_2| = 180°$. In this case, the emission is back-to-back due to the SO mechanism along the transfer direction $+\vec{K}$ $(\theta_{+K} \cong 42°$ and $\theta_{-K} \cong 222°)$.

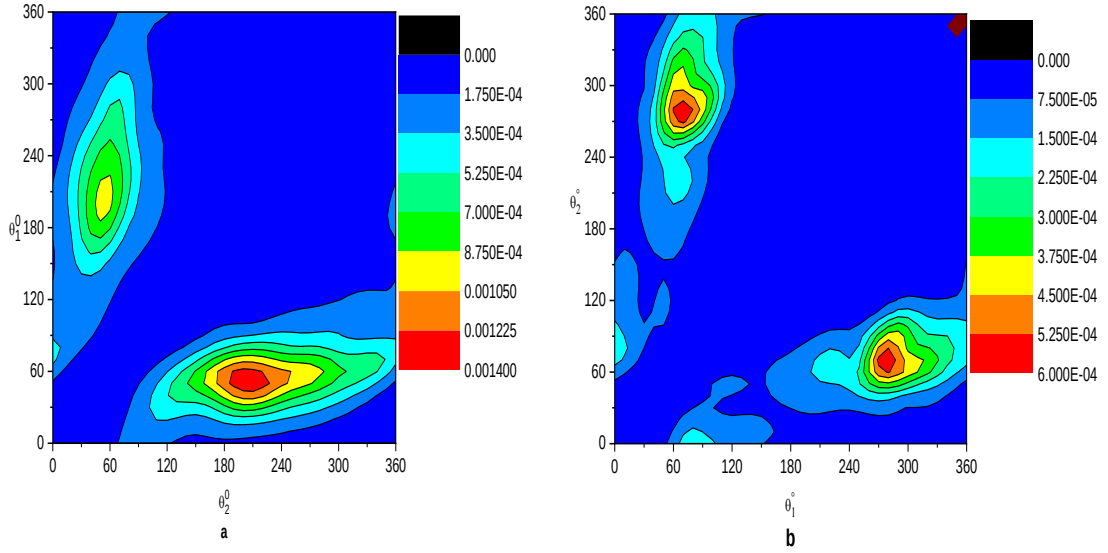

Figure 4-11: Fivefold differential cross section (FDCS) for the double ionization of methane molecular orbital t2z as a function(θ_1, θ_2). The scattered angle$\theta_s = -6°$and the incident electron energy is E_i =612eV. In figure (a): E1=12eV , E2=37eV, and in figure (b): E1 = E2=37eV. **The FDCS is obtained with the second Born approximation and the 2CWG model.**

In figure 4-11 We present a plot of the fivefold angular distribution of the (e,3e) reaction on the t_{2z}-CH_4 orbital, within the second Born approximation and the A3CG model. The kinematical conditions are the same as in fig4-10(a) (for E_1=12eV and E_2=37eV).

In figure (a) The FDCS is represented by two hills extending from $\theta_1 = 150° \rightarrow 300°$(and $\theta_2 = 40° \rightarrow 90°$) for the first hill and from $\theta_1 = 10° \rightarrow 80°$(and $\theta_2 = 100° \rightarrow 360°$) for the second one, where the maximum is localized at $(\theta_1, \theta_2) = (50°, 200°)$ There has been a significant increase in the corresponding amplitude. This situation can be explained by the interference of the TS1 and SO mechanisms, as well as the destructive effect of the TS2, which is characterized by two successive interactions between the incident electron and two target electrons, resulting in their ejection. On the other hand, the second hill has a maximum at $(\theta_1, \theta_2) = (210°, 40°)$with a lower amplitude mainly explained by a dominant SO process.

Figure (b) corresponds to the FDCS of t2z-CH4 double ionization in asymmetric regime (E_1= E_2=37eV). The surface shows two symmetric groups of maxima: a first one extending from $\theta_1 = 40° \rightarrow 100°(\theta_2 = 200° \rightarrow 360°)$ and a symmetric one from $\theta_1 = 200° \rightarrow 360°(\theta_2 = 40° \rightarrow 100°)$ while the maxima are situated at $(\theta_1, \theta_2) = (70°, 280°)$ and symmetrically. The most important observation is that the position of the maximum has shifted and the amplitude has increased, which can be explained by the TS2 contribution. In this case, we can suggest a model in which two successive collisions occur in two stages. The first ejection along $\theta_1 = 70°$ is characterized by an intermediate scattering electron at $\theta_{s1} = -20°$ result after a fast elastic collision since $|\theta_1 - \theta_{s1}| = 90°$between the projectile and one active electron, nevertheless a second electron is ejected during a quasi-elastic collision such as $|\theta_2 - \theta_s| = 280°$ with a second scattered angle $\theta_{s2} = +14°$ in sort that we get $\theta_{s1} + \theta_{s2} = \theta_s = -6°$. However, a similar result was obtained for the (e, 3-1e)-CH_4 experiment [6], in which one of the 37 eV electrons (in the case of symmetrical ejection sharing) and the slower 12 eV electron (in the case of unequal emission energy) were not detected. The TS2 contribution was clearly visible in the 4DCS distribution in various cases, particularly where additional structures appeared on the measurement curve $\theta_b \in [70° - 100°]$ and $\theta_b \in [220° -$

280°], However, the model used in this study could not predict the structures explained by the TS2 mechanism, as it was based on FBA term.

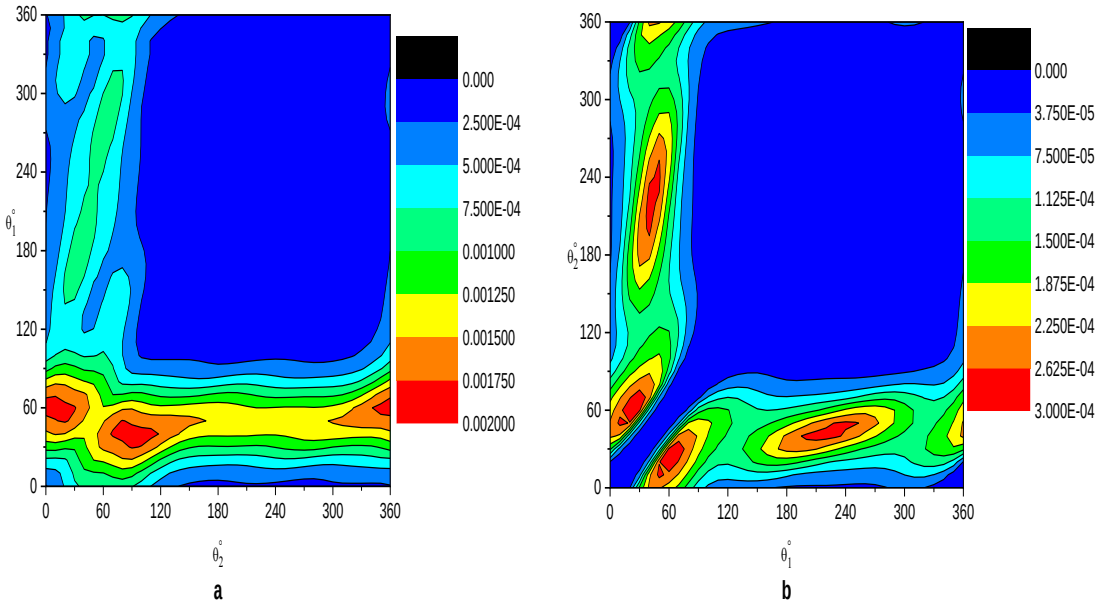

Figure4-12: Fivefold differential cross section (FDCS) for the double ionization of methane molecular orbital t2z as a function($\boldsymbol{\theta_1, \theta_2}$). The scattered angle $\boldsymbol{\theta_s = -6°}$, the incident electron energy is$\boldsymbol{E_i}$ =612eV. In (a): E_1=12eV , E_2=37eV, in (b): E_1 = E_2=37eV. **The FDCS is obtained with the first Born approximation and the 2CWWM model.**

Figure 4-12(a) shows the DI-t2z-CH4 for an asymmetrical ejection energy share of 12 eV and 37 eV. The study is based on the first Born approximation and the A3CWM model, which is an approximate BBK model with a corrected Gamow factor known as the Ward and Macek factor [15] used to describe the coulomb repulsion of the two ejected electrons at a fixed distance. The resulting structures are completely different, where we observe that the angular distribution is in a large continued hill from $\theta_1 = 0°$ to $\theta_1 = 100°$ and θ_2 arrays from $\theta_2 = 0°$ to $\theta_2 = 360°$, while the peaks are located at $(\theta_1, \theta_2) = (60°, 10°)$ and $(\theta_1, \theta_2) = (40°, 90°)$. These infrequent situations may be explained by a special SO process without back-to-back emission, in which the fast electron (37 eV) is ejected at an angle of 10° (or 40° for the second maximum) following its collision with the incident electron. Then, the second electron is emitted at an angle of 60° (or 90° for the second maximum) during the electronic arrangement of the target.

Figure 4-12 (b) displays the FDCS of the CH4-double ionization under the first Born approximation using the A3CWM, where the ejected electrons are both 37eV. The form consists of two large, symmetrical hills set against the middle line ($\theta_1 = \theta_2$) from $\theta_1 = 20°$ to $\theta_1 = 360°$and a second one extending from $\theta_2 = 0°$ to $\theta_2 = 80°$. The first hill contains two maxima situated at $(\theta_1, \theta_2) = (65°, 25°)$ and at $(\theta_1, \theta_2) = (50°, 230°)$(and by symmetry for the second hill). Although the strong repulsion between the two ejected electrons (37eV, 37eV), we may describe the maximum located at $(\theta_1, \theta_2) = (65°, 25°)$ according to an SO mechanism, when one electron collides with the incident electron, the second electron is ejected after the target's electronic reorganization. However, the second maximum $(\theta_1, \theta_2) =$

$(50°, 230°)$ represents a back-to-back emission due to an SO process, where the transfer direction is unfavorable and plays no role.

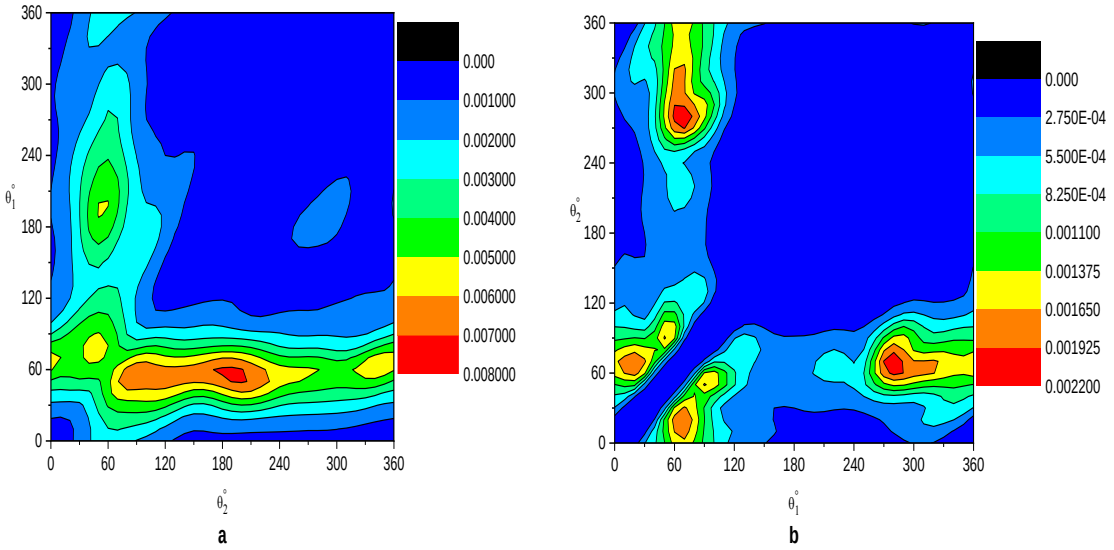

Figure4-13: Fivefold differential cross section (FDCS) for the double ionization of methane molecular orbital t2z as a function($\boldsymbol{\theta_1, \theta_2}$). The scattered angle $\boldsymbol{\theta_s = -6°}$, the incident electron energy is$\boldsymbol{E_i}$ =612eV. In (a): E_1=12eV , E_2=37eV, in (b): $E_1 = E_2$=37eV. **The FDCS is obtained within the second Born approximation and the 2CWWM model.**

The surface curves in Figures 4–13 are obtained under the same kinematic conditions as in Figure4-12, but by using the second Born approximation with the A3CWM model.

As can be seen in Figure 4-13(a), the maxima are delocalized, with a notable increase in magnitude. This may be due to destructive interference effects from the second-order TS2 mechanism. The FDCS is into two large hills extended in the regions: from $\theta_1 = 10°$ to $\theta_1 = 120°$ and $\theta_2 = 0°$ to $\theta_2 = 360°$ and from $\theta_1 = 150°$ to $\theta_1 = 300°$ with many peaks structure distributed on these hills. However, the most important maximum is located at $(\theta_1, \theta_2) = (60°, 190°)$ and can be attributed to by TS1 mechanism governance where we observe one electron ejected along $-\vec{K}$. Then, for the second step of the TS1 mechanism, this ejected electron collides with the second active electron of the target. In our case the slower electron is ejected along $\theta_1 = \theta_{-K} - 90° \approx 60°$and the faster along $\theta_2 = \theta_{-K} + 40° \approx 190°$ such as $|\theta_1 - \theta_2| = 130°$. This group corresponds to forward scattering, which is mainly due to the TS1 mechanism, as was also obtained in the case of the water molecule by Kada et al [16].

In figure 4-13(b) the structure consists of two symmetrical hills, each containing two maximums of different amplitudes. The first one situated at $(\theta_1, \theta_2) = (70°, 25°)$of 2,2*$10^{-3}$au is mostly due to the SO mechanism as in figure 4-12(b), though the second one, located at $(\theta_1, \theta_2) = (70°, 280°)$ this may be due to the interference effects of the TS1 and TS2 processes, as was previously demonstrated. (e,3-1e)-CH4 experience [9].

IV.5 Conclusion

In this work, we reported a theoretical analysis of the fivefold differential cross-section of double ionization of methane by electron impact. The first and second Born approximations were employed alongside two versions of the approximate BBK model, which incorporated separately the Gamow factor and the Ward and Macek factor to describe the repulsion of the two ejected electrons in the residual ion continuum. For the initial state, we used a single-center

wavefunction to describe the target and a plane wave to describe the fast incident electron. It has been clearly demonstrated that the SO mechanism can dominate the first-order reaction, whereas the TS1 mechanism does not appear to be the main process. However, when the second Born approximation was considered, the effects of the TS2 mechanism became apparent. In some cases, dramatic changes to the FDCS structure were observed when the Ward and Macek function was used to correct the behavior in the final state.
Ultimately, we hope that our current results will be verified by an experiment in the near future.

IV.6 References

[1] I. Kada, C. Dal Cappello and A. Mansouri, *Eur. Phys. J. D*, **71** 41(2017).
[2] A. Herbadji, I. Kada, A. Mansouri and C. Dal Cappello, *J. Phys. B: At. Mol. Opt. Phys.*, **54** 215201 (2021).
[3] A. Herbadji doctorate thesis ; University Ferhat ABBAS Setif1-(2022)
[4] C. Schröter, B. El Marji, A. Lahmam-Bennani, A. Duguet, M. Lecas and L. Spielberger, *J. Phys. B: At. Mol. Opt. Phys.*, **31** 131 (1998).
[5] I. Taouil, A. Lahmam-Bennani, A. Duguet, M. Lecas, L.Avaldi, Phys. Rev. Lett. **81**, 4600 (1998)
[6] M. Grin, C. Dal Cappello, R. El Mkhanter, J. Rasch, J.Phys. B **33**, 131 (2000)
[7] H. Hda, C. Dal Cappello, & J. Langlois, Angular distributions of electrons in the (e,3e) reaction. *Zeitschrift für Physik D Atoms, Molecules and Clusters, 29*(1), 25–29(1994).
[8] A. Lahmam-Bennani, A. Duguet, A.M. Grisogono, M. Lucas : J. Phys. B25, 2873 (1992)
[9] E.M. Staicu Casagrande, C. Li, A. Lahmam-Bennani and C. Dal Cappello, *J. Phys. B: At. Mol. Opt. Phys.*, **47** 115203 (2014).
[10] R. El Mir, E.M. Staicu Casagrande, C. Dal Cappello, A. Naja, A. Mansouri, I. Kada, J. Phys. Conf. Ser. 601, 012005 (2015)
[11] Z. Ait Elhadjali, S. Kessal, M.A. Quinto, D. Oubaziz, C. Champion, Int. J. Mass Spectrom. 403, 53–61 (2016)
[12] D. Oubaziz, Z. Ait Elhadjali, M.A. Quinto, R. Boulifa, C. Champion, Eur. Phys. J. D 71, 160 (2017)
[13] A. Lahmam-Bennani, E.M. Staicu-Casagrande, A. Naja, C. Dal Cappello, P. Bolognesi, J. Phys. B At. Mol. Opt. Phys. 43, 105201 (2010)
[14] C. Dal Cappello, I. Kada, A. Mansouri, C. Champion, J. Phys. B Conf. Ser. 288, 012004 (2011)
[15] S.J. Ward and J.H. Macek, *Phys. Rev. A*, **49** 1049 (1994).
[16] I. Kada, A. Mansouri, C. Dal Cappello, P.A. Hervieux and A.C. Roy, *J. Phys. B: At. Mol. Opt. Phys.*, **42** 025201(2009).
[17] W. Sakhraoui, I. Kada, A. Mansouri, and C. Dal Cappello, Eur. Phys. J. D **79**, 75 (2025).

Conclusion

Conclusion

The study of double ionization (DI) processes of atoms and molecules, particularly through electron impact, provides profound insights into the complex dynamics of electron-electron correlations and ionization mechanisms. This work has focused on the double ionization of Neon (Ne) and Methane (CH_4), employing advanced theoretical models such as the First and Second Born Approximations, the BBK (Brauner-Briggs-Klar) model [1], the 2CW and the 2DW models with Gamow [2] and Ward-Macek [3] factors. The findings highlight the intricate interplay between ionization mechanisms, electron correlations, and the role of residual ion states, offering a deeper understanding of many-body interactions in atomic and molecular systems.

The analysis of the fivefold differential cross-section (FDCS) under high-energy electron impact (5500 eV) revealed several observations for neon. The BBK model shows good agreement with the experimental data, particularly with regard to the global contribution of all ion states. The important influence of the ^3P state on the process is also evident, while the impact of the other states is smaller but still significant as they consider electron-electron correlation. However, potential refinements using distorted wave approaches could improve accuracy further, particularly in reproducing finer angular distribution details. Though less prominent, the higher-energy $2s^{-1}2p^{-1}\ ^3P$ state may introduce subtle modifications to the characteristics of the minima and maxima. These observations are consistent with the findings of Kada et al. [4] that comprehensive agreement with experimental data requires contributions from all accessible ion states to be summed.

We conclude that the BBK model successfully captured the essential electron correlation effects, but discrepancies with experimental data, especially at intermediate angles, suggested limitations in treating angular correlations.

When applying the 2DWG model, incorporating distortion effects to the (e,3e)-Ne($2p^6$) it provided improved agreement, particularly in reproducing finer angular structures. These results align with earlier studies by Kada et al. [4] and Herbadji et al. [5] for argon-DI, emphasizing the need for refined theoretical approaches to fully account for electron interactions and ion-recoil dynamics. The study confirms the participation of both forward and backward emission due to the TS1process, and distinguishes apparition of new maxima in different situations (134°, 150°; 330°) where the SO mechanism is the first responsible. Another important remark concerns the underestimation of the theoretical maximum magnitudes in all studied cases needing normalization to experience by factors of about 10. This suggests potential limitations in the model's treatment of post-collision interactions or experimental resolution effects.

In the case of DI of krypton by electron impact of 5,5KeV in a symmetric regime and a coplanar geometry by use of the 2CWG model, our results reveal a good agreement with the experimental angular distribution shape and confirm the dominance of the SO process.

The results suggest that, although the 2DWG model is highly effective, it may not fully capture the intricacies of electron-electron or electron-ion interactions in this configuration. This indicates the need for further theoretical refinement.

The investigation of methane's double ionization introduced additional complexities due to its molecular structure and multicentric nature. The study employed Moccia's monocentric wavefunction [6] approximation to simplify calculations while retaining physical accuracy. For asymmetric energy sharing (E_1 = 12 eV, E_2 = 37 eV), the FDCS exhibited structures consistent with the SO mechanism, though without strict back-to-back emission. In symmetric energy sharing (E_1 = E_2 = 37 eV), the FDCS showed two distinct hills, with maxima suggesting contributions from both SO and Two-Step (TS1) mechanisms. The TS1 process, involving sequential electron collisions, was less dominant than initially expected.
The Second Born Approximation revealed significant contributions from the TS2 mechanism, where the incident electron undergoes two successive collisions with target electrons. This was evident in the dislocation of maxima and increased cross-section amplitudes, particularly for symmetric energy sharing. These findings highlight the importance of higher-order terms in describing DI processes, especially for molecular targets.
The use of the Ward-Macek factor, as a correction to the Gamow factor, introduced notable changes in the FDCS structure. This adjustment accounted for the asymptotic behavior of ejected electrons, leading to more accurate predictions of angular distributions and peak intensities. The results underlined the sensitivity of theoretical models to the treatment of electron-electron repulsion in the final state.

The theoretical frameworks and results presented in this work have several implications, it contributes to the ongoing effort to refine models for DI processes, particularly in addressing discrepancies between theory and experiment. The inclusion of distorted waves, higher-order approximations, and advanced repulsion factors represents a step forward in achieving quantitative accuracy.

Methane, as a key molecule in astrophysical and environmental contexts, benefits from detailed ionization studies. Understanding its behavior under electron impact can inform models of planetary atmospheres, interstellar chemistry, and combustion processes.

While the current models show promising agreement with experimental data, challenges remain in fully capturing the nuances of electron correlations and multicentric effects in molecules.

In conclusion, this work has provided a comprehensive theoretical analysis of double ionization in Neon, Krypton and Methane, shedding light on the underlying mechanisms and the role of electron correlations. The findings demonstrate the power of advanced quantum mechanical models in interpreting experimental data while also highlighting areas for further refinement. As experimental techniques continue to evolve, parallel advancements in theory will be essential to unraveling the full complexity of many-electron dynamics in atomic and molecular systems. The insights gained here pave the way for future studies aimed at achieving a complete and predictive understanding of ionization processes across a wider range of targets and conditions.

References

[1] M. Brauner, J. S. Briggs, and H. Klar, “Triple differential cross sections for double ionization,” *J. Phys. B: At. Mol. Opt. Phys.* 22, 2265 (1989).
[2] C. Dal Cappello, B. Joulakian, and J. Langlois, “Correlated wave-function description of double ionization processes,” *J. Phys. III (France)* 3, 125 (1993).
[3] S. J. Ward and J. H. Macek, “Electron-impact double ionization of helium,” *Phys. Rev. A* 49, 1049 (1994).
[4] I. Kada, C. Dal Cappello, and A. Mansouri, “Theoretical study of electron-impact ionization dynamics,” *Eur. Phys. J. D* 71, 41 (2017).
[5] A. Herbadji, I. Kada, A. Mansouri, and C. Dal Cappello, “Fully differential cross sections for electron-impact double ionization,” *J. Phys. B: At. Mol. Opt. Phys.* 54, 215201 (2021).
[6] R. Moccia, “Correlation effects in atomic wave functions,” *J. Chem. Phys.* 40, 2176 (1964).

Résumé

Cette thèse traite de l'ionisation double des atomes et molécules par impact électronique, un processus fondamental dans la compréhension des interactions particules-matière. Après avoir introduit la théorie de la diffusion et les concepts de sections efficaces, l'étude explore les mécanismes d'ionisation double (shake-off, two-step 1 et two-step 2) en mettant en évidence l'importance des corrélations électroniques. Divers modèles théoriques, tels que BBK (3C), DWBA et 2CWG, sont utilisés pour simuler ces processus. Les résultats obtenus pour des cibles atomiques (Néon, Krypton) et moléculaires (CH_4) sont comparés à des données expérimentales et montrent que la prise en compte des effets de corrélation et de distorsion améliore significativement les prédictions théoriques.

Abstract

This thesis investigates the double ionization of atoms and molecules by electron impact, a key process to understanding particle-matter interactions. After introducing the fundamentals of scattering theory and cross-section concepts, the study focuses on double ionization mechanisms (shake-off, two-step 1, and two-step 2), emphasizing the critical role of electron correlation. Several theoretical models, including BBK (3C), DWBA, and 2CWG, are employed to describe the final-state electron dynamics. Applications to atomic (Neon, Krypton) and molecular (CH_4) targets demonstrate good agreement with experimental data, especially when correlation and distortion effects are included, validating the theoretical approach.

الملخص

تتناول هذه الأطروحة دراسة التأين المزدوج للذرات والجزيئات الناتج عن تصادمات الإلكترونات، وهو عملية أساسية لفهم تفاعلات الجسيمات مع المادة. تبدأ الدراسة بعرض مفاهيم نظرية التشتت ومقاطع التفاعل، ثم تركز على آليات التأين ، مع التأكيد على أهمية الترابط الإلكتروني بين (TS2و TS1) والخطوتين (Shake-off) المزدوج مثل الاهتزاز لوصف هذه العمليات. وقد CWGو2 DWBAو BBK (3C) الإلكترونات. تم استخدام نماذج نظرية متعددة مثل توافقاً جيداً مع البيانات التجريبية، (CH_4) أظهرت النتائج على أهداف ذرية مثل النيون والكربتون وجزيئية مثل الميثان .خاصة عند أخذ تأثيرات الارتباط والتشوه بعين الاعتبار